In-situ Self Assembly of Optoelectronic Quantum Dots Using Reactive Coating

Kimia Rezaei Shad

Thesis submitted to the University of Ottawa in partial fulfillment of the requirements for the Master of Applied Science in Electrical and Computer Engineering

Department of Electrical and Computer Engineering
Faculty of Engineering
University of Ottawa

Abstract

There has been considerable focus on quantum dots (QDs) and nanoparticles (NPs) and their extensive applications. Binary and Ternary QDs such as PbS and $CuInS_2$ (CIS) QDs, owing to their superior chemical, physical, electrical, and optical properties, are utilized in a wide variety of optoelectronic and photonic applications such as solar cells, LEDs, and photodetectors. This research describes an inexpensive approach for fabricating self-assembled binary and ternary quantum dots (QDs), including PbS and CIS, using a reactive blade coating technique based on the in-situ fabrication of QDs from their precursor solutions. Roll-to-roll compatibility makes this technique ideal for scalable nanomanufacturing. For PbS QDs, Pb ink, containing the Pb precursor, was first produced by dissolving lead acetate in Oleic acid and Octadecene, and S ink, containing S precursor, was made by dissolving the sulfur powder in oleylamine (OLA). Fabrication of thin films was conducted by first blade coating the Pb ink and then coating the S ink on top of it. Three different heating methods (vacuum oven, hotplate in the glovebox, and rapid thermal annealing (RTA) were used for heating the blade-coated samples. Different temperatures and heating durations were investigated in each heating method to find the best parameter. Crystallographic structure and the morphology of the synthesized QDs were characterized with X-ray diffractometer (XRD), Energy-dispersive X-ray spectroscopy (EDS), and scanning electron microscopy (SEM). Moreover, UV-vis absorption and photoluminescence (PL) emission tests were executed on the samples to understand the optoelectronic behavior of the QDs. The obtained result confirmed the formation of different shapes of PbS QDs showing PL emission peaks in the UV-vis range that can be used in optoelectrical applications.

Furthermore, the facile blade coating technique mentioned above was also used for synthesizing CIS QDs, which are more environmentally friendly particles compared to PbS QDs. In the CIS blade coating process, first CuIn ink was prepared by dissolving copper iodide and indium acetate in OLA, and S ink was prepared by dissolving S powder in OLA. The in-situ fabrication of CIS QDs was performed by first blade-coating one layer of CuIn ink, followed by blade-coating one layer of S ink on top of that. The blade-coated samples were heated with the RTA method, which was selected as the best heating method for preparing PbS QDs (details mentioned in Chapter 3).

Different heating temperatures and durations were tried to heat the blade-coated samples with RTA. XRD, SEM, EDS, and transmission electron microscope (TEM) tests were investigated on CIS QDs to understand their crystal structure and morphology. Moreover, UV-test and photoluminescence tests were also executed on the samples to check their optoelectronic properties.

Another step towards industrialization of the in-situ reactive blade coating system was achieved using different techniques to get a full-coverage uniform thin film. Using UV-ozone cleaning, oxygen plasma cleaning, and silanization process, we were able to get full-coverage uniform CIS thin films (1 × 1 inch). This investigated technique is useful for comprehending the steps required to produce uniform, high-quality thin films using a roll-to-roll compatible, simple method on a large scale.

Acknowledgment

Prior to anything else, I would like to express my sincerest gratitude to my supervisor, Professor Ghassan Jabbour, for his invaluable guidance, ongoing encouragement, and abundant support throughout my research. Joining his lab and conducting research under his supervision has been a fantastic opportunity for me. I am profoundly grateful for his direction, forbearance, understanding, and financial assistance, during my study at uOttawa.

I would like to thank Dr. Mutalifu Abulikemu and Dr. Choi for being such kind and generous mentors, for sharing their vast knowledge as well as valuable time, and for providing guidance when there was an obstacle in my research.

Also, I would like to thank the Center for Research in Photonics (CRPUO) lab manager Dr. Antony Olivera, Howard Northfield, Spyridon Ntais, and the CRPuO administrative staff for granting us access to the NanoFab lab facilities and required training. I would like to express my gratitude to Dr. Neeraj Joshi and Ms. Yun Liu for their training and use of the instruments at the Centre for Advanced Material Research (CAMaR) at the Department of Chemistry and Biomolecular Sciences and to Dr. Jeffrey Ovens for his use of the University of Ottawa's X-ray Core Facility.

Last but not least, I would like to extend my sincere gratitude and appreciation to my family and friends for their continuous support and motivation throughout my academic career.

Table of Contents

List of Figures

List of Tables

Abbreviations

ODE	1-Octadecene
CIS QDs	Cupper Indium Sulfide Quantum dots
EDS	Energy-dispersive X-ray spectroscopy
FTO	Fluorine-doped Tin Oxide
IPA	Isopropyl alcohol
PbS QDs	Lead Sulfide Quantum dots
NPs	Nanoparticles
OA	Oleic acid
OLA	Oleylamine
PL	Photoluminance
PV	Photovoltaic
P3HT:PCBM	poly(3-hexylthiophene-2,5-diyl):[6,6]-phenyl C61 butyric acid methyl ester
QDs	Quantum dots
RTA	Rapid thermal annealing
R2R	Roll-to-Roll
SEM	Scanning electron microscopy
S	Sulfur
XRD	X-ray diffractometer

Chapter 1 . Introduction

Nanotechnology has become the dominant technology in many fields, including engineering, electronics, chemistry, physics, material science, and biomaterials[1,2].

Nanoparticles (NPs) are one of the building blocks of nanotechnology, and they have attracted considerable attention due to their wide array of applications, such as optoelectronics, biology, biomedical, photocatalysis, and industrial applications. Particles with at least one dimension within the nanometer range are classified as NPs. In contrast to their bulk counterparts, NPs have distinct properties and can be engineered to demonstrate quantum confinement and enhanced surface effects [3–9].

Quantum dots (QDs) are among the most popular NPs with all three dimensions on the order of nm and are usually categorized as zero dimensional materials. Their crystal structure and composition can be engineered to create specific optical and electronic characteristics not observed in the respective bulk material[10,11]. QDs can be classified based on their properties and constituents. This classification can include the following:

1- Semiconductor QDs (nanocrystals), 2- Metal-based QDs such as Copper, Lead, Zinc, and Indium, and 3- Metal alloy-based QDs (bimetallic or trimetallic) such as Cu-In, Au-Ag, Pt-Ru-Sn

The quantum confinement effect observed in semiconductor QDs has garnered great interest because it enables the material properties of these structures to be manipulated[12]. These controllable characteristics include absorption and emission when exposed to radiation and chemical and physical properties, which are determined by their size and bandgaps[13–15]. The quantum size effect can be tailored to different applications, such as optoelectronic, optical, biological, and biomedical applications[16–19]. Fig. 1.1 illustrates using QDs in various applications[13].

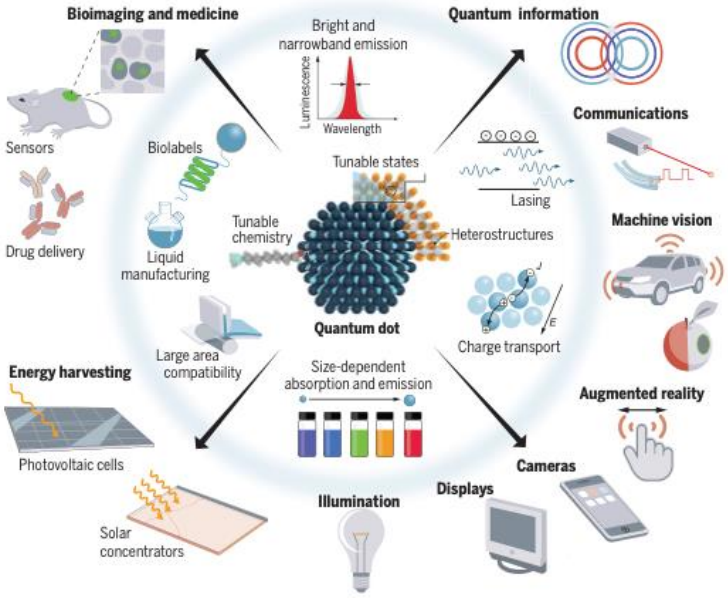

Figure 1.1 - Quantum dots different applications[13].

Semiconductor QDs have many applications, but their use in optical and optoelectronic applications has been prevalent. This popularity can be attributed to their large surface-to-volume ratio, which absorbs more light when they are under radiation and emits bright and relatively narrow light spectrum[13,20]. Moreover, they have a tunable bandgap that can be adjusted by changing their size, which can result in absorbing light at different ranges, from UV-Vis to IR range[21,22]. As a result, QDs can have great potential to be used in lasers, light-emitting diodes (LEDs), solar cells, photodetectors, optical fibres, and biomedical imaging[20–24]. Also, optoelectronic devices based on QDs have a future scope for telecommunication, medical applications, and military devices[25–27].

In the area of binary QDs, lead chalcogenides (PbS, PbSe, PbTe) have been extensively investigated for their attractive UV-vis-near-IR optical properties and their potential use in IR photodetectors, solar cells, and lasers[28–31]. PbS QDs are the most commonly used lead chalcogenide structure in photodetector and solar cell applications[32–34]. With a bandgap of 0.41 eV at ambient temperature, an absorption edge of 3200 nm, and a large exciton Bohr radius of 18 nm, PbS facilitates the observation of quantum size effects[32,35]. Also, PbS has favourable optical features such as multiple carrier generation, high molar excitation coefficient, and a wide range of spectral responses that make these QDs good candidates for photovoltaic devices[36–38].

According to several reports, PbS has shown a high photoluminescence quantum yield and good stability when compared to other materials, such as PbSe QDs[39–41].

Solar cells, LEDs, sensors, optical fibres, optoelectronic integrated circuits, and photodetectors are photovoltaic devices fabricated using different shapes and sizes of PbS QDs[42–46]. Furthermore, many composites of PbS with other organic or inorganic structures have been fabricated to increase the efficiency of optoelectronic devices, in which PbS plays a key role[47–49]. In addition, PbS has been utilized (occasionally as an additive or in a nanocomposite structure) to improve the performance of various applications, including photocatalytic and telecommunication applications[50–52].

Specially designed PbS QDs have been widely studied for their unique properties for the above reasons[53,54]. The synthesis of PbS QDs has been widely investigated, and a variety of methods have been used.

Hines method is the most famous method for synthesizing PbS QDs and is counted as a hot injection method. In this method, a solution containing Pb precursor and some ligands is first prepared, then the sulfur solution is quickly added to it while heated. After several steps of precipitation and centrifugation, the monodisperse PbS QDs are obtained[55].

It is important to note that time-consuming processes, such as the Hines method, result in additional organic solvents, materials, and energy being consumed, ultimately increasing the price of QDs. In order to enhance the market penetration of such vital nanocrystals, it is essential to find alternative synthesis methods for producing homogenous PbS QDs that dramatically reduce the cost. Moreover, low-cost organized QDs thin films with functional periodic patterns are crucial for various applications in optoelectronics, photovoltaics, and chemical and biological ones[56,57].

Structures such as PbS QDs have been intensively studied over the last two decades because of their controllable shape and size for optoelectronic applications[58]. Despite this, their use on a large scale is limited due to lead toxicity. Thus, serious efforts are needed to decrease such toxicity to acceptable levels [59–61]. One ultimate solution is to avoid having toxic elements in the materials used for given applications. Research efforts have been growing to substitute binary structures of PbS QDs with ternary semiconductor QDs, such as $CuInS_2$ (CIS) with I-III−VI_2,

which are inexpensive heavy metal-free materials and have low toxicity[62,63]. CIS has a direct bandgap of 1.5 eV and a high absorption coefficient in the visible/NIR region that correlates well with the solar emission range[64,65]. Moreover, as a ternary material, CIS allows further tuning of optical properties by changing the ratio of Cu to In in its lattice[66].

Chalcopyrite, zinc-blende, and wurtzite are the three most common crystal structures of $CuInS_2$. Chalcopyrite is the most frequent CIS structure at room temperature. Some of these structures can be stable even above 1100 K. However, the CIS QDs with wurtzite and zinc-blend structures can be synthesized at much lower temperatures because of the high surface-to-volume ratio and lower surface energy in smaller sizes[67,68]. The chalcopyrite structure of CIS has been studied for its high tolerance to having a wide variety of anions and cations off-stoichiometry, in addition to its adjustable band gap and photoluminescence[69]. Meanwhile, in zinc-blende and wurtzite crystal structures, metal atoms are randomly located in the sublattice of cations[70]. Because of the differences among the three mentioned structures, various optical characteristics can be achieved by altering the crystalline phase of CIS QDs[71].

CIS QDs have been made with a hot injection, solvothermal, or other colloidal synthesis methods[67],[103]. Similar to PbS, the procedures for synthesizing CIS QDs are considered time-consuming and wasteful of a significant amount of chemicals. The previously utilized techniques for synthesizing CIS QDs may not be suited for large-scale manufacturing due to the aforementioned factors.

CIS QDs have very high potential to be used in optoelectronic applications similar to PbS because of their features such as enhanced charge-transport properties, size-tunable absorption and emission spectra, broad absorption cross sections, and exceptional radiation toughness and defect resistance[73,74]. They can be used in LEDs, solar cells and photodetectors and are environmentally friendly alternatives to toxic conventional binary structures such as CdS, CdSe, and PbS, and may lead to increased device efficiency[75–77]. Moreover, they can be used for biomedical applications such as biological cell imaging and fluorescent probes[62,78].

Also, $CuInS_2$ structures can be used for photocatalytic applications because of their attractive features, such as strong visible-to-NIR light absorption efficiency and tunable bandgap[78]. They can be used as a photocatalyst for producing hydrogen with a reasonable efficiency[79] or increase the photoresponse range of a composite photocatalyst[80].

In most cases, for depositing NPs and QDs on surfaces or forming them directly into thin films, conventional liquid-based methods require prior preparation of colloidal solutions of NPs and QDs followed by purification and washing processes to obtain a uniform and narrow size distribution, and the functionalization of substrate surfaces (and/or the particles) to obtain homogeneous ordered assembly of thin layers. As a result, this results in more processing time and increased costs. Some of the most popular conventional methods of depositing and synthesizing NPs are described in more detail in Chapter 2 (literature review).

In light of the above and the details described in Chapter 2, Jabbour's group has introduced some in-situ reactive printing and coating methods to synthesize self-assembled metallic NPs such as silver and gold NPs with uniform order and size[81,82]. In one of their works for synthesizing gold NPs with reactive inkjet printing, they used low cost precursors and solvents with almost zero dangerous byproducts. Also, the synthesis and printing process time was less than one minute, which is far less than most other preparation techniques for gold NPs[81].

It is worth noting that a short shelf lifetime, leading to a colloidal solution of NPs with a broad size range, is observed for commercial colloidal QDs and NPs[83]. However, in the in-situ reactive printing method mentioned above, the ink containing the precursors can be stored for months and years without any reaction or formation of NPs until they are printed on top of each other.

In the in-situ reactive printing process, the precursor inks are printed on each other using silicon or glass substrates. The sizes of the self-assembled homogenous gold NPs achieved were about 8±2 nm, smaller than the ones produced by traditional synthesizing techniques[81]. However, inkjet printing is an expensive technique because of the high cost of printer cartridges that clog with time and raise the cost of NPs or QDs production. Thus, a quicker and more financially viable reactive printing or coating method must be developed to meet the low cost and widespread application of QDs or NPs with uniform size distribution.

Several roll-to-roll-compatible techniques, including blade coating, gravure printing, and slot die coating, can implement an efficient coating process. In this regard, Jabbour's group synthesized and deposited silver NPs on a glass substrate, textiles, and a surgical mask with an in-situ reactive blade coating method. These blade-coated thin films were highly disinfectant against SARS-CoV-2[82]. Compared to in-situ reactive inkjet printing, in-situ reactive blade coating is a quicker and

more cost-effective method worthy of investigation for making low-cost, ubiquitous QDs. A schematic of a roll-to-roll blade-coating system is shown in Fig. 1.3.

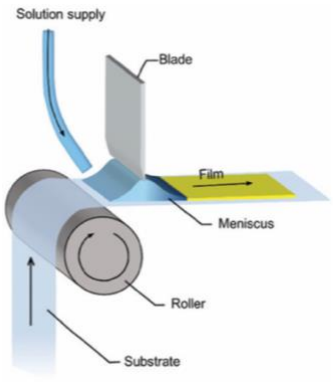

Figure 1.2 - Schematic of a roll-to-roll blade-coating system[84].

Here, in this thesis, I used in-situ reactive blade coating to synthesize binary and ternary QDs such as PbS and $CuInS_2$. Blade coating was chosen for this study due to its potential for roll-to-roll QDs production. In this synthesizing method, QDs with uniform sizes and ordered layers were generated on the surface of substrates. Successful implementation of this low-cost method could significantly reduce QDs ' prices when used by the industry.

For each of the investigated QDs, different factors, such as the precursor concentration, and parameters for different heating procedures, such as the heating time and temperature, were investigated.

The main objectives of this research are the followings:

1. Analyze in-situ self-assembly of PbS and $CuInS_2$ in a roll-to-roll compatible, reactive blade coating technique.
2. Investigate various heating methods, temperatures, and heating durations for drying the blade-coated samples and evaluate their impact on the coating uniformity and QD size range.
3. Illustrate the potential of the in-situ reactive blade-coated samples for photovoltaic devices by performing UV-Vis absorption measurements and photoluminescence tests on the synthesized QDs.

Chapter 2 will describe an overview of different synthesizing and coating methods for PbS and $CuInS_2$. It will also demonstrate the application of these QDs in different optoelectrical and photovoltaic devices.

Chapter 3 will present the synthesizing process of PbS QDs using an in-situ reactive blade coating method and the various heating methods used for drying the blade-coated samples. It will also discuss the precursors used for synthesizing these QDs and the different parameters investigated for synthesizing and drying them. The characterization techniques, the analysis, and their results will also be described. The UV-vis and photoluminescence results of PbS QDs will also be presented in this chapter to demonstrate the potential of these QDs in optoelectronic devices.

Chapter 4 will demonstrate the fabrication process of self-assembled $CuInS_2$ QDs using the reactive blade coating method. Then the discussion will be followed by various characterization tests and their results. Different parameters investigated for these QDs will be explained, and the efforts undertaken to create a uniformly thin film will be investigated.

Chapter 5 will demonstrate the overall conclusion of the in-situ reactive blade coating manufacturing of self-assembled binary and ternary QDs, which are viable materials for photovoltaics and optoelectronics in the future. Also, we will comment on the possible extension of such facile synthesizing and coating techniques for usage on an industrial scale.

Chapter 2 . Background

2.1 Nanomaterials and nanoparticles

Nanoparticles (NPs) are tiny particles with at least one dimension less than 100 nanometers. They can be made from a various materials, such as metals, metal oxides, polymers, and ceramics. Due to their ultra-small dimension, high surface-to-volume ratio, and quantum effects, NPs possess unique physical, chemical, and biological properties. Their optical, magnetic, electrical, and catalytic properties are distinct from their bulk counterparts[85]. These characteristics make NPs applicable to various applications, including electronics, energy, medicine, and environmental services[86], to mention a few.

NPs have a large surface area compared to their volume because of their tiny size. This expanded surface area makes NPs more reactive and improves their potential physical and/or chemical attachment to other materials. Also, specific NPs can self-assemble into organized structures due to their size and structure. This characteristic has potential use in nanotechnology, including manufacturing nanoscale electrical devices[87].

2.2 Quantum dots

Quantum dots (QDs) are nanoscale semiconductor particles with zero dimensions, and their electrical and optical properties differentiate them from bulk materials. QDs may produce multiple wavelengths of light based on their size, making them ideal for various applications, including lighting, displays, and biomedical imaging. In addition to their usage in photography and displays, QDs are being studied for various applications, such as solar cells, sensors, and single-electron transistors[88].

The size and composition of QDs control their electrical and optical characteristics. When light or heat excites a QD, one electron is elevated to a higher energy level. This electron can then recombine with a hole to release energy as a photon of light. Because the energy of the released photon is proportional to the energy difference between the starting and final states of the electron (which is proportional to the size of the QD), the size of the QD determines the colour and wavelength of the produced light[89].

2.2.1 Quantum confinement effect

Quantum confinement is a phenomenon that happens when a material's dimensions are decreased to a few nanometers or less. When a material is shrunk to this level, the confinement of electrons alters the material's electrical and optical characteristics. This confinement leads to the quantization of the electronic energy levels, resulting in variety of unique and fascinating features[90].

One of the most significant effects of quantum confinement is that the material's bandgap changes when its size is decreased. In this regard, the bandgap of nanoscale materials can be controlled by varying their shape and dimension[91]. This gives rise to more degrees of freedom to control the quantum effects in 1 dimension (1D), 2D, or 3D.

Fig. 2.1, from left to right, illustrates the transition in electronic energy levels from bulk semiconductors to small nanocrystal semiconductors (QDs) and then to a cluster of only a few atoms. When the QD size decreases, the bandgap increases with more distinct energy levels appearing at the band edges, as seen in Fig. 2.1. The phenomenon associated with the band gap widening is known as the "quantum confinement effect"[92].

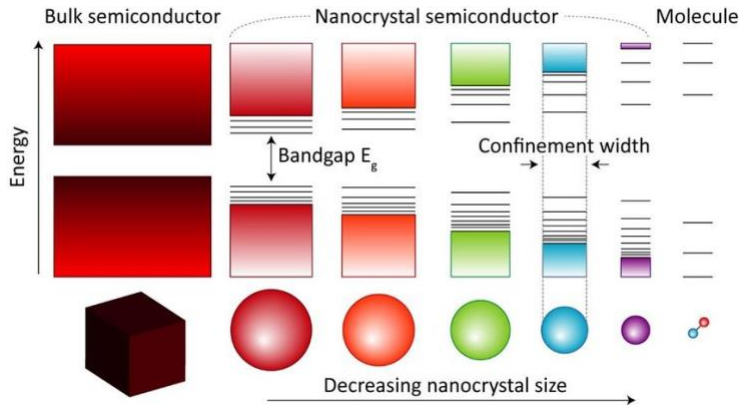

Figure 2.1 - Quantum confinement effect: Comparison of bulk, semiconductor nanocrystals (QDs), and molecules reveals the size-dependent bandgap of nanocrystals and the creation of distinct states near the band edge[92].

Changes in dimension significantly impact the density of states (DOS). The energy of the bands of a bulk semiconductor is proportional to their square root. Moreover, in a 2D quantum well, excitons can travel in two dimensions but are limited in the lateral dimension. This leads to a stepwise DOS with a constant dependence in which all energies are available but only rise in

quantifiable steps. With a quantum wire, the exciton can only go in one direction. Thus, a DOS with an inverse square energy dependency is produced. Here, the DOS only grows in quantifiable increments but decreases rapidly between each quantified step. Lastly, 0D, quantum confinement in all 3 dimensions, QDs exhibit a DOS with states permitted only at specific energies as shown in Fig. 2.2[93].

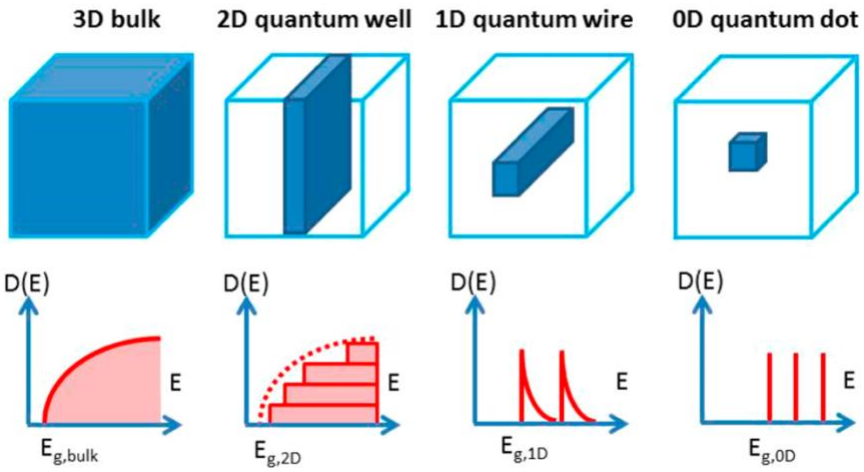

Figure 2.2 - Schematic representation of a three-dimensional (3D) bulk semiconductor and the related two-dimensional (2D), one-dimensional (1D), and zero-dimensional (0D) quantum nanostructures. The joint density of states D(E) between the conduction band (CB) and the valence band (VB) is represented as a function of the energy [93].

As a further consequence of the quantum confinement effect, the state density of a material varies when its size is diminished. Due to the quantization of energy levels, the density of states in nanoscale materials is discrete, whereas it is continuous in bulk materials. This discrete state density significantly affects nanoscale materials' optical and electrical characteristics. QDs offer various potential uses in fields such as electronics, photonics, and sensing due to the quantum confinement effect's distinctive features[94].

2.3 PbS quantum dots and nanoparticles

A significant interest has been generated in synthesizing PbS QDs and NPs due to their large size tunability over the UV-Vis-NIR region and strong quantum confinement effect[95]. PbS is a direct bandgap semiconductor with a 0.41 eV bandgap and a large 18 nm exciton Bohr radius.

2.3.1 Synthesis of PbS quantum dots and nanoparticles

Top-down and bottom-up are two ways to approach PbS NPs. In the top-down approach, PbS NPs are synthesized using various methods by reducing the size or breaking down the bulk structure to the nanoscale size. For instance, PbS QDs and NPs have been synthesized using top-down methods such as vacuum evaporation of bulk PbS and solid-state grinding synthesis[96,97]. These approaches require complicated manufacturing equipment and cannot produce particles with tunable sizes. In bottom-up approaches, which are most common for synthesizing PbS NPs, NPs are formed from tiny atoms and molecules. Some of these synthesizing methods, such as the aqueous solution phase method and synthesis with the help of glass fabrication and polymer films, have been tried to achieve PbS QDs and NPs[98–100].

2.3.1.1 *Wet-chemical methods*

Among the various bottom-up approaches for synthesizing nanomaterials, direct chemical synthesis methods, such as wet-chemical synthesis, are major methods for synthesizing binary NPs and QDs. Wet-chemical synthesis techniques demonstrate controllability and reproducibility to a great degree for producing nanocrystals and are established as effective, inexpensive ways to produce PbS QDs of excellent quality. Some of the most famous wet-chemical synthesis approaches for synthesizing PbS particles are solvothermal and hot injection methods[101].

- Solvothermal synthesizing method

A solvothermal method is one of the popular methods used for synthesizing PbS QDs. Cheng et al. synthesized PbS QDs using a sulfur stock solution containing sulfur powder in Oleylamine (OLA) and a lead solution containing lead chloride in OLA. The sulfur stock solution was added to the Pb solution, and it was stirred and heated to make PbS QDs, followed by the centrifugation and washing process[102]. Moreover, in another study, Zhang et al. synthesized PbS NPs with different shapes using lead acetate as the Pb source and thiourea as the sulfur source. The two precursors were put in a stainless-steel autoclave, and then L-cysteine was added. L-cysteine is an amino acid, and different concentrations of it affect the growth and final shape of PbS particles. Different solvents, such as water, ethanol, and ethylene glycol, were added to the autoclave and heated for a different amount of time to make PbS particles with different shapes[103].

- Hot injection method

A hot injection is one of the most famous synthesizing methods to produce monodispersed colloidal NPs and QDs with homogenous sizes and shapes[104]. Using this wet-chemical synthesis method, a cold solution containing one or more precursors is rapidly injected into a hot solution containing other precursors or surfactants and a solvent with a high boiling point[105].

Conventional theories state that nucleation and diffusion-controlled growth are the most significant variables in colloidal synthesis for controlling size distribution. Several papers on the synthesis of uniform nanocrystals over the past two decades have popularized the hot-injection approach for obtaining uniform nanocrystals of diverse materials, such as metals, semiconductors, and oxides. The mechanism of making NPs and QDs in the hot injection method is based on nucleation and growth[106]. A schematic of the formation mechanism of NPs in this synthesizing method is shown in Fig. 2.3. The time development of the number of particles and the relative standard deviation of the size distribution is depicted in the Figure.

Based on the Figure, stable nuclei can grow into bigger particles during the nucleation phase, and the number of particles in the solution grows fast, accompanied by a broadening of the size distribution. The relative standard deviation of the size distribution, σ_r, achieves its maximum value at the end of the nucleation period. The process then enters the growth phase, during which the number of particles remains constant, and their size distribution narrows[107].

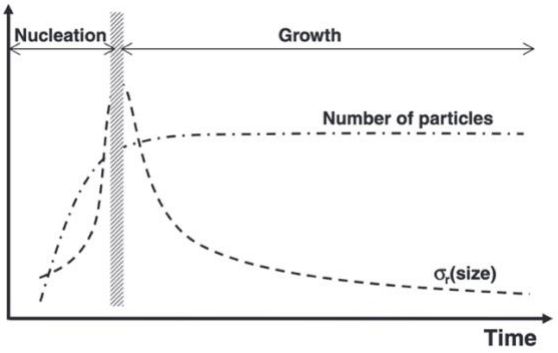

Figure 2.3 - Schematic illustration of the size-distribution control process in the hot injection method[107].

- Hines method

Hines method is the most famous method used for synthesizing PbS QDs. An investigation into how parameters of the synthesis affect the shape of QDs was conducted in this method. In the

Hines method, the synthesis of size-tunable PbS QDs was accomplished utilizing economical and comparatively clean precursors. Lead oleate was used as the lead precursor, and bis(trimethylsilyl)sulfide (TMS) was used as the sulfur source. Moreover, Oleic acid (OA) was used as the stabilizing agent and growth solvent, and Octadecene (ODE) was used as a non-coordinating high-boiling solvent for sulfur precursor. Oleic acid controls particles' nucleation and growth by affecting monomers' reactivity. PbO was first dissolved easily in OA for synthesis, then TMS in ODE was injected into it after heating. When the S precursor was added to the Pb-oleate mixture, the reaction vessel's quick brown colour shift indicated a fast nucleation event. Neither stacking faults nor lattice defects were present in the achieved nanocrystals. The sizes of the QDs achieved by this method were in the range of 2-7 nm[55].

Moreover, this synthesis technique led to the generation of various particle shapes. As soon as sulfur solution was injected into the reaction, particles removed from the reaction appeared to have sharp angles and facets, so they grew along the crystal's favoured orientations. However, the decreasing number of sharp edges on the particles due to increased heating time suggests that extended heating tends to smooth the morphology of the particles[55].

Many other reports follow the Hines method as their reference for synthesizing PbS QDs, mainly with some modification or changes in the precursors, ligands, or solvents. Also, sometimes, they use the same precursors and ligands but change the heating duration and temperature of synthesizing process[108]. Other lead precursors such as lead acetate and lead chloride and other sulfur precursors such as thioacetamide, Na_2S, sulfur powder, and thiourea have been used as precursors for this specific hot injection synthesizing method[109]. In the mentioned Hines method, TMS was used as the sulfur precursor, which is expensive and toxic, has a bad smell, and is a very reactive material. As a result, a glovebox or another vacuum system is needed during the synthesizing process, which makes this process unsuitable for industrial applications. In a recent study, Owen et al. synthesized PbS QDs with tiny diameters and a narrow range of sizes. In their report, they used thiourea as the sulfur source. Due to the toxicity of thiourea, gloveboxes may be necessary during certain steps of the QDs synthesis[110].

The sulfur powder can be used as a substitution for TMS (trimethylsilyl) and thiourea in synthesizing. Sulfur powder is a more environmentally friendly alternative as it does not produce the harmful byproducts that TMS and thiourea can produce during synthesis. Additionally, sulfur

powder is less toxic and has a lower cost than TMS and thiourea, making it a more attractive option for green chemistry applications. Another ligand that can be used in the hot injection synthesizing process (close to the Hines method) is Oleylamine (OLA, $C_{18}H_{35}NH_2$)[111]. Oleylamine is an organic solvent that can act as capping and reducing agents in wet-chemical synthesizing processes. It is composed of a long hydrocarbon chain and one amino group.

Sulfur powder was used instead of TMS in the Hines method by Cademartiri et al. for the first time[112]. In their synthesizing method, lead chloride was used as the lead source and added to Oleylamine to make a suspension. While heating, S precursor in OLA was injected into it. The sizes of the spherical QDs obtained from their synthesis were 2-6 nm by changing the $PbCl_2$:OLA ratio[112]. Figure 2.4 shows the same synthesizing process in another report[113]. Using $PbCl_2$ and S powder as lead and sulfur sources for synthesizing PbS nanocrystals, among other precursors, offers the advantages of using a sustainable and stable S source, involves practical synthetic procedures, and is relatively inexpensive[111].

Moreover, lead oleate or oleic acid lead salt used as a lead precursor in the Hines method can be made with lead acetate in oleic acid (OA) instead of lead oxide in OA. For instance, Deng et al. used lead acetate in OA and n-decane as the lead precursor to synthesize PbS QDs with the hot injection method[109]. Also, in another report, lead oleate was prepared by using lead acetate as a lead source, OA, and hexadecane in a three-neck flask under nitrogen gas, without using air-sensitive compounds throughout the reaction procedure, and then used as a lead precursor for the hot injection synthesis of PbS QDs[114]. Also, in another report, PbS QDs were synthesized with a hot injection method using lead precursor, which was prepared by adding lead oxide or lead acetate trihydrate to OA, a stabilizing agent, and dissolving the mixture in ODE, a non-coordinating solvent, for use in solar cells with high power conversion efficiency. Using lead acetate instead of lead oleate in the PbS synthesizing process can have the beneficiary of using a more stable soluble salt with a lower melting point and better availability[115–117].

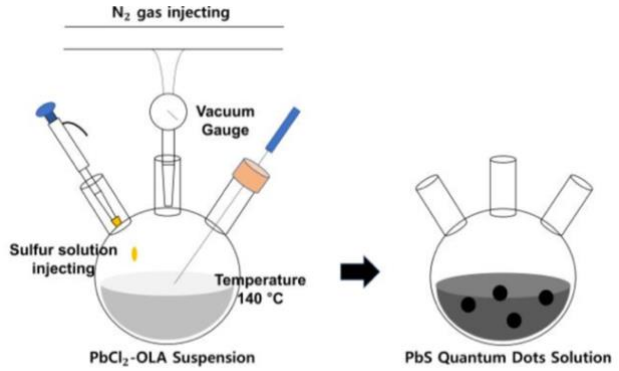

Figure 2.4 - Schematic diagram of PbS QDs synthesizing process[113].

Some of the problems of these synthesis methods (solvothermal and hot injection, for instance) include high reaction temperatures, making them difficult to control and potentially causing damage to the materials being synthesized. Additionally, these methods may need to be better suited for mass production, as they can be time-consuming and require specialized equipment. Additionally, the excessive use of surfactants can be problematic, as they may not be removed entirely from the final product and can affect the properties of the synthesized material[82,118].

2.3.2 Self-assembled thin-film nanostructures

In addition to colloidal NPs and QDs, which can be used for various purposes, self-assembled NPs or QDs thin films have also captured the attention of many researchers over the last decade. They can be used in chemical, biological, electrical, and optical applications[119]. To mention a few applications, the thin films of self-assembled QDs have been used in solar cells, sensors, LEDs, photodetectors, bioimaging, photocatalysis and water splitting[120–124]. Binary and ternary semiconductor QD and NP thin films, including PbS QDs thin films, are among the most prominent examples of self-assembled thin film structures employed in numerous applications[125,126].

An inorganic semiconductor thin film, such as a coating made of PbS QDs, is affected by particle shape, size, and packing. So, the production of NPs and the creation of thin-film structures can significantly affect the characteristics of films. Having mentioned that, it is evident that finding the best fabrication method for making thin films is crucial. Fast, easy, and inexpensive solution-based thin-film deposition approaches have been widely used in various applications[127,128]. Some of these thin film deposition techniques will be discussed thoroughly in section 2.4 of this

thesis. As a whole, PbS QDs and NPs self-assembled thin films can be produced with vast depositing methods. Optoelectronic devices such as photovoltaic cells and photodetectors can be fabricated using PbS thin films since these thin films possess several desirable properties such as direct bandgap and large exciton Bohr radius[129,130].

2.1 Optoelectronic applications of PbS nanoparticles and quantum dots

PbS NPs and QDs can have various applications. Their applications can include optical and electrical applications such as solar cells, LEDs, sensors, and photodetectors. As mentioned earlier, PbS QDs have some amazing features, making them suitable candidates for optoelectronic applications. As mentioned previously, PbS QDs are semiconductors with direct bandgap and a large Bohr radius of 18 nm. Additionally, they have characteristics like multiple carrier production and a high molar extinction coefficient that make them suitable for solar devices[44,44]. Some of the most famous optical applications of PbS QDs and NPs are mentioned below.

2.1.1 Solar cells

Renewable clean energies have been promoted to combat global warming and environmental pollution, especially solar energy. QD-based solar cells with high power conversion efficiency have emerged as one of the most promising candidates for solar cells thanks to their multiple charge carrier generation feature[131,132]. Moreover, the potential of solution-processed photovoltaic solar cells based on colloidal lead chalcogenide QDs is enormous. Among lead chalcogenides, PbS QDs with narrow bandgaps, large Bohr radius, and high absorption coefficients are good candidates for QD solar cells.

In Figs. 2.5(d) and (e) spin-coated PbS layers were used to form colloidal QDs solar cells, showing photovoltaic efficiency of 5.5%[192] and 8%[193]. Also, in another work, shown in Fig. 2.5(f), researchers achieved 10.7% efficiency from a QD solar cell consisting of a layer of PbS QDs, with the help of a self-assembled monolayer (SAM) as a buffer layer between the ZnO layer and PbS QDs layer. The buffer layer had the role of decreasing interface carrier recombination and enhancing electron collection[133].

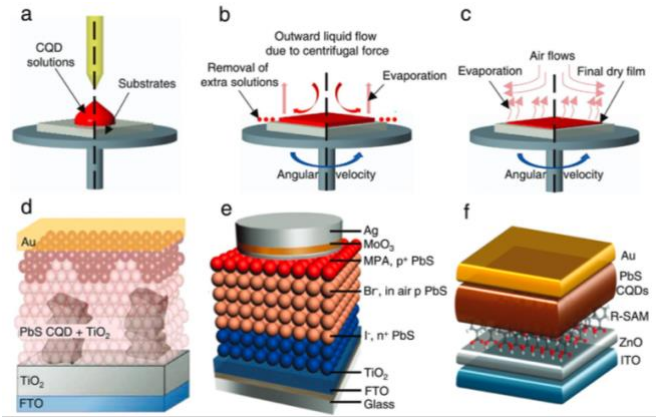

Figure 2.5 - a–c) Schematic illustration of spin coating process showing the different steps involved. d) Schematic drawings of the cross section of depleted bulk heterojunction PbS QD solar cells. e) Schematics of inverted quantum junction PbS QD solar cells with a color gradient indicating the charge depleted portion of the device using mercaptopropionic acid, bromide, and iodide for the solid-state ligand exchange. f) Schematic of a prototypical PbS QD device structure, including a SAM between the ZnO and the PbS CQD film[134].

Blade-coated PbS QDs have also been used in QD solar cells. Blade coating is an inexpensive, simple method for depositing QDs on different substrates and making good quality uniform thin films on a large scale. Blade coating deposition can happen on various substrates with few amounts of waste. More details about the blade coating technique will be mentioned in section 2.4. Solar cells have been fabricated using blade-coated PbS QDs with 10.01% photovoltaic efficiency, a performance comparable to that of solar cells fabricated with spin-coated PbS QDs layer[135]. Also, in another report, Kirmani et al. fabricated QD solar cells with more than 10% efficiency, using blade coated PbS layer, with one oxygen doping step to make PbS layer in ambient conditions regardless of seasonal fluctuations in relative humidity[136]. It is worth mentioning that in solar cells made with blade-coated PbS QDs layer compared to solar cells with spin-coated PbS QDs layer, less amount of solution was used, leading to negligible solution waste, which makes blade coating a more efficient method that might be incorporated in fabricating solar cells based on such materials on an industrial scale[136].

2.1.2 LEDs

LEDs or light-emitting diodes are semiconductor devices that emit light upon current flow through the device. LEDs can be manufactured with various materials, such as different organic and inorganic structures [137]. LEDs manufactured with epitaxy from direct-bandgap semiconductors

are relatively expensive and problematic to integrate with other materials that do not have specific lattice matching. On the contrary, LEDs fabricated with colloidal semiconductor QDs are more economical, solution-processable, and can be directly merged with silicon[138] or any other material. Lead chalcogenides have been used in LEDs, and they possess the highest recorded photoluminescence quantum yield across typical near infrared QDs emitters, with PbS QDs varying between 60% at wavelength of 1 μm and 30% at 1.5 μm[139]. Zhang et al. fabricated an LED device using PbS QDs -silicone nanocomposite that showed good long-term stability[43]. In another work, Sun et al. used spin-coated PbS QDs layers as emitters in the LED structure. They achieved 2.0% external quantum efficiency by controlling the spacing between PbS dots. They adjusted the distance between QDs in the range of 1.3 nm by using linker molecules with three to eight CH_2 groups[140]. Moreover, an LED having a 4.9% power conversion efficiency was achieved by Gong et al. using PbS QDs in a mixed halide perovskite matrix[141].

2.1.3 Sensors and photodetectors

Photodetectors are light-sensitive sensors that convert photon energy into an electrical signal. Utilizing semiconductor materials with strong light extinction coefficients, carriers with high mobility, and the capacity to absorb light in a range where silicon cannot is one way to increase the performance of photodetectors[142,143]. Semiconductor QDs in photodetectors may increase light trapping and strong nonlinear interactions due to their specific characteristics, such as charge carrier confinement and adjustable bandgaps[104,144]. Among different semiconductors, PbS QDs have been used in several photodetectors[145]. Lacovo et al. fabricated PbS QDs photoconductors with high detectivity and responsivity. They used simple, low-cost fabrication and deposition procedures (drop casting) to make PbS photoconductors[46]. In another report, layer-by-layer spray-coated PbS QDs were used to fabricate a photodetector. The whole process of device fabrication, including the spray coating step, is shown in Fig. 2.6. The performance of the aforementioned photodetector device in terms of detectivity and responsiveness was rather good, and it demonstrated exceptional potential for usage in large-scale production[146].

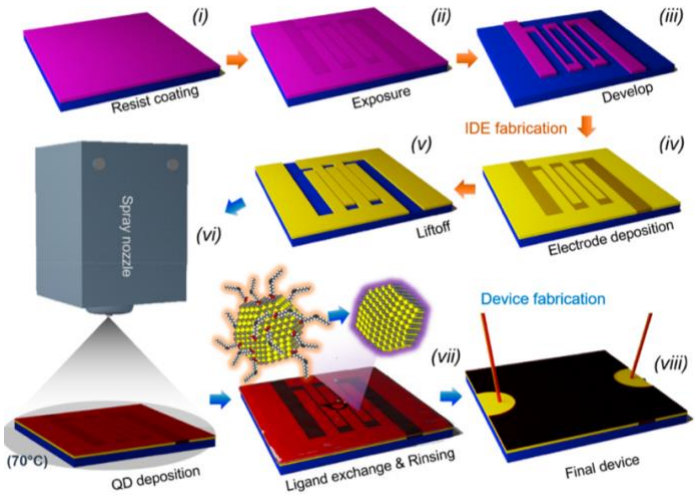

Figure 2.6 - Schematic for the photodetector device fabrication processes, including inter-digitated electrode (IDE) substrate made by a lithography process (i–v), QDs' deposition process via spray coating (vi), ligand exchange treatment process (vii) and final device structure (viii)[146].

2.2 $CuInS_2$ (CIS) nanoparticles and quantum dots

Several studies have been conducted on $CuInS_2$ (CIS) NPs and QDs, ternary structures that are remarkably cheap and have low toxicity. They may be a better alternative for optoelectronic, catalytic, and biological usage than toxic binary structures such as PbS[67,147]. With a direct bandgap of 1.5 eV, CIS exhibits a strong absorption coefficient in the visible and near-infrared regions, matching the spectrum of solar emissions. The three main crystal structures of CIS NPs are shown in Fig. 2.7. Chalcopyrite is the most common CIS structure at ambient temperature. A key characteristic of the chalcopyrite structure of CIS is its ability to tolerate a wide range of anions and cations off stoichiometry, as well as its tunable band gap and photoluminescence. $CuInS_2$ has a tetragonal crystal structure when crystallized as chalcopyrite, composed of two interlocking lattices of sulfur and metal ions. In other words, in the CIS chalcopyrite structure, each S atom is surrounded by two In and two Cu atoms[148].

Two other CIS structures are zincblende and wurtzite. The chalcopyrite is thermodynamically preferred at room temperature, as mentioned above, whereas the zinc-blende and wurtzite structures are stable from 1253 to 1318 K and 1318 K to the CIS melting temperature, which is 1400 K, respectively. At room temperature, the zincblende and wurtzite structures may transform into chalcopyrite. However, zinc-blende and wurtzite structure nanocrystals can be synthesized at a significantly lower temperature due to their reduced surface energy in the nano-scale region[67].

The choice between the three structures depends on the conditions such as temperature, pH value, and growth condition under which CIS is formed. For instance, an active ligand species has been reported to be crucial to forming CIS NPs with wurtzite structures by capturing the metal ions to control the nucleation and growth of the NPs[149].

Various optical and electrical properties can be obtained from CIS QDs/NPs by modifying their crystalline phase [150–152]. Since optoelectronic usage of CIS QDs is the primary appeal of these materials, as far as this thesis is concerned, the discussion below will be confined to highlighting a few advancements in areas such as manufacturing and synthesis of CIS QDs for use in optoelectronic applications.

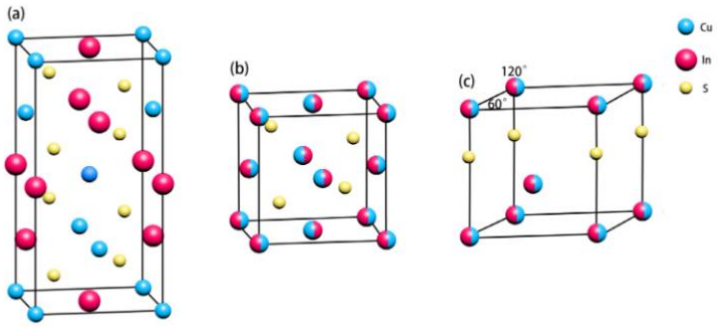

Figure 2.7 - Structure of (a) chalcopyrite, (b) zinc-blende and (c) wurtzite $CuInS_2$[67].

2.2.1 Synthesizing and printing of CIS nanoparticles

$CuInS_2$ NPs and QDs have been synthesized with various methods such as hot injection method similar to PbS QDs, solvothermal methods[76], solid-state reaction[153], microwave irradiation[154], hydrothermal synthesis[155], and thermolysis methods[156]. For example, Yue et al. synthesized 2-4 nm CIS QDs with a solvothermal method for electron acceptors in hybrid solar cells. In their method, 4-bromothiophenol (HSPh) was used as both reducing and capping agents and the precursors contained $CuCl_2$, $InCl_3$ as the copper and indium source, and Na_2S as the sulfur source. In this method, $CuCl_2$ and $InCl_3$ were first dissolved in ethanol, followed by the addition of HSPh solution under stirring. Na_2S in ethanol was then added, and an autoclave was used to heat the resulting solution to facilitate the formation of the QDs. After cooling the autoclave to room temperature, the QDs were obtained by centrifugation of the resulting colloidal solution, followed by multiple washing steps in ethanol and drying under vacuum[75]. In another report,

Wang et al. synthesized chalcopyrite CIS structures with one step hot injection method. In this method, they added two metal precursors, CuI and $In(Ac)_3$, to oleylamine, followed by degassing the mixture to remove oxygen. Afterward, the solution was heated, and a sulfur precursor was rapidly injected. The sulfur precursor contained dissolved sulfur powder in oleylamine, octadecene, or diphenylphosphine. It has been observed that the three sulfur precursor solutions exhibit notably distinct reactivities toward the formation of CIS QDs. The synthesizing process is shown in Fig. 2.8. After adding sulfur solution to Cu and In solution, both Cu^+ and In^{3+} cations react with DPP-S (diphenylphosphine-sulfur) to make Cu-In-(DPP-S)x structure, which will decompose at a specific temperature to make CIS QDs. This approach resulted in the synthesis of high-quality chalcopyrite CIS structures, which were subsequently deposited using drop casting to form QDs solar cells[65].

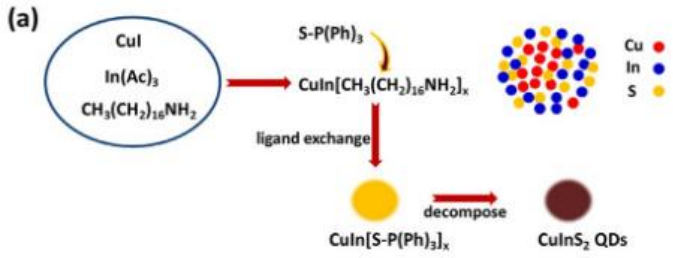

Figure 2.8 - (a) Schematic diagram of the evolution of CIS QDs[65].

Also, Pan et al. synthesized CIS nanocrystals with a hot injection method using Cu(dedc)2 and In(dedc)3 as copper and Indium sources (dedc as diethyl dithiocarbamate), dodecanthiol (DDT) as sulfur source and capping agent, and oleylamine as the activation agent. Oleic acid was also used as a capping agent. By modifying the concentration and type of capping agent, reaction temperature, precursor ratios, and amount of added oleylamine, they could synthesize zinc-blende, and wurtzite CIS structures having an average size of 2 to 30 nm[150]. There are many more examples of chalcopyrite, zinc-blende, and wurtzite CIS structures synthesized with hot injection or solvothermal methods used in solar cells and LEDs. Just as in the PbS case, extra steps were required to produce CIS QDs, including purification, sonication, and long processing and heating times. Moreover, the amount of waste product from this synthesis approach is high. In addition, coating such pre-made QDs into thin films requires extra time consuming steps leading to more cost[156,161].

2.2.2 Optoelectronic applications of CIS quantum dots

CIS QDs synthesized with different methods have been used in optoelectronic applications such as solar cells and LEDs.

2.2.2.1 *Solar cells*

CIS QDs have been used as sensitizers in solar cells[156]. For instance, Peng et al. have used solvothermal synthesized 3.5 nm CIS QDs chemically linked to pentatitanate nanobelt films with the help of a linker molecule. The nanobelts sensitized with CIS QDs were used in a solar cell as a photoanode and showed good photovoltaic conversion good efficiency (about 1.05%)[162].

2.2.2.2 *LEDs*

Due to their vast and colour-tunable emissions, and massive Stokes shifts, $CuInS_2$-based QDs are developing as low-hazard materials alternatives for LED fabrication. Bai et al. fabricated an LED structure using hydroxyl-terminated CIS-based QDs. In their study, the CIS-based QDs were used as an emitter layer. The resulting LEDs showed good luminescence properties and a 3.22% external quantum efficiency. The mentioned CIS QDs were synthesized with the hot injection method prior to LED fabrication[163].

2.3 Thin-film deposition

In recent years, coating and printing techniques have been widely used for thin-film deposition on both large and small scales. There are lots of widespread printing and coating techniques available for depositing thin films of NPs and QDs. Among these techniques, roll-to-roll printing is a desired coating choice. In the roll-to-roll printing technique, a flexible substrate is continuously transferred between huge rollers, and deposition can occur successively to build several films and layers. The outcome is rolls of coated flexible substrates produced in an economical and convenient approach, compared to conventional coating methods such as drop and dip coating. Many manufacturing industries, including IT, electronics and computers, energy, textiles, medicine, metal products, and life science, to mention a few, use the roll-to-roll deposition technique. Finding a convenient QDs and/or NPs thin film deposition technology compatible with the roll-to-roll process would be an ideal choice for industrial mass production in various technological fields, including displays, solar cells, medicine delivery, etc. [164]. Here, we will describe some popular printing and coating methods that can be used to fabricate NPs- and QDs-based thin films.

2.3.1 Printing techniques

In printing, a shape or pattern is directly transferred on a substrate during deposition. So in this process, deposition and patterning are happening at the same time. Some famous printing methods compatible with the roll-to-roll process are gravure printing, flexographic printing, screen printing, and inkjet printing. The mentioned printing methods have been widely used for printing different NPs and QDs. The gravure printing process, also called rotogravure printing, is a high-quality, high-speed, long-run printing process mainly used for producing large volumes of magazines and newspapers. In this printing method, the ink is transferred to the substrate's surface by rotating engraved cylinders[165]. NPs have been printed using gravure printing on flexible substrates for electrochemical sensors[166]. A simple schematic of the gravure printing technique is shown in Fig. 2.9[167].

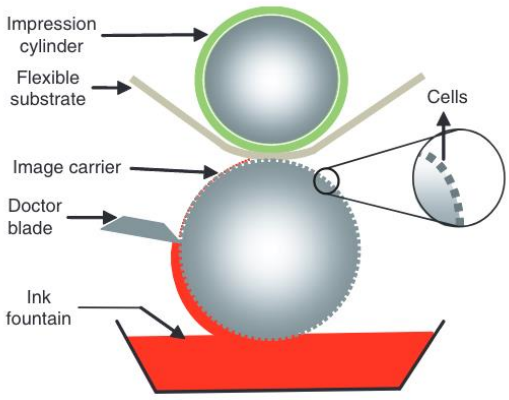

Figure 2.9 - Structure of Gravure printing technique[167].

Flexographic printing is another printing technique that is somehow related to the gravure printing technique. Flexographic printing or flexo printing is a relief printing technique in which ink is transferred from a raised printing plate cylinder to the surface of the substrate using quick-drying inks. This printing technique is faster than gravure printing and can be used to print on various substrates such as paper and plastic, but sometimes the film quality is much better in gravure printing[168]. Different NPs, such as ZnO and In_2O_3, have been printed by flexo-printing to be used in sensors and transistors[169,170].

Screen printing is another method to produce a printed design by forcing ink through a stencil formed on a mesh screen. Screen printing can be performed on flat or curved surfaces made up of

paper, fabric, plastic, ceramic, and metal[171]. This technique has been used to print organic and inorganic NPs for stretchable electronics, sensors, and electrochemical applications[172–174]. Figure 2.10 shows a schematic of the materials available for preparing printable ink for screen printing of stretchable electronics[175].

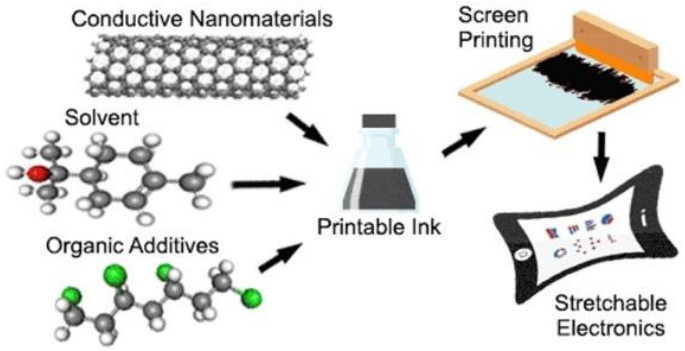

Figure 2.10 - Schematic of materials used to prepare a printable ink for screen printing[175].

In all the mentioned printing techniques, the substrate briefly comes into contact with some elements of the printing process[176]. Among the noncontact printing approaches, inkjet printing is the most popular due to its simplicity. In such technique, the ink is forced into a nozzle forming a droplet that is ejected onto a substrate. No physical contact between the printing head and the substrate occurs during this process. Ink viscosity and concentration of particles, velocity of the ink droplet, ink surface tension and the wettability on a given surface are some significant factors in the inkjet printing process[177].

In the inkjet printing process, dimensionless fluid mechanics quantities such as the Reynolds number, Weber number, and Ohnesorge number must fall within an acceptable range for it to be successful[177,178]. In materials and device research, various types of inks have been used in inkjet printing, including semiconductor NPs, metal NPs, conducting polymers, and metal-organic hybrids in flexible electronics, sensors, light-emitting diodes, and solar cells[179,180]. There are two modes for inkjet printing technique. One is drop-on-demand inkjet printing, and the other is continuous inkjet printing, as shown in Fig. 2.11[181]. Also, inkjet printers may use piezoelectric or thermal printheads to form and eject the ink droplets. Drop-on-demand inkjet printing has been used to fabricate PbS directly on papers at room temperature[182]. Also, inkjet-printed PbS NPs have been used in fully printed low-cost photodetectors[183].

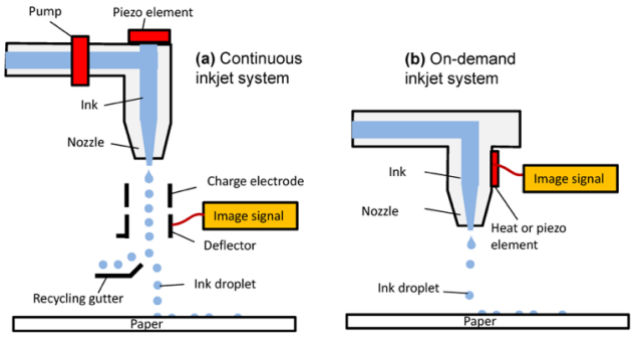

Figure 2.11 - Schematic showing a. continuous inkjet printing, b. drop on demand inkjet printing[184].

2.3.2 Coating techniques

Many coating techniques have been used for depositing QDs and NPs on top of different substrates. Some of the most well-known coating methods, such as spin, spray, dip, drop, and blade coating, are mentioned below. These techniques have varying precision, cost, and scalability levels, making it essential to select the most appropriate technique for a specific application.

2.3.2.1 *Spin coating*

Spin coating is a method that uses centrifugal force to distribute a given liquid into thin films on a given flat substrate. In this coating method, a rigid substrate is spun quickly after having the liquid dropped onto it. Rotation is carried out until the excess solution spins off the substrate and the required film thickness is left behind. The factors which can affect the film's thickness and the final quality are surface wettability, solutions' viscosity, spin duration, density of the solution, spin rate, and solvent evaporation rate. Spin coating often necessitates drying or heating, regardless of the deposited medium. This coating technique is a typical technique for deposition of polymers, NPs, QDs, and biomaterials[185]. The schematic of the spin coating process is shown in Fig. 2.12.

Incidentally, Fig. 2.5(a-c) shows the process of spin coating of PbS QDs, in which the obtained thin film was used as the absorber layer of a solar cell. The electron and hole transport layers were made with spin coating in the quantum dot solar cell. The steps of spin coating of PbS QDs shown are: liquid disposing, spin-up, liquid outflow, spin-off, and evaporation and drying[134]. In another report, spin-coated CIS QDs were fabricated to be used in photovoltaic (PV) cells. In such report, P3HT: PCBM, a copolymer, was blended with CIS QDs to result in hybrid PV cells with increased quantum efficiency[186].

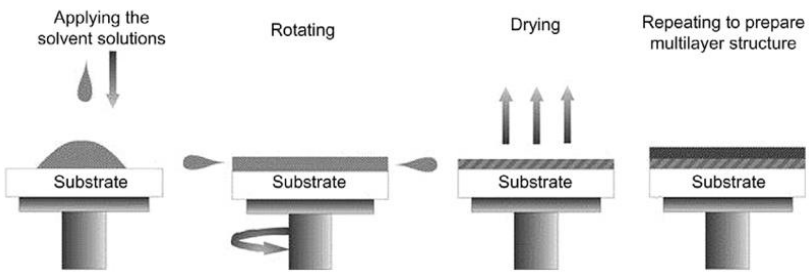

Figure 2.12 - Schematic diagram of the spin-coating method[187].

2.3.2.2 *Spray coating*

In the spray coating process, the substrate is coated by a device containing a nozzle that sprays liquid base material above the surface of the substrate. The liquid is atomized at the spray front head's nozzle, generating a steady stream of spray droplets. The droplets are generated by pressurized gas, air, or an ultrasonic system. The parameters affecting the final quality of the thin film and the coating efficiency include substrate surface characteristics such as surface tension and viscosity, coating velocity, droplet size distribution, distance between spray nozzles (and between nozzles and substrate), wetting mechanism and gas flow[188]. Figure 2.13 illustrates a schematic representation of the spray coating process at two different times of the spray pass, one at the beginning of the spray coating process and one close to the end of the process. Fig. 2.6(vi) shows the photodetector device fabrication process, in which the QD layer containing PbS QDS was obtained by the spray coating method driven by high-pressure N_2 pulses[146].

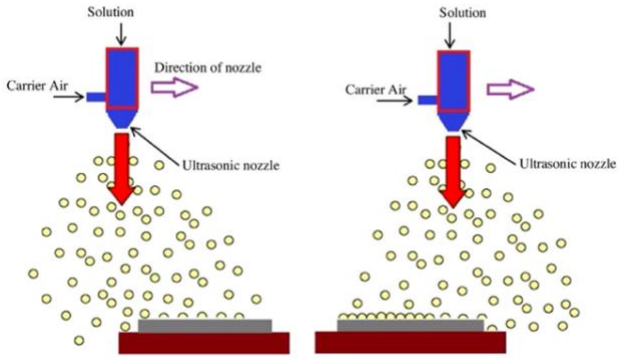

Figure 2.13 - Schematic diagram of the spray coating process, shown at two different times of a spray pass[189].

2.3.2.3 *Chemical bath deposition*

Chemical bath deposition is a popular technique for coating NPs on top of different substrates. In this technique, a reactive solution containing the precursors is prepared. Then the clean substrate was vertically immersed in the heated solution. In this deposition method, solid thin films of materials are formed from solution via nucleation and particle growth. The nucleus refers to the minimal number of ions or molecules required for any precipitate to form a stable phase in contact with a solution. After the nucleus formation, the precipitation and combination of particles continue to make a thin film. Film growth can occur either by ion-by-ion condensing of the components on the surface of the substrates or by deposition of colloidal particles from the solution on the substrate, depending on the deposition conditions. Different substrates, such as semiconductors, insulators, and metals, can be used in this deposition technique, as the deposition method is being processed at low temperatures[190]. The experimental setup of the chemical bath deposition technique is shown in Fig. 2.14[191]. Factors that affect thin film formation include stirring speed, solution bath temperature, solution concentration, and the PH of the solution[192]. It has been demonstrated that PbS and CIS QDs, and NPs, can be deposited on various substrates using this coating method [193–196].

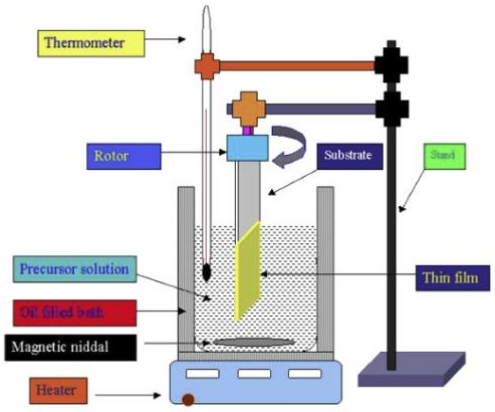

Figure 2.14 - Setup of chemical bath deposition technique[191].

2.3.2.4 *Dip coating*

A Schematic of a dip coating method is shown in Fig. 2.15. The sample is immersed in a nanoparticle-containing solution in this coating method in the first step. Then, the sample is left in the solution for a sufficient time for NPs to deposit. The solution wets the substrate's two surfaces

during immersion. Then after giving the sample a reasonable period of immersion, the sample is withdrawn from the solution, and a wet film is achieved. The evaporation process starts after the wet film is removed and starts to dry. A couple of factors will affect the dip coating process and the film's final quality, such as time spent immersed, liquid viscosity, evaporation duration, and speed of substrate removal[197]. Solar cells incorporating QDs have been fabricated by depositing PbS and CIS QDs onto substrates with dip coating techniques [198,199].

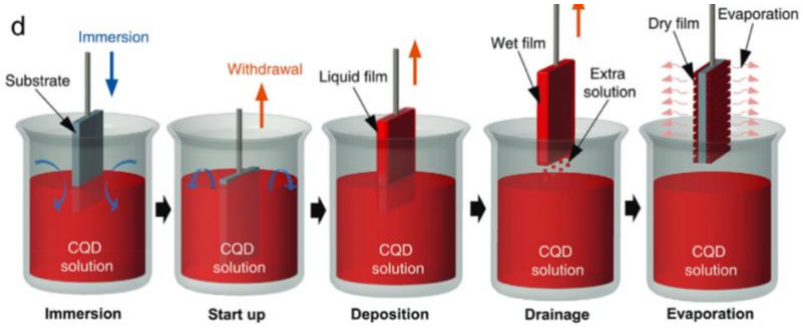

Figure 2.15 - d) Schematic illustration of the dip coating process[134].

2.3.2.5 *Drop coating*

The simplest and most straightforward NP deposition technique is drop coating. According to this method, as seen in Fig. 2.16(a), a drop of a QDs or NPs solution is dropped directly onto the substrate, and the solvent is then allowed to evaporate completely, froming a thin film of QDs or NPs. The resulting thin films are affected by several factors, such as solvent evaporation rate, solvent viscosity, diffusion of the droplet, etc.[200]. Figure 2.16 shows a drop coating technique for depositing PbS QDs on a substrate for use in QDs solar cells (QDSC).[201]. CIS QDs were dropped casted on TiO_2 substrate resulting in highly efficient solar cells[65].

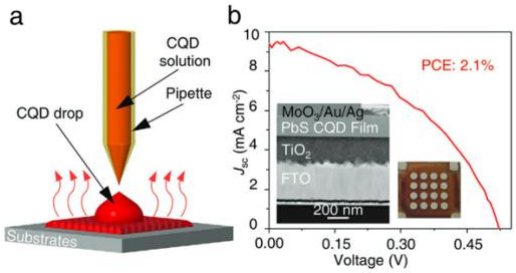

Figure 2.16 - a) Schematic of the drop coating process. b) J–V curves of the PbS QDSC fabricated by single-layer drop coating, leading to a PCE of 2.1%. Insets are a cross-sectional TEM image of the device structure and a photograph of a drop-coated QDSC[134,201].

2.3.2.6 Blade coating

Blade coating or doctor blade coating technique, also known as knife coating, produces thin films with precise thicknesses. This coating technique is closely connected to industrial processes such as roll-to-roll printing. It has been employed in the large-scale production of thin films and in different applications such as printing procedures, textiles, and ceramic industries[202–204]. Blade coating involves spreading the solution over the surface of a substrate using a blade and making a homogeneous thin film. The blade-to-substrate distance, blade velocity, angle between the blade and substrate, surface wettability, and solution characteristics such as solution viscosity, solution concentration, and evaporation rate of the solution can control the thickness and quality of the final achieved thin film[205,206].

Another important factor is surface wettability. The surface wettability of a substrate can be improved by using cleaning processes such as UV-ozone and plasma before the coating process. By using these cleaning procedures, a significant portion of the contaminants on top of the surfaces of the substrates will be removed, resulting in increased surface wettability[207,208].

Another way to change the wettability of the surface is silanization, which is the process of using a silane solution to functionalize and improve the wettability of the silicon substrate. Surface modification through silanization is focused on producing a silyl ether; hence, the free hydroxy groups can be recovered by cleaving this silicon–oxygen link to alter the surface chemistry and wettability[209]. The silanazation process or the mentioned cleaning processes can be performed on the substrate surface, to improve the surface's wettability before the blade coating process begins.

In blade coating, unlike spin coating, the low boiling point solvent is not needed in blade coating, the area may be expanded with relative ease, and nearly all of the material is utilized with no considerable waste[210]. Additionally, this deposition technique can be used for single or multilayer coatings, and single and multiple layers can be deposited without a buffer solution[211]. Moreover, the blade-coating technique, hugely noteworthy in industrial manufacturing, can deliver faster processing than other fluid processing methods like spray coating and inkjet printing[208,212].

Blade-coating is a straightforward, cost-effective, and roll-to-roll compatible method for fabricating layers necessary for optoelectronic devices. With the blade coating technique, different types of solar cells, such as perovskite solar cells and various light-emitting diodes (LEDs), including organic light-emitting diodes (OLEDs), can be manufactured[213–215]. The schematic of a fully printable perovskite solar cell structure and the blade coating equipment used for printing the solar cell is shown in Fig. 2.17. In this solar cell, all layers, except the Ag top electrodes, were prepared using blade-coating method [213].

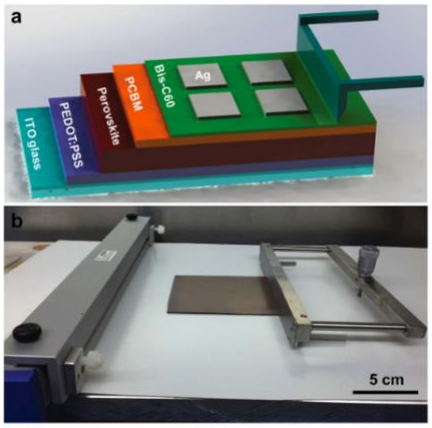

Figure 2.17 - a) Schematic illustration of a fully printable perovskite solar cell. b) Blade-coating equipment with as-prepared 10 cm × 10 cm perovskite film[213].

Blade coating has also been used for depositing the PbS passive ink on a substrate to be used in QD solar cells. Figure 2.18 shows the blade-coating process of PbS ink and pictures of its blade-coated films. As can be seen in the Figure, good-quality PbS thin films were achieved at comparatively low temperatures. The PbS ink was prepared before the blade coating process by the hot injection method[38].

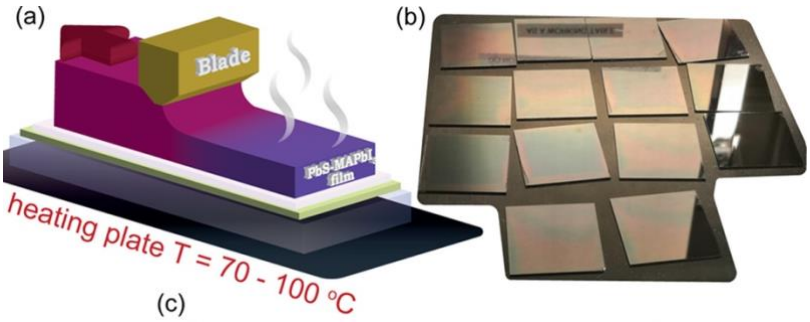

Figure 2.18 - Blade-coated films of PbS-$MAPbI_3$ (capping ligand) inks from DFP. (a) Scheme of the blade-coating process. (b) Photograph of the blade-coated films from PbS-MAPbI3 inks on 3 × 3cm^2 substrates[38].

Ink of PbS colloidal QDs was deposited on silicon substrates to make transistors. In this case, the hot injection method was used to prepare the PbS colloidal ink before the blade coating step[216]. Moreover, ball-milled synthesized CIS QDs have been blade-coated on TiO_2 substrates to be used in solar cells. The cell efficiency achieved from the mentioned solar cell device was 2.01% [217]. Altaf et al. also have blade-coated CIS ink, prepared with hot injection method, on a Fluorine-doped Tin Oxide (FTO) substrate to be used as photoanodes in photoelectrochemical water-splitting devices. In the mentioned report, different crystal structures of CIS were synthesized, and chalcopyrite CIS thin film showed the best photoelectrochemical performance compared to other CIS crystal structures[70].

2.3.3 Printing approach to the *in-situ* synthesis of nanoparticles and quantum dots

Traditionally, thin films of QDs were achieved using a colloidal solution containing presynthesized QDs (e.g., PbS and CIS QDs)[55,150]. However, one cannot self-assemble QDs or NPs on demand and at selected locations over a given surface or inside nanopores using such approach.

To mitigate this, there are some synthesizing techniques called in-situ reactive methods, in which synthesizing and depositing NPs and QDs on substrates happen simultaneously. An example of in-situ reactive deposition is the reactive inkjet printing of gold NPs by Jabbour's group[118]. Based on their work, in the in-situ reactive inkjet printing process of gold NPs, two inks were used: the gold precursor ink and the reducer ink. In the mentioned process, NPs production, thin film formation, and patterning all occur at predetermined locations throughout the surface of the substrate in response to application demand. An added advantage of this approach is the reduction of waste products, energy use, and fabrication[141].

A schematic of the whole in-situ reactive inkjet printing technique used for acquiring gold NPs is shown in Fig. 2.19. According to the Figure, gold NPs were produced by injecting cartridge A with a solvent combination including a capping/reducing agent and a dispersion solvent which contained 1 mL OLA in 10 mL 1,2-dichlorobenzene. Also, cartridge B was injected with gold (III) chloride trihydrate ($HAuCl_4.3H_2O$) in 10 mL dimethyl sulfoxide as gold precursor ink. Cartridge A prints the ink on a clean silicon substrate to begin the synthesis, followed by cartridge B, printing on top of the former droplets using the same printing conditions at ambient temperature. The printed substrate is then heated in an oven at 120 °C for three hours, creating Au NPs on the surface of the substrate[118].

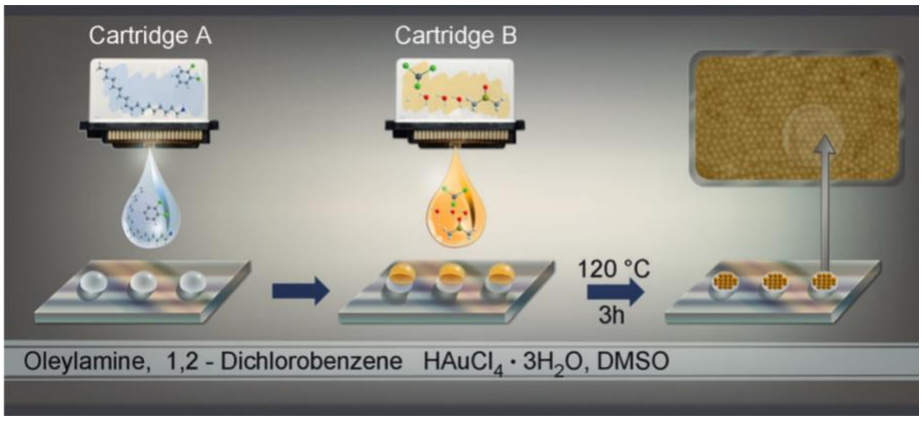

Figure 2.19 - A schematic description of the in situ synthesis of self-assembled Au NPs through reactive inkjet printing[118].

Although inkjet printing has clear benefits, it has some limitations, such as expensive cartridges with a high potential to clog over time, which can increase the price of final products. Moreover, inkjet is rather a slow process compared to blade coating in the fabrication of thin films! Jabbour's group extended the reactive in-situ self-assembly approach of NPs to blade coating. In this case, silver NPs have been synthesized and deposited simultaneously on a glass substrate, fabric, and surgical mask with an in-situ reactive blade coating method. The resulting structures were used successfully for disinfection against SARS-CoV-2 [82]. Compared to in-situ reactive inkjet printing, in situ reactive blade coating method is a quicker and more economically viable reactive printing process that can meet the demands of low-cost and widespread NPs and QDs use[82].

Figure 2.20 shows the in-situ reactive blade coating process of silver NPs on top of a surgical mask. In-situ reactive blade coating is useful for impregnating porous and fibrous surfaces with

Ag NPs, since the starting inks are molecular and have a greater potential to penetrate sub-nanometer voids than pre-prepared NPs. To immunize commercial fabrics and face masks against SARS-CoV-2, the reducer ink (Fig. 2.20(A)) was blade-coated on a single-use face mask, and then silver precursor ink was coated on top of the reducer ink (Fig. 2.20(B)). The substrates were then placed in an oven and heated at 120 °C for two hours, and silver NPs were formed on the surface of the mask[82].

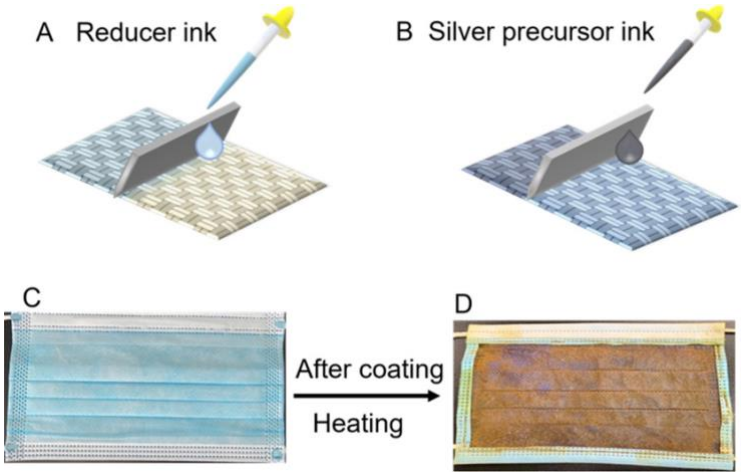

Figure 2.20 - In situ fabrication process of a Ag nanoparticle-impregnated face mask. (A) Coating of the oleylamine-based reducer ink followed by (B) adding the silver precursor ink on top of the previously coated reducer ink. The surface texture of the face mask before (C) and after (D) in situ fabrication of Ag NPs via in-situ reactive blade coating[82].

2.4 References

[1] Schmid G 2010 *Nanoparticles: from theory to application* (Weinheim, Germany: Wiley-VCH)

[2] Jr C P P and Owens F J 2003 *Introduction to Nanotechnology* (John Wiley & Sons)

[3] McNamara K and Tofail S A M 2017 Nanoparticles in biomedical applications *Advances in Physics: X* **2** 54–88

[4] Tanabe K 2007 Optical radiation efficiencies of metal nanoparticles for optoelectronic applications *Materials Letters* **61** 4573–5

[5] Stark W J, Stoessel P R, Wohlleben W and Hafner A 2015 Industrial applications of nanoparticles *Chem. Soc. Rev.* **44** 5793–805

[6] Beydoun D, Amal R, Low G and McEvoy S Role of Nanoparticles in Photocatalysis

[7] De M, Ghosh P S and Rotello V M 2008 Applications of Nanoparticles in Biology *Advanced Materials* **20** 4225–41

[8] Bundschuh M, Filser J, Lüderwald S, McKee M S, Metreveli G, Schaumann G E, Schulz R and Wagner S 2018 Nanoparticles in the environment: where do we come from, where do we go to? *Environ Sci Eur* **30** 6

[9] Biswas P and Wu C-Y 2005 Nanoparticles and the Environment *Journal of the Air & Waste Management Association* **55** 708–46

[10] Klimov V I 2017 *Nanocrystal Quantum Dots* (CRC Press)

[11] Masumoto Y and Takagahara T 2013 *Semiconductor Quantum Dots: Physics, Spectroscopy and Applications* (Springer Science & Business Media)

[12] B nyai L and Koch S W 1993 *Semiconductor Quantum Dots* (World Scientific)

[13] García de Arquer F P, Talapin D V, Klimov V I, Arakawa Y, Bayer M and Sargent E H 2021 Semiconductor quantum dots: Technological progress and future challenges *Science* **373** eaaz8541

[14] Coe-Sullivan S 2009 Quantum dot developments *Nature Photon* **3** 315–6

[15] Bukowski T J and Simmons J H 2002 Quantum Dot Research: Current State and Future Prospects *Critical Reviews in Solid State and Materials Sciences* **27** 119–42

[16] Jamieson T, Bakhshi R, Petrova D, Pocock R, Imani M and Seifalian A M 2007 Biological applications of quantum dots *Biomaterials* **28** 4717–32

[17] Reshma V G and Mohanan P V 2019 Quantum dots: Applications and safety consequences *Journal of Luminescence* **205** 287–98

[18] Chow W W and Jahnke F 2013 On the physics of semiconductor quantum dots for applications in lasers and quantum optics *Progress in Quantum Electronics* **37** 109–84

[19] Routzahn A L, White S L, Fong L-K and Jain P K 2012 Plasmonics with Doped Quantum Dots *Isr. J. Chem.* **52** 983–91

[20] Wu J, Chen S, Seeds A and Liu H 2015 Quantum dot optoelectronic devices: lasers, photodetectors and solar cells *J. Phys. D: Appl. Phys.* **48** 363001

[21] Konstantatos G and Sargent E H 2013 *Colloidal Quantum Dot Optoelectronics and Photovoltaics* (Cambridge University Press)

[22] Yuan T, Meng T, He P, Shi Y, Li Y, Li X, Fan L and Yang S 2019 Carbon quantum dots: an emerging material for optoelectronic applications *J. Mater. Chem. C* **7** 6820–35

[23] Gil H M, Price T W, Chelani K, Bouillard J-S G, Calaminus S D J and Stasiuk G J 2021 NIR-quantum dots in biomedical imaging and their future *iScience* **24** 102189

[24] Jorge P, Martins M, Trindade T, Santos J and Farahi F 2007 Optical Fiber Sensing Using Quantum Dots *Sensors* **7** 3489–534

[25] Agarwal T 2014 Optoelectronics Devices with their Applications *ElProCus - Electronic Projects for Engineering Students*

[26] Huwer J, Stevenson R M, Skiba-Szymanska J, Ward M B, Shields A J, Felle M, Farrer I, Ritchie D A and Penty R V 2017 Quantum-Dot-Based Telecommunication-Wavelength Quantum Relay *Phys. Rev. Applied* **8** 024007

[27] Azzazy H M E, Mansour M M H and Kazmierczak S C 2007 From diagnostics to therapy: Prospects of quantum dots *Clinical Biochemistry* **40** 917–27

[28] Shuklov I A and Razumov V F 2020 Lead chalcogenide quantum dots for photoelectric devices *Russ. Chem. Rev.* **89** 379–91

[29] Shrestha A, Batmunkh M, Tricoli A, Qiao S Z and Dai S 2019 Near-Infrared Active Lead Chalcogenide Quantum Dots: Preparation, Post-Synthesis Ligand Exchange, and Applications in Solar Cells *Angew. Chem. Int. Ed.* **58** 5202–24

[30] Hu J, Shi Y, Zhang Z, Zhi R, Yang S and Zou B 2019 Recent progress of infrared photodetectors based on lead chalcogenide colloidal quantum dots *Chinese Phys. B* **28** 020701

[31] Liu C and Heo J 2013 Lead Chalcogenide Quantum Dot-Doped Glasses for Photonic Devices *Int J Appl Glass Sci* **4** 163–73

[32] Moreels I, Justo Y, De Geyter B, Haustraete K, Martins J C and Hens Z 2011 Size-Tunable, Bright, and Stable PbS Quantum Dots: A Surface Chemistry Study *ACS Nano* **5** 2004–12

[33] McDonald S A, Konstantatos G, Zhang S, Cyr P W, Klem E J D, Levina L and Sargent E H 2005 Solution-processed PbS quantum dot infrared photodetectors and photovoltaics *Nature Materials* **4** 138–42

[34] Cao Y, Stavrinadis A, Lasanta T, So D and Konstantatos G 2016 The role of surface passivation for efficient and photostable PbS quantum dot solar cells *Nat Energy* **1** 1–6

[35] Lee S-M, Jun Y, Cho S-N and Cheon J 2002 Single-Crystalline Star-Shaped Nanocrystals and Their Evolution: Programming the Geometry of Nano-Building Blocks *J. Am. Chem. Soc.* **124** 11244–5

[36] Clark S W, Harbold J M and Wise F W 2007 Resonant Energy Transfer in PbS Quantum Dots *J. Phys. Chem. C* **111** 7302–5

[37] Kim D, Kim D-H, Lee J-H and Grossman J C 2013 Impact of Stoichiometry on the Electronic Structure of PbS Quantum Dots *Phys. Rev. Lett.* **110** 196802

[38] Sukharevska N, Bederak D, Goossens V M, Momand J, Duim H, Dirin D N, Kovalenko M V, Kooi B J and Loi M A 2021 Scalable PbS Quantum Dot Solar Cell Production by Blade Coating from Stable Inks *ACS Appl. Mater. Interfaces* **13** 5195–207

[39] Dai Q, Wang Y, Zhang Y, Li X, Li R, Zou B, Seo J, Wang Y, Liu M and Yu W W 2009 Stability Study of PbSe Semiconductor Nanocrystals over Concentration, Size, Atmosphere, and Light Exposure *Langmuir* **25** 12320–4

[40] Antu A D, Jiang Z, Premathilka S M, Tang Y, Hu J, Roy A and Sun L 2018 Bright Colloidal PbS Nanoribbons *Chem. Mater.* **30** 3697–703

[41] Greben M, Fucikova A and Valenta J 2015 Photoluminescence quantum yield of PbS nanocrystals in colloidal suspensions *Journal of Applied Physics* **117** 144306

[42] Xue Y, Yang F, Yuan J, Zhang Y, Gu M, Xu Y, Ling X, Wang Y, Li F, Zhai T, Li J, Cui C, Chen Y and Ma W 2019 Toward Scalable PbS Quantum Dot Solar Cells Using a Tailored Polymeric Hole Conductor *ACS Energy Lett.* **4** 2850–8

[43] Zhang X, Chen Y, Lian L, Zhang Z, Liu Y, Song L, Geng C, Zhang J and Xu S 2021 Stability enhancement of PbS quantum dots by site-selective surface passivation for near-infrared LED application *Nano Res.* **14** 628–34

[44] Ankah G N, Büchele P, Poulsen K, Rauch T, Tedde S F, Gimmler C, Schmidt O and Kraus T 2016 PbS quantum dot based hybrid-organic photodetectors for X-ray sensing *Organic Electronics* **33** 201–6

[45] Sun X, Dai R, Chen J, Zhou W, Wang T, Kost A R, Tsung C-K (Frank) and An Z 2014 Enhanced thermal stability of oleic-acid-capped PbS quantum dot optical fiber amplifier *Opt. Express, OE* **22** 519–24

[46] De Iacovo A, Venettacci C, Colace L, Scopa L and Foglia S 2016 PbS Colloidal Quantum Dot Photodetectors operating in the near infrared *Sci Rep* **6** 37913

[47] Zhang J-Y, Xu J-L, Chen T, Gao X and Wang S-D 2019 Toward Broadband Imaging: Surface-Engineered PbS Quantum Dot/Perovskite Composite Integrated Ultrasensitive Photodetectors *ACS Appl. Mater. Interfaces* **11** 44430–7

[48] Xin X, Zhang Y, Guan X, Cao J, Li W, Long X and Tan X 2019 Enhanced Performances of PbS Quantum-Dots-Modified MoS2 Composite for NO2 Detection at Room Temperature *ACS Appl. Mater. Interfaces* **11** 9438–47

[49] Shen K, Baig S, Jiang G, Paik Y, Kim S J and Wang M R 2017 Improved light emitting UV curable PbS quantum dots-polymer composite optical waveguides *Optics Communications* **402** 606–11

[50] Shi X-F, Xia X-Y, Cui G-W, Deng N, Zhao Y-Q, Zhuo L-H and Tang B 2015 Multiple exciton generation application of PbS quantum dots in ZnO@PbS/graphene oxide for enhanced photocatalytic activity *Applied Catalysis B: Environmental* **163** 123–8

[51] Mughal F, Muhyuddin M, Rashid M, Ahmed T, Akram M A and Basit M A 2019 Multiple energy applications of quantum-dot sensitized TiO2/PbS/CdS and TiO2/CdS/PbS hierarchical nanocomposites synthesized via p-SILAR technique *Chemical Physics Letters* **717** 69–76

[52] Sarma S, Datta P, Barua K Kr and Karmakar S 2009 Synthesis, Characterization and Application Of PbS Quantum Dots *AIP Conference Proceedings* **1147** 436–42

[53] Anon Significantly enhanced energy conversion efficiency of CuInS2 quantum dot sensitized solar cells by controlling surface defects | Elsevier Enhanced Reader

[54] Wang J S, Ullrich B, Brown G J and Wai C M 2013 Morphology and energy transfer in PbS quantum dot arrays formed with supercritical fluid deposition *Materials Chemistry and Physics* **141** 195–202

[55] Hines M A and Scholes G D 2003 Colloidal PbS Nanocrystals with Size-Tunable Near-Infrared Emission: Observation of Post-Synthesis Self-Narrowing of the Particle Size Distribution *Advanced Materials* **15** 1844–9

[56] Kim J Y, Voznyy O, Zhitomirsky D and Sargent E H 2013 25th Anniversary Article: Colloidal Quantum Dot Materials and Devices: A Quarter-Century of Advances *Adv. Mater.* **25** 4986–5010

[57] McMillan R A, Paavola C D, Howard J, Chan S L, Zaluzec N J and Trent J D 2002 Ordered nanoparticle arrays formed on engineered chaperonin protein templates *Nature Mater* **1** 247–52

[58] Zhao N, Osedach T P, Chang L-Y, Geyer S M, Wanger D, Binda M T, Arango A C, Bawendi M G and Bulovic V 2010 Colloidal PbS Quantum Dot Solar Cells with High Fill Factor *ACS Nano* **4** 3743–52

[59] Ayoubi M, Naserzadeh P, Hashemi M T, Reza Rostami M, Tamjid E, Tavakoli M M and Simchi A 2017 Biochemical mechanisms of dose-dependent cytotoxicity and ROS-mediated apoptosis induced by lead sulfide/graphene oxide quantum dots for potential bioimaging applications *Sci Rep* **7** 12896

[60] Zamani H, Moradshahi A, Jahromi H D and Sheikhi M H 2014 Influence of PbS nanoparticle polymer coating on their aggregation behavior and toxicity to the green algae Dunaliella salina *Aquatic Toxicology* **154** 176–83

[61] Chen J, Kong Y, Wang W, Fang H, Wo Y, Zhou D, Wu Z, Li Y and Chen S 2016 Direct water-phase synthesis of lead sulfide quantum dots encapsulated by β-lactoglobulin for in vivo second near infrared window imaging with reduced toxicity *Chem. Commun.* **52** 4025–8

[62] Pons T, Pic E, Lequeux N, Cassette E, Bezdetnaya L, Guillemin F, Marchal F and Dubertret B 2010 Cadmium-Free $CuInS_2$/ZnS Quantum Dots for Sentinel Lymph Node Imaging with Reduced Toxicity *ACS Nano* **4** 2531–8

[63] Fuhr A S, Yun H J, Makarov N S, Li H, McDaniel H and Klimov V I 2017 Light Emission Mechanisms in $CuInS_2$ Quantum Dots Evaluated by Spectral Electrochemistry *ACS Photonics* **4** 2425–35

[64] Nose K, Soma Y, Omata T and Otsuka-Yao-Matsuo S 2009 Synthesis of Ternary $CuInS_2$ Nanocrystals; Phase Determination by Complex Ligand Species *Chem. Mater.* **21** 2607–13

[65] Wang G, Wei H, Shi J, Xu Y, Wu H, Luo Y, Li D and Meng Q 2017 Significantly enhanced energy conversion efficiency of CuInS2 quantum dot sensitized solar cells by controlling surface defects *Nano Energy* **35** 17–25

[66] Fitzmorris R C, Oleksak R P, Zhou Z, Mangum B D, Kurtin J N and Herman G S 2015 Structural and optical characterization of CuInS2 quantum dots synthesized by microwave-assisted continuous flow methods *J Nanopart Res* **17** 319

[67] Liu L, Li H, Liu Z and Xie Y-H 2018 Structure and band gap tunable CuInS2 nanocrystal synthesized by hot-injection method with altering the dose of oleylamine *Materials & Design* **149** 145–52

[68] Qi Y, Liu Q, Tang K, Liang Z, Ren Z and Liu X 2009 Synthesis and Characterization of Nanostructured Wurtzite $CuInS_2$: A New Cation Disordered Polymorph of $CuInS_2$ *J. Phys. Chem. C* **113** 3939–44

[69] Ming S-K, Taylor R A, McNaughter P D, Lewis D J, Leontiadou M A and O'Brien P 2021 Tunable structural and optical properties of CuInS 2 colloidal quantum dots as photovoltaic absorbers *RSC Adv.* **11** 21351–8

[70] Tuc Altaf Ç and Demirci Sankir N 2019 Colloidal synthesis of CuInS2 nanoparticles: Crystal phase design and thin film fabrication for photoelectrochemical solar cells *International Journal of Hydrogen Energy* **44** 18712–23

[71] Gong F, Tian S, Liu B, Xiong D and Zhao X 2014 Oleic acid assisted formation mechanism of CuInS 2 nanocrystals with tunable structures *RSC Adv.* **4** 36875–81

[72] Omata T, Nose K, Kurimoto K and Kita M 2014 Electronic transition responsible for size-dependent photoluminescence of colloidal CuInS 2 quantum dots *J. Mater. Chem. C* **2** 6867

[73] McDaniel H, Fuke N, Makarov N S, Pietryga J M and Klimov V I 2013 An integrated approach to realizing high-performance liquid-junction quantum dot sensitized solar cells *Nat Commun* **4** 2887

[74] Castro S L, Bailey S G, Raffaelle R P, Banger K K and Hepp A F 2004 Synthesis and Characterization of Colloidal CuInS 2 Nanoparticles from a Molecular Single-Source Precursor *J. Phys. Chem. B* **108** 12429–35

[75] Yue W, Han S, Peng R, Shen W, Geng H, Wu F, Tao S and Wang M 2010 CuInS2 quantum dots synthesized by a solvothermal route and their application as effective electron acceptors for hybrid solar cells *J. Mater. Chem.* **20** 7570

[76] Li T-L and Teng H 2010 Solution synthesis of high-quality CuInS 2 quantum dots as sensitizers for TiO 2 photoelectrodes *Journal of Materials Chemistry* **20** 3656–64

[77] Chang S, Zhao Y, Tang J, Bai Z, Zhao L and Zhong H 2020 Balanced Carrier Injection and Charge Separation of CuInS 2 Quantum Dots for Bifunctional Light-Emitting and Photodetection Devices *J. Phys. Chem. C* **124** 6554–61

[78] Long Z, Zhang W, Tian J, Chen G, Liu Y and Liu R 2021 Recent research on the luminous mechanism, synthetic strategies, and applications of CuInS 2 quantum dots *Inorg. Chem. Front.* **8** 880–97

[79] Li T-L, Cai C-D, Yeh T-F and Teng H 2013 Capped CuInS2 quantum dots for H2 evolution from water under visible light illumination *Journal of Alloys and Compounds* **550** 326–30

[80] Yuan Y-J, Fang G, Chen D, Huang Y, Yang L-X, Cao D-P, Wang J, Yu Z-T and Zou Z-G 2018 High light harvesting efficiency CuInS 2 quantum dots/TiO 2 /MoS 2 photocatalysts for enhanced visible light photocatalytic H 2 production *Dalton Trans.* **47** 5652–9

[81] Abulikemu M, Da'as E H, Haverinen H, Cha D, Malik M A and Jabbour G E 2014 In Situ Synthesis of Self-Assembled Gold Nanoparticles on Glass or Silicon Substrates through Reactive Inkjet Printing *Angewandte Chemie* **126** 430–3

[82] Abulikemu M, Tabrizi B E A, Ghobadloo S M, Mofarah H M and Jabbour G E 2022 Silver Nanoparticle-Decorated Personal Protective Equipment for Inhibiting Human Coronavirus Infectivity *ACS Appl. Nano Mater.* **5** 309–17

[83] Ahmed S R, Kim J, Tran V T, Suzuki T, Neethirajan S, Lee J and Park E Y 2017 In situ self-assembly of gold nanoparticles on hydrophilic and hydrophobic substrates for influenza virus-sensing platform *Sci Rep* **7** 44495

[84] Lu Z, Wang C, Deng W, Achille M T, Jie J and Zhang X 2020 Meniscus-guided coating of organic crystalline thin films for high-performance organic field-effect transistors *J. Mater. Chem. C* **8** 9133–46

[85] Schmid G 2011 *Nanoparticles: From Theory to Application* (John Wiley & Sons)

[86] Santos C S C, Gabriel B, Blanchy M, Menes O, García D, Blanco M, Arconada N and Neto V 2015 Industrial Applications of Nanoparticles – A Prospective Overview *Materials Today: Proceedings* **2** 456–65

[87] Böker A, He J, Emrick T and Russell T P 2007 Self-assembly of nanoparticles at interfaces *Soft Matter* **3** 1231–48

[88] Jacak L, Hawrylak P and Wojs A 2013 *Quantum Dots* (Springer Science & Business Media)

[89] Bera D, Qian L, Tseng T-K and Holloway P H 2010 Quantum Dots and Their Multimodal Applications: A Review *Materials* **3** 2260–345

[90] Beard M C, Luther J M, Semonin O E and Nozik A J 2013 Third Generation Photovoltaics based on Multiple Exciton Generation in Quantum Confined Semiconductors *Acc. Chem. Res.* **46** 1252–60

[91] Rabouw F T and de Mello Donega C 2016 Excited-State Dynamics in Colloidal Semiconductor Nanocrystals *Top Curr Chem (Z)* **374** 58

[92] Akkerman Q 2019 *Lead Halide Perovskite Nanocrystals: A New Age of Semiconductive Nanocrystals*

[93] Katan C, Mercier N and Even J 2019 Quantum and Dielectric Confinement Effects in Lower-Dimensional Hybrid Perovskite Semiconductors *Chem. Rev.* **119** 3140–92

[94] Edvinsson T 2018 Optical quantum confinement and photocatalytic properties in two-, one- and zero-dimensional nanostructures *R. Soc. open sci.* **5** 180387

[95] Wise F W 2000 Lead Salt Quantum Dots: the Limit of Strong Quantum Confinement *Acc. Chem. Res.* **33** 773–80

[96] Kaito C, Saito Y and Fujita K 1987 A New Preparation Method of Ultrafine Particles of Metallic Sulfides *Jpn. J. Appl. Phys.* **26** L1973

[97] Wang W, Liu Y, Zhan Y, Zheng C and Wang G 2001 A novel and simple one-step solid-state reaction for the synthesis of PbS nanoparticles in the presence of a suitable surfactant *Materials Research Bulletin* **36** 1977–84

[98] Nenadovic M T, Comor M I, Vasic Vesna and Micic O I 1990 Transient bleaching of small lead sulfide colloids: influence of surface properties *J. Phys. Chem.* **94** 6390–6

[99] Wang S and Yang S 2000 Preparation and Characterization of Oriented PbS Crystalline Nanorods in Polymer Films *Langmuir* **16** 389–97

[100] Borrelli N F and Smith D W 1994 Quantum confinement of PbS microcrystals in glass *Journal of Non-Crystalline Solids* **180** 25–31

[101] Pottathara Y B, Grohens Y, Kokol V, Kalarikkal N and Thomas S 2019 Synthesis and Processing of Emerging Two-Dimensional Nanomaterials *Nanomaterials Synthesis* (Elsevier) pp 1–25

[102] Cheng H, Wang Y, Dai H, Han J-B and Li X 2015 Nonlinear Optical Properties of PbS Colloidal Quantum Dots Fabricated via Solvothermal Method *J. Phys. Chem. C* **119** 3288–92

[103] Zhang B, Guo F, Yang L and Wang J 2014 Tunable synthesis of multi-shaped PbS via l-cysteine assisted solvothermal method *Journal of Crystal Growth* **405** 142–9

[104] Murray C B, Norris D J and Bawendi M G 1993 Synthesis and characterization of nearly monodisperse CdE (E = sulfur, selenium, tellurium) semiconductor nanocrystallites *J. Am. Chem. Soc.* **115** 8706–15

[105] Tyagi A K and Ningthoujam R S 2021 *Handbook on Synthesis Strategies for Advanced Materials: Volume-I: Techniques and Fundamentals* (Singapore: Springer Singapore)

[106] de Mello Donegá C, Liljeroth P and Vanmaekelbergh D 2005 Physicochemical Evaluation of the Hot-Injection Method, a Synthesis Route for Monodisperse Nanocrystals *Small* **1** 1152–62

[107] Kwon S G and Hyeon T 2011 Formation Mechanisms of Uniform Nanocrystals via Hot-Injection and Heat-Up Methods *Small* **7** 2685–702

[108] Yarema M, Yarema O, Lin W M M, Volk S, Yazdani N, Bozyigit D and Wood V 2017 Upscaling Colloidal Nanocrystal Hot-Injection Syntheses via Reactor Underpressure *Chem. Mater.* **29** 796–803

[109] Deng D, Cao J, Xia J, Qian Z, Gu Y, Gu Z and Akers W J 2011 Two-Phase Approach to High-Quality, Oil-Soluble, Near-Infrared-Emitting PbS Quantum Dots by Using Various Water-Soluble Anion Precursors *European Journal of Inorganic Chemistry* **2011** 2422–32

[110] Hendricks M P, Campos M P, Cleveland G T, Jen-La Plante I and Owen J S 2015 A tunable library of substituted thiourea precursors to metal sulfide nanocrystals *Science* **348** 1226–30

[111] Zuo X, Chang K, Zhao J, Xie Z, Tang H, Li B and Chang Z 2016 Ultrasmall PbS quantum dots: a facile and greener synthetic route and their high performance in luminescent solar concentrators *J. Mater. Chem. A* **4** 51–8

[112] Cademartiri L, Bertolotti J, Sapienza R, Wiersma D S, von Freymann G and Ozin G A 2006 Multigram Scale, Solventless, and Diffusion-Controlled Route to Highly Monodisperse PbS Nanocrystals *J. Phys. Chem. B* **110** 671–3

[113] Seo K-H, Jang J, Kang I M and Bae J-H 2021 Improving of Sensitivity of PbS Quantum Dot Based SWIR Photodetector Using P3HT *Materials* **14** 1488

[114] Zhang H, Selopal G S, Zhou Y, Tong X, Benetti D, Jin L, Navarro-Pardo F, Wang Z, Sun S, Zhao H and Rosei F 2017 Controlled synthesis of near-infrared quantum dots for optoelectronic devices *Nanoscale* **9** 16843–51

[115] Wang Y, Lu K, Han L, Liu Z, Shi G, Fang H, Chen S, Wu T, Yang F, Gu M, Zhou S, Ling X, Tang X, Zheng J, Loi M A and Ma W 2018 In Situ Passivation for Efficient PbS Quantum Dot Solar Cells by Precursor Engineering *Advanced Materials* **30** 1704871

[116] Yin S, Ho C H Y, Ding S, Fu X, Zhu L, Gullett J, Dong C and So F 2022 Enhanced Surface Passivation of Lead Sulfide Quantum Dots for Short-Wavelength Photodetectors *Chem. Mater.* **34** 5433–42

[117] Ganguly A, Choudhury M, Nath S S and Gope G 2017 Synthesis and characterization of one pot synthesized PVA capped PbS quantum dots *2017 Devices for Integrated Circuit (DevIC)* 2017 Devices for Integrated Circuit (DevIC) pp 141–3

[118] Abulikemu M, Da'as E H, Haverinen H, Cha D, Malik M A and Jabbour G E 2014 In Situ Synthesis of Self-Assembled Gold Nanoparticles on Glass or Silicon Substrates through Reactive Inkjet Printing *Angewandte Chemie* **126** 430–3

[119] Chopra K 2012 *Thin Film Device Applications* (Springer Science & Business Media)

[120] Chopra K L, Paulson P D and Dutta V 2004 Thin-film solar cells: an overview *Prog. Photovolt: Res. Appl.* **12** 69–92

[121] Singh J, Teo J H S, Xu Y, Premachandran C S, Chen N, Kotlanka R, Olivo M and Sheppard C J R 2008 A two axes scanning SOI MEMS micromirror for endoscopic bioimaging *J. Micromech. Microeng.* **18** 025001

[122] He Y, Hamann T and Wang D 2019 Thin film photoelectrodes for solar water splitting *Chem. Soc. Rev.* **48** 2182–215

[123] Singh J, Khan S A, Shah J, Kotnala R K and Mohapatra S 2017 Nanostructured TiO2 thin films prepared by RF magnetron sputtering for photocatalytic applications *Applied Surface Science* **422** 953–61

[124] Zou C, Chang C, Sun D, Böhringer K F and Lin L Y 2020 Photolithographic Patterning of Perovskite Thin Films for Multicolor Display Applications *Nano Lett.* **20** 3710–7

[125] Nair P K, Nair M T S, Castillo A, Ayala I T, Gomezdaza O and Hu H 1998 Semiconductor thin films by chemical bath deposition for solar energy related applications *Solar Energy Materials and Solar Cells*

[126] Babu Krishna Moorthy S 2015 *Thin Film Structures in Energy Applications* (Cham: Springer International Publishing)

[127] Eslamian M 2017 Inorganic and Organic Solution-Processed Thin Film Devices *Nano-Micro Lett.* **9** 3

[128] Lin Z, Huang Y and Duan X 2019 Van der Waals thin-film electronics *Nat Electron* **2** 378–88

[129] Patel J, Mighri F, Ajji A, Tiwari D and Chaudhuri T K 2014 Spin-coating deposition of PbS and CdS thin films for solar cell application *Appl. Phys. A* **117** 1791–9

[130] Khanzode P M, Halge D I, Narwade V N, Dadge J W and Bogle K A 2021 Highly photoresponsive visible light photodetector using nano PbS thin film on paper *Optik* **226** 165933

[131] Semonin O E, Luther J M, Choi S, Chen H-Y, Gao J, Nozik A J and Beard M C 2011 Peak External Photocurrent Quantum Efficiency Exceeding 100% via MEG in a Quantum Dot Solar Cell *Science* **334** 1530–3

[132] Kamat P V 2013 Quantum Dot Solar Cells. *The Next Big Thing* in Photovoltaics *J. Phys. Chem. Lett.* **4** 908–18

[133] Kim G-H, García de Arquer F P, Yoon Y J, Lan X, Liu M, Voznyy O, Yang Z, Fan F, Ip A H, Kanjanaboos P, Hoogland S, Kim J Y and Sargent E H 2015 High-Efficiency Colloidal Quantum Dot Photovoltaics via Robust Self-Assembled Monolayers *Nano Lett.* **15** 7691–6

[134] Zhao Q, Han R, Marshall A R, Wang S, Wieliczka B M, Ni J, Zhang J, Yuan J, Luther J M, Hazarika A and Li G 2022 Colloidal Quantum Dot Solar Cells: Progressive Deposition Techniques and Future Prospects on Large-Area Fabrication *Advanced Materials* **34** 2107888

[135] Aqoma H and Jang S-Y 2018 Solid-state-ligand-exchange free quantum dot ink-based solar cells with an efficiency of 10.9% *Energy Environ. Sci.* **11** 1603–9

[136] Kirmani A R, Sheikh A D, Niazi M R, Haque M A, Liu M, de Arquer F P G, Xu J, Sun B, Voznyy O, Gasparini N, Baran D, Wu T, Sargent E H and Amassian A 2018 Overcoming

the Ambient Manufacturability-Scalability-Performance Bottleneck in Colloidal Quantum Dot Photovoltaics *Advanced Materials* **30** 1801661

[137] Kressel H 2012 *Semiconductor Lasers and Herterojunction LEDs* (Elsevier)

[138] Cho K-S, Lee E K, Joo W-J, Jang E, Kim T-H, Lee S J, Kwon S-J, Han J Y, Kim B-K, Choi B L and Kim J M 2009 High-performance crosslinked colloidal quantum-dot light-emitting diodes *Nature Photon* **3** 341–5

[139] Weidman M C, Beck M E, Hoffman R S, Prins F and Tisdale W A 2014 Monodisperse, Air-Stable PbS Nanocrystals *via* Precursor Stoichiometry Control *ACS Nano* **8** 6363–71

[140] Sun L, Choi J J, Stachnik D, Bartnik A C, Hyun B-R, Malliaras G G, Hanrath T and Wise F W 2012 Bright infrared quantum-dot light-emitting diodes through inter-dot spacing control *Nature Nanotech* **7** 369–73

[141] Gong X, Yang Z, Walters G, Comin R, Ning Z, Beauregard E, Adinolfi V, Voznyy O and Sargent E H 2016 Highly efficient quantum dot near-infrared light-emitting diodes *Nature Photon* **10** 253–7

[142] Banerjee D and Chattopadhyay K K 2018 Hybrid Inorganic Organic Perovskites *Perovskite Photovoltaics* (Elsevier) pp 123–62

[143] Konstantatos G and Sargent E H 2011 Colloidal quantum dot photodetectors *Infrared Physics & Technology* **54** 278–82

[144] Brus L 1986 Electronic wave functions in semiconductor clusters: experiment and theory *J. Phys. Chem.* **90** 2555–60

[145] Zhao D, Huang J, Qin R, Yang G and Yu J 2018 Efficient Visible–Near-Infrared Hybrid Perovskite:PbS Quantum Dot Photodetectors Fabricated Using an Antisolvent Additive Solution Process *Advanced Optical Materials* **6** 1800979

[146] Chen W, Tang H, Chen Y, Heger J E, Li N, Kreuzer L P, Xie Y, Li D, Anthony C, Pikramenou Z, Ng K W, Sun X W, Wang K and Müller-Buschbaum P 2020 Spray-deposited PbS colloidal quantum dot solid for near-infrared photodetectors *Nano Energy* **78** 105254

[147] Booth M, Brown A P, Evans S D and Critchley K 2012 Determining the Concentration of $CuInS_2$ Quantum Dots from the Size-Dependent Molar Extinction Coefficient *Chem. Mater.* **24** 2064–70

[148] Leach A D P and Macdonald J E 2016 Optoelectronic Properties of $CuInS_2$ Nanocrystals and Their Origin *J. Phys. Chem. Lett.* **7** 572–83

[149] Kuzuya T, Hamanaka Y, Itoh K, Kino T, Sumiyama K, Fukunaka Y and Hirai S 2012 Phase control and its mechanism of CuInS2 nanoparticles *Journal of Colloid and Interface Science* **388** 137–43

[150] Pan D, An L, Sun Z, Hou W, Yang Y, Yang Z and Lu Y 2008 Synthesis of Cu−In−S Ternary Nanocrystals with Tunable Structure and Composition *J. Am. Chem. Soc.* **130** 5620–1

[151] Xie B-B, Hu B-B, Jiang L-F, Li G and Du Z-L 2015 The phase transformation of CuInS2 from chalcopyrite to wurtzite *Nanoscale Res Lett* **10** 86

[152] Connor S T, Hsu C-M, Weil B D, Aloni S and Cui Y 2009 Phase Transformation of Biphasic Cu $_2$ S−CuInS $_2$ to Monophasic CuInS $_2$ Nanorods *J. Am. Chem. Soc.* **131** 4962–6

[153] Yoshino K, Ikari T, Shirakata S, Miyake H and Hiramatsu K 2001 Sharp band edge photoluminescence of high-purity CuInS2 single crystals *Appl. Phys. Lett.* **78** 742–4

[154] Chumha N, Thongtem T, Thongtem S, Tantraviwat D, Kittiwachana S and Kaowphong S 2016 A single-step method for synthesis of CuInS2 nanostructures using cyclic microwave irradiation *Ceramics International* **42** 15643–9

[155] Liu S, Zhang H, Qiao Y and Su X 2012 One-pot synthesis of ternary CuInS 2 quantum dots with near-infrared fluorescence in aqueous solution *RSC Advances* **2** 819–25

[156] Peng Z, Liu Y, Shu W, Chen K and Chen W 2012 Synthesis of Various Sized CuInS $_2$ Quantum Dots and Their Photovoltaic Properties as Sensitizers for TiO $_2$ Photoanodes *Eur. J. Inorg. Chem.* **2012** 5239–44

[157] Li H, Luo D, Liu L, Xiong D and Peng Y 2021 Improved efficiency and carrier dynamic transportation behavior in perovskite solar cells with CuInS $_2$ quantum dots as hole-transport materials *Dalton Trans.* **50** 8837–44

[158] Liu Y, Zhang Z, Gao H, Zhang H and Mao Y 2019 A novel inorganic hole-transporting material of CuInS2 for perovskite solar cells with high efficiency and improved stability *Organic Electronics* **75** 105430

[159] Feng J, Han J and Zhao X 2009 Synthesis of CuInS2 quantum dots on TiO2 porous films by solvothermal method for absorption layer of solar cells *Progress in Organic Coatings* **64** 268–73

[160] Park S H, Hong A, Kim J-H, Yang H, Lee K and Jang H S 2015 Highly Bright Yellow-Green-Emitting CuInS $_2$ Colloidal Quantum Dots with Core/Shell/Shell Architecture for White Light-Emitting Diodes *ACS Appl. Mater. Interfaces* **7** 6764–71

[161] Voigt D, Bredol M and Gonabadi A 2021 A general strategy for CuInS2 based quantum dots with adjustable surface chemistry *Optical Materials* **115** 110994

[162] Peng Z, Liu Y, Chen K, Yang G and Chen W 2014 Fabrication of the protonated pentatitanate nanobelts sensitized with CuInS2 quantum dots for photovoltaic applications *Chemical Engineering Journal* **244** 335–42

[163] Bai Z, Ji W, Han D, Chen L, Chen B, Shen H, Zou B and Zhong H 2016 Hydroxyl-Terminated CuInS 2 Based Quantum Dots: Toward Efficient and Bright Light Emitting Diodes *Chem. Mater.* **28** 1085–91

[164] Søndergaard R R, Hösel M and Krebs F C 2013 Roll-to-Roll fabrication of large area functional organic materials *Journal of Polymer Science Part B: Polymer Physics* **51** 16–34

[165] Grau G, Cen J, Kang H, Kitsomboonloha R, Scheideler W J and Subramanian V 2016 Gravure-printed electronics: recent progress in tooling development, understanding of printing physics, and realization of printed devices *Flex. Print. Electron.* **1** 023002

[166] Reddy A S G, Narakathu B B, Atashbar M Z, Rebros M, Rebrosova E and Joyce M K 2011 Gravure Printed Electrochemical Biosensor *Procedia Engineering* **25** 956–9

[167] Reddy A S G, Narakathu B B, Atashbar M Z, Rebros M, Rebrosova E, Bazuin B J, Joyce M K, Fleming P D and Pekarovicova A 2011 Printed Capacitive Based Humidity Sensors on Flexible Substrates *Sen Lett* **9** 869–71

[168] Liu X and Guthrie J T 2003 A review of flexographic printing plate development *Surface Coatings International Part B: Coatings Transactions* **86** 91–9

[169] Assaifan A K, Lloyd J S, Samavat S, Deganello D, Stanton R J and Teng K S 2016 Nanotextured Surface on Flexographic Printed ZnO Thin Films for Low-Cost Non-Faradaic Biosensors *ACS Appl. Mater. Interfaces* **8** 33802–10

[170] Leppäniemi J, Huttunen O-H, Majumdar H and Alastalo A 2015 Flexography-Printed In2O3 Semiconductor Layers for High-Mobility Thin-Film Transistors on Flexible Plastic Substrate *Advanced Materials* **27** 7168–75

[171] Zhang Y, Zhu Y, Zheng S, Zhang L, Shi X, He J, Chou X and Wu Z-S 2021 Ink formulation, scalable applications and challenging perspectives of screen printing for emerging printed microelectronics *Journal of Energy Chemistry* **63** 498–513

[172] Cinti S, Arduini F, Moscone D, Palleschi G and Killard A 2014 Development of a Hydrogen Peroxide Sensor Based on Screen-Printed Electrodes Modified with Inkjet-Printed Prussian Blue Nanoparticles *Sensors* **14** 14222–34

[173] Wan H, Sun Q, Li H, Sun F, Hu N and Wang P 2015 Screen-printed gold electrode with gold nanoparticles modification for simultaneous electrochemical determination of lead and copper *Sensors and Actuators B: Chemical* **209** 336–42

[174] Torres-Rivero K, Florido A and Bastos-Arrieta J 2021 Recent Trends in the Improvement of the Electrochemical Response of Screen-Printed Electrodes by Their Modification with Shaped Metal Nanoparticles *Sensors* **21** 2596

[175] Zavanelli N and Yeo W-H 2021 Advances in Screen Printing of Conductive Nanomaterials for Stretchable Electronics *ACS Omega* **6** 9344–51

[176] Søndergaard R, Hösel M, Angmo D, Larsen-Olsen T T and Krebs F C 2012 Roll-to-roll fabrication of polymer solar cells *Materials Today* **15** 36–49

[177] Hoath S D 2016 *Fundamentals of Inkjet Printing: The Science of Inkjet and Droplets* (John Wiley & Sons)

[178] Singh M, Haverinen H M, Dhagat P and Jabbour G E 2010 Inkjet Printing-Process and Its Applications *Adv. Mater.* **22** 673–85

[179] Nayak L, Mohanty S, Nayak S K and Ramadoss A 2019 A review on inkjet printing of nanoparticle inks for flexible electronics *J. Mater. Chem. C* **7** 8771–95

[180] Calvert P 2001 Inkjet Printing for Materials and Devices *Chem. Mater.* **13** 3299–305

[181] Lau G-K and Shrestha M 2017 Ink-Jet Printing of Micro-Electro-Mechanical Systems (MEMS) *Micromachines* **8** 194

[182] Teranishi R 2002 Direct fabrication of patterned PbS and CdS on organic sheets at ambient temperature by on-site reaction using inkjet printer *Solid State Ionics* **151** 97–103

[183] YousefiAmin A, Killilea N A, Sytnyk M, Maisch P, Tam K C, Egelhaaf H-J, Langner S, Stubhan T, Brabec C J, Rejek T, Halik M, Poulsen K, Niehaus J, Köck A and Heiss W 2019 Fully Printed Infrared Photodetectors from PbS Nanocrystals with Perovskite Ligands *ACS Nano* acsnano.8b09223

[184] Anon DP3: Digital Print Preservation Portal | Inkjet

[185] Zhang J X J and Hoshino K 2019 Fundamentals of nano/microfabrication and scale effect *Molecular Sensors and Nanodevices* (Elsevier) pp 43–111

[186] Nam M, Lee S, Park J, Kim S-W and Lee K-K 2011 Development of Hybrid Photovoltaic Cells by Incorporating CuInS $_2$ Quantum Dots into Organic Photoactive Layers *Jpn. J. Appl. Phys.* **50** 06GF02

[187] Dobrzański L A and Szindler M 2012 Sol gel TiO2 antireflection coatings for silicon solar cells *J. Achiev. Mater. Manuf. Eng.* **52** 7–14

[188] Mishra A, Bhatt N and Bajpai A K 2019 Nanostructured superhydrophobic coatings for solar panel applications *Nanomaterials-Based Coatings* (Elsevier) pp 397–424

[189] Zabihi F, Xie Y, Gao S and Eslamian M 2015 Morphology, conductivity, and wetting characteristics of PEDOT:PSS thin films deposited by spin and spray coating *Applied Surface Science* **338** 163–77

[190] Hodes G 2007 Semiconductor and ceramic nanoparticle films deposited by chemical bath deposition *Phys. Chem. Chem. Phys.* **9** 2181

[191] Pawar S M, Pawar B S, Kim J H, Joo O-S and Lokhande C D 2011 Recent status of chemical bath deposited metal chalcogenide and metal oxide thin films *Current Applied Physics* **11** 117–61

[192] Mane R S and Lokhande C D 2000 Chemical deposition method for metal chalcogenide thin ®lms *Materials Chemistry and Physics*

[193] Rajathi S, Kirubavathi K and Selvaraju K 2017 Structural, morphological, optical, and photoluminescence properties of nanocrystalline PbS thin films grown by chemical bath deposition *Arabian Journal of Chemistry* **10** 1167–74

[194] Chen Y, Zhang X, Tao Q, Fu W, Yang H, Su S, Mu Y, Zhou L and Li M 2015 High catalytic activity of a PbS counter electrode prepared via chemical bath deposition for quantum dots-sensitized solar cells *RSC Adv.* **5** 1835–40

[195] Ho Yeon D, Chandra Mohanty B, Lee S M and Soo Cho Y 2015 Effect of band-aligned double absorber layers on photovoltaic characteristics of chemical bath deposited PbS/CdS thin film solar cells *Sci Rep* **5** 14353

[196] Wang Y, Rui Y, Zhang Q, Li Y and Wang H 2013 A Facile in Situ Synthesis Route for CuInS $_2$ Quantum-Dots/In $_2$ S $_3$ Co-Sensitized Photoanodes with High Photoelectric Performance *ACS Appl. Mater. Interfaces* **5** 11858–64

[197] Landau L and Levich B 1988 Dragging of a Liquid by a Moving Plate *Dynamics of Curved Fronts* ed P Pelcé (San Diego: Academic Press) pp 141–53

[198] Crisp R W, Kroupa D M, Marshall A R, Miller E M, Zhang J, Beard M C and Luther J M 2015 Metal Halide Solid-State Surface Treatment for High Efficiency PbS and PbSe QD Solar Cells *Sci Rep* **5** 9945

[199] Ilaiyaraja P, Rakesh B, Das T K, Mocherla P S V and Sudakar C 2018 CuInS2 quantum dot sensitized solar cells with high VOC ≈ 0.9 V achieved using microsphere-nanoparticulate TiO2 composite photoanode *Solar Energy Materials and Solar Cells* **178** 208–22

[200] Cui H-Q, Peng R-X, Song W, Zhang J-F, Huang J-M, Zhu L-Q and Ge Z-Y 2019 Optimization of Ethylene Glycol Doped PEDOT:PSS Transparent Electrodes for Flexible Organic Solar Cells by Drop-coating Method *Chin J Polym Sci* **37** 760–6

[201] Fischer A, Rollny L, Pan J, Carey G H, Thon S M, Hoogland S, Voznyy O, Zhitomirsky D, Kim J Y, Bakr O M and Sargent E H 2013 Directly Deposited Quantum Dot Solids Using a Colloidally Stable Nanoparticle Ink *Advanced Materials* **25** 5742–9

[202] Conway R 2016 Coating of textiles *Handbook of Technical Textiles* (Elsevier) pp 211–29

[203] Pierre A, Sadeghi M, Payne M M, Facchetti A, Anthony J E and Arias A C 2014 All-Printed Flexible Organic Transistors Enabled by Surface Tension-Guided Blade Coating *Adv. Mater.* **26** 5722–7

[204] Francis L F and Roberts C C 2016 Dispersion and Solution Processes *Materials Processing* (Elsevier) pp 415–512

[205] Vand V 1948 Viscosity of Solutions and Suspensions. I. Theory *J. Phys. Chem.* **52** 277–99

[206] Mishra P C, Mukherjee S, Nayak S K and Panda A 2014 A brief review on viscosity of nanofluids *Int Nano Lett* **4** 109–20

[207] O'Kane D F and Mittal K L Plasma cleaning of metal surfaces

[208] Vig J R 1985 UV/ozone cleaning of surfaces *J. Vac. Sci. Technol. A* **3**

[209] Brehm M, Scheiger J M, Welle A and Levkin P A 2020 Reversible Surface Wettability by Silanization *Adv. Mater. Interfaces* **7** 1902134

[210] Chang Y-H, Tseng S-R, Chen C-Y, Meng H-F, Chen E-C, Horng S-F and Hsu C-S 2009 Polymer solar cell by blade coating *Organic Electronics* **10** 741–6

[211] Tseng S-R, Meng H-F, Lee K-C and Horng S-F 2008 Multilayer polymer light-emitting diodes by blade coating method *Appl. Phys. Lett.* **93** 153308

[212] Yang J, Lim E L, Tan L and Wei Z 2022 Ink Engineering in Blade-Coating Large-Area Perovskite Solar Cells *Advanced Energy Materials* **12** 2200975

[213] Yang Z, Chueh C-C, Zuo F, Kim J H, Liang P-W and Jen A K-Y 2015 High-Performance Fully Printable Perovskite Solar Cells via Blade-Coating Technique under the Ambient Condition *Adv. Energy Mater.* **5** 1500328

[214] Han D, Khan Y, Ting J, King S M, Yaacobi-Gross N, Humphries M J, Newsome C J and Arias A C 2017 Flexible Blade-Coated Multicolor Polymer Light-Emitting Diodes for Optoelectronic Sensors *Adv. Mater.* **29** 1606206

[215] Chang H-W, Lee Y-T, Tseng M-R, Jang M-H, Yeh H-C, Luo F-T, Meng H-F, Chen C-T, Chi Y, Qiu Y, Duan L, Lin H-W, Horng S-F and Zan H-W 2014 General application of blade coating to small-molecule hosts for organic light-emitting diode *Synthetic Metals* **196** 99–109

[216] Balazs D M, Dirin D N, Fang H-H, Protesescu L, ten Brink G H, Kooi B J, Kovalenko M V and Loi M A 2015 Counterion-Mediated Ligand Exchange for PbS Colloidal Quantum Dot Superlattices *ACS Nano* **9** 11951–9

[217] Mousavi-Kamazani M, Salehi Z and Motevalli K 2017 Enhancement of quantum dot-sensitized solar cells performance using CuInS2–Cu2S nanocomposite synthesized by a green method *Appl. Phys. A* **123** 691

[218] Magdassi S and Kamyshny A 2017 *Nanomaterials for 2D and 3D Printing* (John Wiley & Sons)

Chapter 3 . PbS quantum dots

The following article is going to be submitted for publication.

Synthesis of Self-Assembled PbS Quantum Dots Using Reactive Blade Coating

Kimia Rezaei Shad[1], Mutalifu Abulikemu[1], and Ghassan E. Jabbour[1]*

[1]School of Electrical Engineering and Computer Science, University of Ottawa, 800 King Edward Ave., Ottawa, ON, Canada K1N 6N5

*Corresponding Author: gja@uOttawa.ca

3.1 Abstract

Most techniques for synthesizing and depositing PbS QDs can be considered high-cost and unsuitable for future large-scale fabrication. In this chapter, in-situ reactive synthesis of PbS QDs/NPs via blade coating will be presented. The impact of various heating methods, such as oven, hotplate, and rapid thermal annealing (RTA), on the formation of QDs/NPs of PbS will be presented for the first time. In this regard, different sizes and shapes of PbS QDs/NPs have been realized by changing some experimental parameters, such as heating time and temperature. The PbS QDs/NPs were characterized with XRD, SEM, EDS, UV-vis and photoluminescence tests to to understand their properties better. The facile reactive blade coating synthesizing method for synthesizing PbS QDs/NPs can be easily scaled up to large-scale synthesis, such as roll-to-roll (R2R) manufacturing techniques for various optoelectronic applications, thus reducing cost and time to market.

KEYWORDS: PbS QDs, blade coating, in-situ reactive synthesis, roll-to-roll manufacturing technique, photodetectors.

3.2 Introduction

Quantum dots (QDs) have attracted great attention for the last two decades owing to their outstanding optical properties attributed to the quantum size effect observed, which allows for tuning the band gap of nanocrystals[1,2]. This tunable bandgap can result in getting desired features such as different colour emissions under excitation. QDs can be synthesized using a variety of techniques, including chemical, physical, and biological approaches[3–5]. Chemical synthesizing techniques are the most well-studied and adaptive ones[6]. QDs have been made with several chemical synthesizing methods, such as hydrothermal routes[7,8], sol-gel method[9], hot injection method[10], solvothermal methods[11], and microwave synthesis[12]. The desirable qualities of QDs have led to their widespread use in QD light-emitting diodes[13], colour conversion layers in OLED displays[14], solar cells[15], and photodetectors[16].

Since printed electronic devices are easy to manufacture and can be flexible, they have attracted a lot of attention in recent years. Compared to traditional production processes like sputtering[17] and chemical bath deposition[18], which require complex manufacturing processes and relatively expensive equipment, printing technologies can offer competitive advantages in terms of product performance and fabrication cost. Inkjet printing[13,14], microcontact printing[19], electrohydrodynamic nanoprinting[20], and roll-to-roll (R2R) printing[21] are just a few of the several printing processes available. Some of these printing techniques were used for depositing thin films of binary QDs for various electrical and optical applications. Kurley et al. synthesized CdTe QDs by hot injection to be used in R2R-printed solar cells[21]. Arango et al.[22] printed CdSe QDs as a photosensitive layer by microcontact stamping method for photovoltaic devices. In another work, ZnO QDs, PbS QDs, and FeS_2 nanocrystals were fabricated by inkjet printing and utilized in photodetectors[23]. Also, In another study, inkjet-printed PbS QDs were used in an IR QD photodetector[24]. The printing methods used in the mentioned printed binary QD layers were ex-situ, which means the inks containing the QDs were prepared prior to the printing process. These conventional methods for synthesizing and printing QDs in separate steps are costly and environmentally unfriendly due to the high amount of materials waste and the need for multiple processes to synthesize the QDs and deposit them into thin films for a given application.

Meanwhile, some promising methods exist for directly fabricating thin films by in-situ printing or coating from commercially available precursor sources. These methods can be called in-situ reactive methods. In these methods, synthesizing and printing the QDs are simultaneously performed, which leads to simple, cheap, fast, and easy-to-control processes. Also, the in-situ reactive methods involve low chemical waste and are more suitable for large-scale fabrications[25]. In-situ reactive inkjet printing was used by Jabbour's group for the first time to synthesize Au NPs[25]. This method can facilitate the use of Au NPs for complex optoelectronic applications. Although inkjet printing is a fascinating manufacturing technique to synthesize nanoparticles, it can be expensive due to the high cost of cartridges, which may clog over time. In another work, Jabbour et al. used an in-situ reactive blade coating method for synthesizing silver NPs on a glass substrate, textile, and a surgical mask to be used against SARS-CoV-2 with high disinfection[26]. In-situ reactive blade coating method is a faster and more economically feasible technique than in-situ reactive inkjet printing. To our knowledge, in-situ reactive preparation of binary QDs/NPs has not been reported.

Here, we synthesized PbS QDs/NPs with an in-situ reactive blade coating method for the first time. Among binary QDs, lead chalcogenides have received considerable attention for UV-vis-near IR optical applications. Researchers have studied numerous optoelectronic applications using PbS and PbSe, including solar cells[30,31], photodetectors[32,33], and light-emitting diodes (LEDs)[34]. PbS is a direct bandgap semiconductor with a 0.41 eV bandgap and 3200 nm absorption edge at room temperature[35]. It is an exciting material for the study of quantum effects and has a large 18 nm exciton Bohr radius and properties such as multiple carrier generation[36]. A variety of methods have been used to synthesize PbS QDs/NPs with different shapes, such as chemical bath deposition[18], hot injection[37], controlled precipitation with an ultrasonic bath[38], in situ halide passivation[39], electrochemical deposition[40], and bacterial biosynthesis[41]. However, in-situ reactive synthesis of binary PbS QDs/NPs directly on substrates yet to be reported. We used the in-situ reactive method for synthesizing PbS QDs/NPs, using various methods for heating them, such as heating samples on a hotplate, in a vacuum oven, and with rapid thermal annealing (RTA). Each heating method had specific features that this study will discuss thoroughly. Also, different parameters, such as different heating temperatures and heating durations, have been investigated in the synthesis and heating of these QDs/NPs. The best heating method and parameters were chosen to be utilized in optical devices. The in-situ reactive

blade coating method used here for the preparation of PbS QDs/NPs can be used on large manufacturing scales leading to lower total fabrication costs.

3.3 Experimental

3.3.1 Materials

Lead acetate trihydrate ($Pb(CH_3COO)_2.3H_2O$), oleylamine (OLA) ($C_{18}H_{35}NH_2$), sulfur (100%), oleic acid (OA) (90 %), and 1-octadecene (ODE) (90 %) were used for making the solutions for the blade coating process without further treatment. Isopropyl alcohol (IPA) was used for washing silicon substrates, and acetone (C_3H_6O) and toluene (TOL) were used for diluting the solution containing the QDs/NPs during the photoluminance (PL) test. Silicon substrates (1 × 1 inch) were utilized as working substrates. Carbon steel sterile blades were used for the blade coating process.

3.3.2 PbS QDs synthesis

3.3.2.1 *Precursor preparation*

Two solutions (inks) were prepared prior to the blade coating process. For the first solution (the Pb ink), lead acetate trihydrate (189 mg) was dissolved in the mixture of 0.39 ml OA and 3.8 ml ODE, then heating up to 180 °C for 30 min under continuous stirring. Similarly, for the second solution (the S ink), sulfur (51 mg) was dissolved in 6.5 ml OLA followed by heating the solution at 180 °C for 30 min under stirring. These two inks (Pb ink and S ink) were the initial precursor inks for the blade coating process.

3.3.2.2 *Substrate preparation*

Silicon substrates (1 × 1 $inch^2$) were used for the blade coating process. First, the substrates were washed with soap and rinsed with DI water, followed by 10 min sonication in DI water and IPA, then dried using an air gun, respectively. The surface treatment was performed by UV-Ozone for 10 min before the blade coating process.

3.3.2.3 *Blade coating process*

A Schematic of PbS QD/NP synthesis is shown in Fig. 3.1. Figures 3.1(a) and 3.1(b) show the preparation of Pb and S inks, respectively. First, two droplets (about 0.05 ml) of the as-prepared Pb ink were blade coated on top of the silicon substrate by a surgical razor blade (Fig. 3.1(c)).

Then, two droplets of the as-prepared S ink were blade coated on top of the first layer (Pb ink), shown in Fig. 3.1(d). The angle between the blade and the silicon substrate was kept at 50° during the blade coating process. In the final step (Fig. 3.1(e)), the substrates were heated with three different methods to yield films with dark brown colour. The heating methods used were: 1) vacuum oven, 2) hotplate in a glovebox, and 3) RTA (Fig 3.1.e). Parameters such as time, temperature, and concentration were investigated for their impact on the synthesis results.

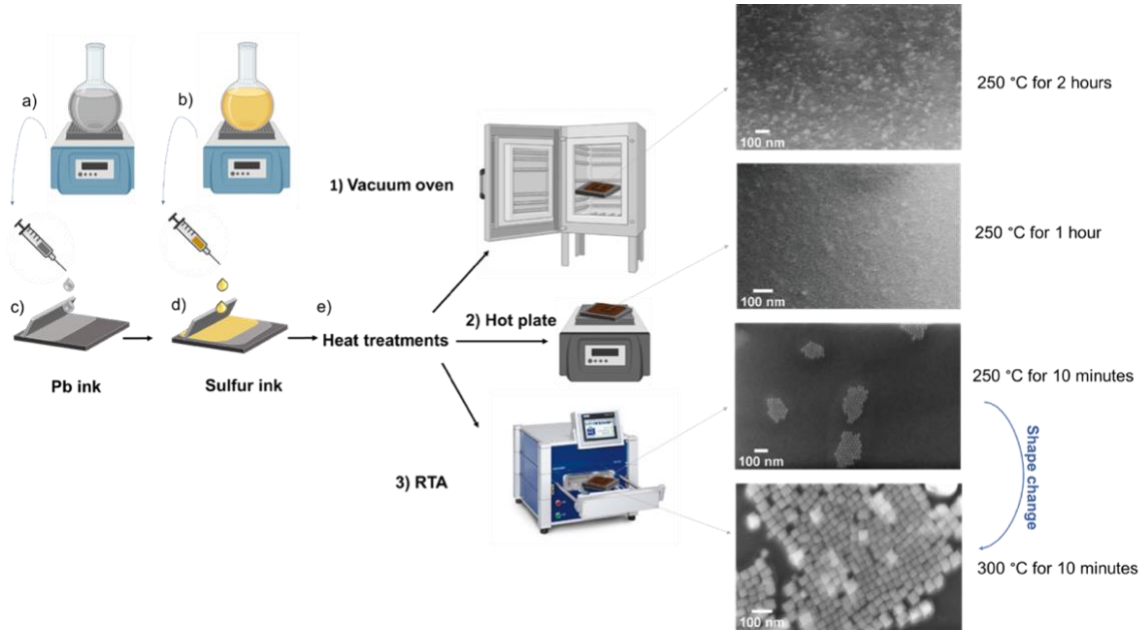

Figure 3.1 - Schematic of in situ reactive blade coating process of self-assembled PbS QDs/NPs. a) preparation of Pb ink. b) preparation of S ink. c) blade coating the Pb ink. d) blade coating the S ink on top of the first ink (Pb ink). e) formation of PbS QDs/NPs after the heating treatment with 1) vacuum oven, 2) hotplate, and 3) RTA heating methods. A representative SEM images for each heating method is also shown (far right).

For comparison, spin coating was also tried for fabricating PbS QDs/NPs thin films. Similar to blade coating, a layer of Pb ink was first deposited on a clean silicon substrate. After spin coating of Pb ink using a rate of 1000 rpm, a layer of S ink was deposited and on top using the same spin rate. Shortly after the second cycle of spin coating, the substrates were heated using the aforementioned three methods.

3.3.3 Heating methods

3.3.3.1 Vacuum oven

Vacuum oven is the first heating method used to heat the coated substrates. In this method, blade coating was carried out in a room environment; the sample was placed in the oven immediately after blade coating. In the following step, the oven was purged with nitrogen for five minutes, and then a vacuum was applied. This process was repeated several times to ensure the oven atmosphere contained no oxygen. Finally, after putting the oven under a complete vacuum with pressure around 0.1 Pa to 1×10^{-6} Pa, the oven was turned on and set to the desired temperature. Parameters such as time & temperature were investigated.

3.3.3.2 Hotplate in glovebox

The second heating method is using a hotplate in an inert glovebox. In this method, all the needed materials were first placed in the glovebox, which was purged with nitrogen. After purging the glovebox for 30 minutes, the blade coating procedure was performed. Then right after blade coating, the substrate was placed on the hotplate set at the desired temperature. Various parameters, including time and temperature, were investigated here as well.

3.3.3.3 Rapid thermal annealing (RTA)

The third heating method is RTA. Here the samples were blade coated in normal operating laboratory environment, then placed in the RTA. For optimization of process conditions, the RTA had four main steps for heating and cooling down to room temperature. The first step was purging. The chamber of the RTA was purged with nitrogen for a specific time before the heating process started. As shown in Table 3.1, the chamber of RTA was purged with nitrogen for 30 min before the heating process started to minimize the presence of oxygen in the RTA chamber environment. All the other steps were completed under nitrogen environment. The second step was the ramp up step. In this step, the temperature was increased to desired values. The third step was the holding (soaking) step, where the substrate was maintained at that temperature for the specified time. Table 3.1 lists the holding temperature values and times. The fourth step was the cooling step. In this step, the chamber was cooled from the desired temperature to room temperature. After the cooling step, the sample was taken out from the RTA. In all samples heated with vacuum oven, hotplate

in glovebox, and RTA, 1 ml of S ink was diluted with 3 ml OLA before blade coating. Table 3.1 shows the experimental parameters investigated for each heating method.

Table 3.1- Different heating method experimental parameters and estimation of the corresponding average size of PbS QDs/NPs as obtained via SEM and calculations based on XRD results.

Heating method	Sample	Temperature	Time	Average size from SEM (nm)	Calculated size from XRD (nm)
Vacuum oven	S_1	200 °C	3 h	Incomplete Drying (ID)	16.2
	S_2	250 °C	1 h	ID	10.1
	S_3	250 °C	2 h	12.8	13
	S_4	250 °C	3 h	24	20
Hotplate in glovebox	S_1	200 °C	2 h	ID	9.8
	S_2	250 °C	1 h	6.8	8.8
	S_3	250 °C	2 h	8.5	13.5
	S_4	250 °C	3 h	9.2	15
	S_5	300 °C	1 h	8.4	10
RTA	S_1	250 °C	10 min	15.8	18
	S_2	300 °C	10 min	32	30
	S_3	350 °C	3 min	24	27
	S_4	350 °C	10 min	82	55

3.3.4 Characterization

Various characterization techniques were used to investigate the PbS QDs/NPs. In this regard, absorption measurements were carried out with UV-vis Cary 7000 Spectrophotometer using the 280-800 nm wavelength range. Photoluminescence (PL) measurements were performed with a Horiba fluorescence spectrometer in the UV-vis range (400-700 nm). Crystalline phase investigations of the samples were carried out using X-ray diffraction (XRD) analysis-Rigaku Ultima IV Diffractometer with Cu target ($k\alpha = 1.54$). The range of angle 2θ was between 20-65° using a Cu-sealed tube, and the scan speed was adjusted to 0.5°/min at a 40 kV voltage. The surface morphology, structure, and size distribution of the QDs/NPs were characterized by a Scanning

Electron Microscope (SEM) system (Zeiss Gemini 500 device). Energy-dispersive X-ray spectroscopy (EDS) analysis was carried, in the SEM chamber, for elemental analysis of the NPs and QDs.

3.4 Results and Discussion

The full method for blade coating PbS QDs/NPs was described in the experimental section and illustrated in Fig. 3.1. Briefly, two layers of Pb ink and S ink were blade coated on top of each other to make the PbS thin film. First, The Pb ink was blade coated on the silicon substrate (Fig. 3.1(c)), and then the S ink was blade coated on top (Fig. 3.1(d)). The reason we first blade coated Pb ink (containing OA and ODE) and then S ink (containing OLA) on top of it on the silicon substrate, is better wetting and lower contact angle between the Pb ink and silicon substrate, compared to doing the reverse steps (first blade coat S ink on silicon substrate) (Fig. 3.2). The photos of contact angle measurement tests of S ink and Pb ink on top of glass and silicon substrates are shown in Fig. 3.2, which confirms our statement above for both glass and silicon substrates. Then, the sample was heated to make the PbS QDs/NPs (Fig. 3.1(e)). Three different heating methods were used for heating the blade-coated substrate: 1) Vacuum oven, 2) Hotplate in the glovebox, and 3) RTA, which are shown in Fig. 3.1(e). The SEM images of the representative samples achieved from each heating method are shown in Figure 3.1.

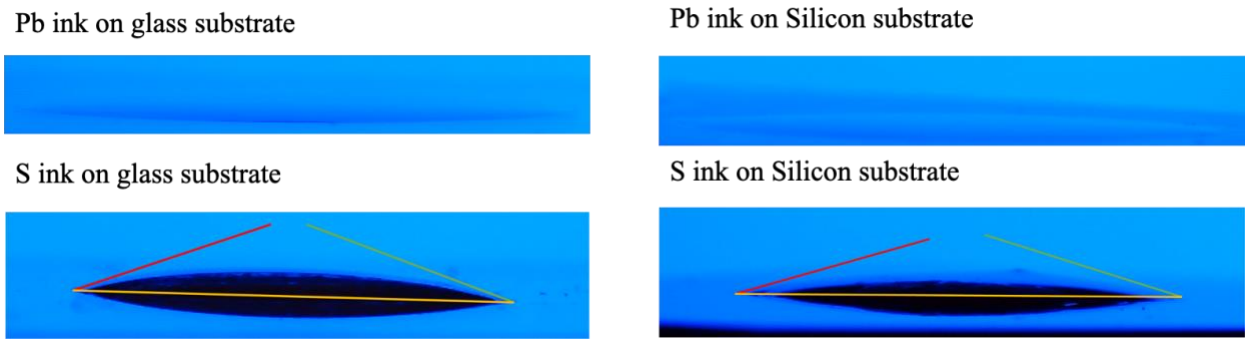

Figure 3.2- Contact angle of two precursor inks on top of the glass and silicon substrates. a) Pb ink on a glass substrate with a contact angle of < 2 °, b) Pb ink on a silicon substrate with a contact angle of < 2 °, c) S ink on a glass substrate with a contact angle of (12± 2) °, and d) S ink on silicon substrate with a contact angle of (9± 2) °.

3.4.1 X-ray diffraction analysis

The XRD data of the synthesized PbS QDs/NPs with various drying methods are shown in Fig. 3.3 and Fig. A1, which agreed with the standard JCPDS PbS data (card No. 05-0592), confirming the purity and cubic structure of synthesized PbS nanocrystals. Moreover, the calculated mean value of the lattice constant (5.921 Å) is in good agreement with the reported value (a = 5.936 Å). The following relationship was used for calculating the lattice constant 'a' for PbS cubic structure nanocrystals (Eq. (1)). Where in this formula, 'd' is d-spacing (interplanar pacing), and 'h k l' are miller indices.

$$a = d\sqrt{(h^2 + k^2 + l^2)} \qquad (1)$$

The average size of QDs/NPs synthesized with various methods was estimated with Debye-Sherrer equation (Eq. (2)). In this formula, D is the size of QD/NP, k is the shape factor that normally is considered as 0.94, λ is the XRD wavelength (for Cu target $\lambda = 1.54$ Å), β is the full width at half maximum (FWHM) which shows line broadening in radians, and θ is the Bragg angle.

$$D = \frac{k\lambda}{\beta \cos\theta} \qquad (2)$$

The average sizes of QDs/NPs estimated with eq. (2) for different investigated parameters are given in Table 3.1. As shown in Table 3.1, for samples heated at 200 °C for 3 h, 250 °C for 1 h, 2 h, and 3 h in vacuum oven, the predicted size of QDs/NPs based on the FWHM of XRD peaks is approximately 16.2 nm, 10.1 nm, 13 nm, and 20 nm, respectively. For the case of the hotplate in glovebox, QDs heated at 200 °C for 2 h, 250 °C for 1 h, 2 h, 3 h, and 300 °C for 1 h had an estimated diameter of 9.8 nm, 8.8 nm, 13.5 nm, 15 nm, and 10 nm, respectively. The average size of QDs/NPs in samples heated using RTA at 250 °C for 10 min, 300 °C for 10 min, and 350 °C for 3 min and 10 min was 18 nm, 30 nm, 27 nm, and 55 nm, respectively. For all QDs/NPs samples, the particles grew larger as the heating time and temperature increased.

Figure 3.3 shows the XRD pattern of PbS QDs/NPs synthesized under different heating methods. In Fig. 3.3(a), various temperatures and times were investigated for a hotplate in inert glovebox environment. The intensity of almost all of the PbS peaks becomes stronger, indicating an increase in the crystallinity of QDs/NPs with rising temperature (from 200 °C to 250 °C and 300 °C) for a

similar heating duration. In addition, as shown in Fig. 3.3(a), extending the heating period from 1 h to 3 h at 250 °C increases the intensity of the peaks, which also results in higher crystallinity. PbS QDs/NPs heated in a vacuum oven for various times and temperatures are shown in Fig. 3.3(b). As indicated in Fig. 3.3(b), increasing the temperature of the vacuum oven from 200 °C to 250 °C for 3 h heating time causes the intensity of the peak of (200) to increase, same for samples heated using the hotplate in a glovebox. Similarly, as shown in Fig. 3.3(b), increasing the heating period from 1 h to 3 h at 250° C in the vacuum oven, an increase in the intensity of (200) XRD is observed. Figure 3.3(c) shows XRD patterns of PbS QDs/NPs heated with the RTA. The sharpness of most of the peaks increases as the RTA temperature rises from 250 °C to 300 °C and 350 °C, indicating an increase in the degree of crystallinity of the QDs/NPs. This behavior was seen in all of the investigated heating methods and is in accord with other reports on NPs, including nanostructured magnetically tunable ceramics and nanostructured calcium phosphate[42–45]. One possible reason for this phenomenon can be the recovery of internal strain[46]. The crystallinity of samples heated in a vacuum oven and RTA is higher (XRD peaks are sharper) than the crystallinity of samples heated with a hotplate in a glovebox. The reason can be the more homogenous and efficient heating provided by the RTA compared with the standard chemical laboratory hot plate[47].

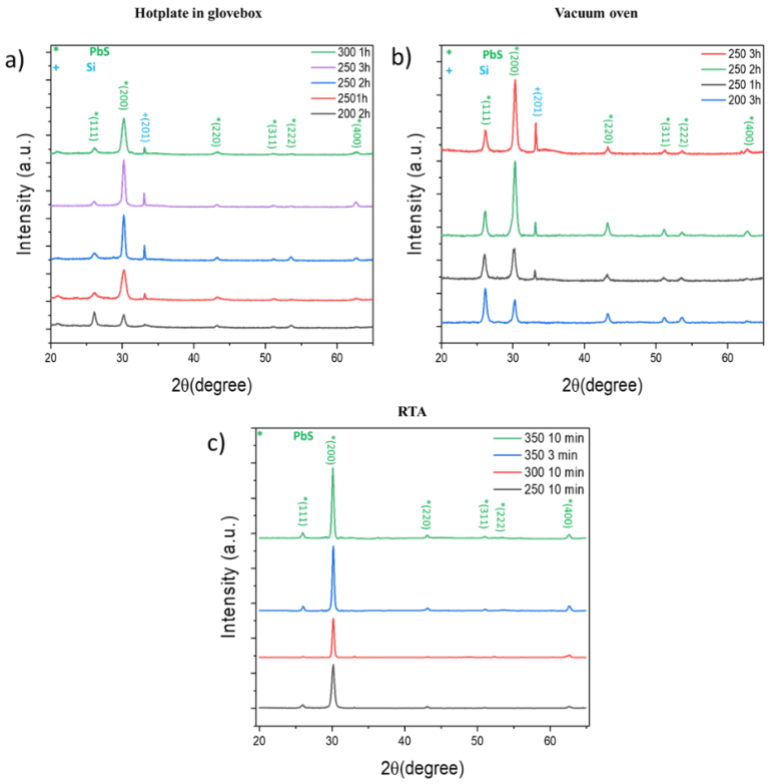

Figure 3.3 - XRD patterns of PbS QDs/NPs synthesized using an in situ reactive blade coating method and a) dried on a hotplate in glovebox heating, b) in vacuum oven heating, and c) in the RTA at different temperatures and times.

Figure A1 shows XRD peaks of PbS QDs heated on a hotplate at 250 °C for 3 h with different S ink concentrations. The S ink was diluted from top to bottom with 5 ml, 4 ml, and 3 ml OLA before blade coating, respectively. The SEM figures taken from these samples will be shown and discussed in the SEM part and Fig. A2.

Also, Fig. 3.4 shows the XRD of the PbS sample heated in the RTA at 300° C for 10 min under an oxygen environment. All previous samples heated using the RTA were kept under a nitrogen environment to avoid oxidation. Figure 3.4(a) shows the XRD peaks of the sample heated in oxygen, where most of the XRD peaks are related to $PbSO_4$ instead of PbS. Figure 3.4(b) shows samples heated at 300°C in nitrogen and oxygen for 10 min. It can be seen that the (200) peak of PbS is very weak in the sample under oxygen compared with the sample under nitrogen. In this case, most of the peaks are related to $PbSO_4$. The SEM and EDS tests taken from the sample treated in oxygen can be seen in Fig. A3, which will be discussed in the SEM part.

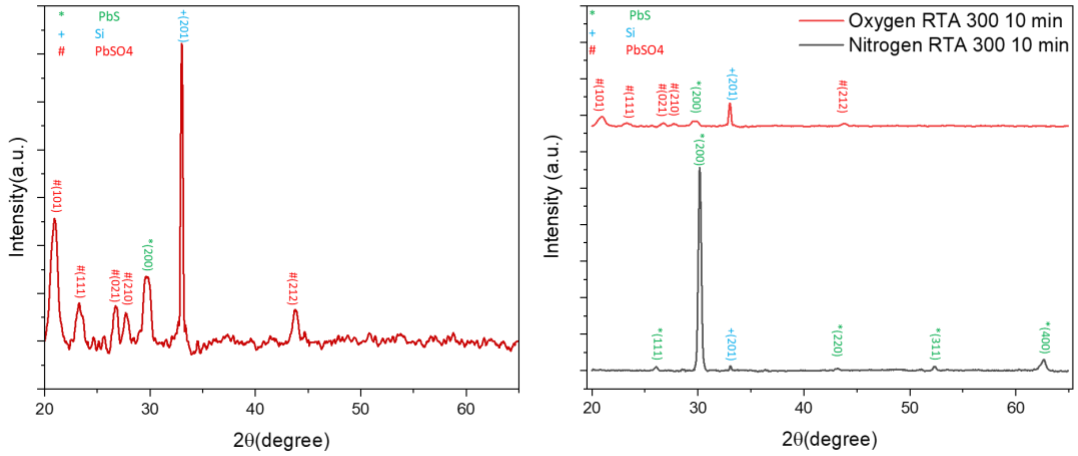

Figure 3.4 - XRD patterns of PbS QDs/NPs synthesized using in-situ reactive blade coating method dried with RTA at 300 °C for 10 min in a) oxygen environment and b) nitrogen environment.

3.4.2 Scanning Electron Microscope

Figures 3.5 to 3.8 show SEM images of the as-synthesized PbS samples, which were prepared using various heating methods. From Table 3.1, in all samples, the average size of QDs/NPs estimated from SEM figures is in agreement with the estimation of size of QDs/NPs using the FWHM of XRD peaks of the samples. Figure 3.5 shows different magnifications of SEM images for PbS QDs/NPs heated in the RTA under different conditions. Figures 3.5(a-b) and (d-e) show SEM images taken for PbS QDs/NPs heated in the RTA at 250 °C for 10 min. In this case, an average size of (15.8±2) nm (Fig. 3.5(c)) was seen. Whereas, at 300 °C and 10 min heat treatment time, the average particle size is (32±3.5) nm (Fig. 3.5(f)). A shape transition is seen from spherical to cubic when increasing the heating temperature. The possible reasons for this shape change, and a series of controlled experiments to investigate the conditions that give rise to this observation, will be explained in the next paragraph. SEM images of PbS NPs heated in an RTA at 350 °C for 3 min, and 10 min are also presented in Figs. 3.5(g-h) and (k-m), respectively. The average size of the obtained NPs is about (24±4) nm (Fig. 3.5(i)) for 3 min and (82±50) nm (Fig. 3.5(n)) for 10 min heating duration, respectively. As shown in Fig. 3.5, the QDs/NPs grow in size as the temperature rises and as the heating duration increases. At temperatures below 250 °C, the samples were not well-dried, so they weren't tested with RTA. As anticipated, the NPs grow much larger at temperatures higher than 350 °C, and thus, no investigation was performed.

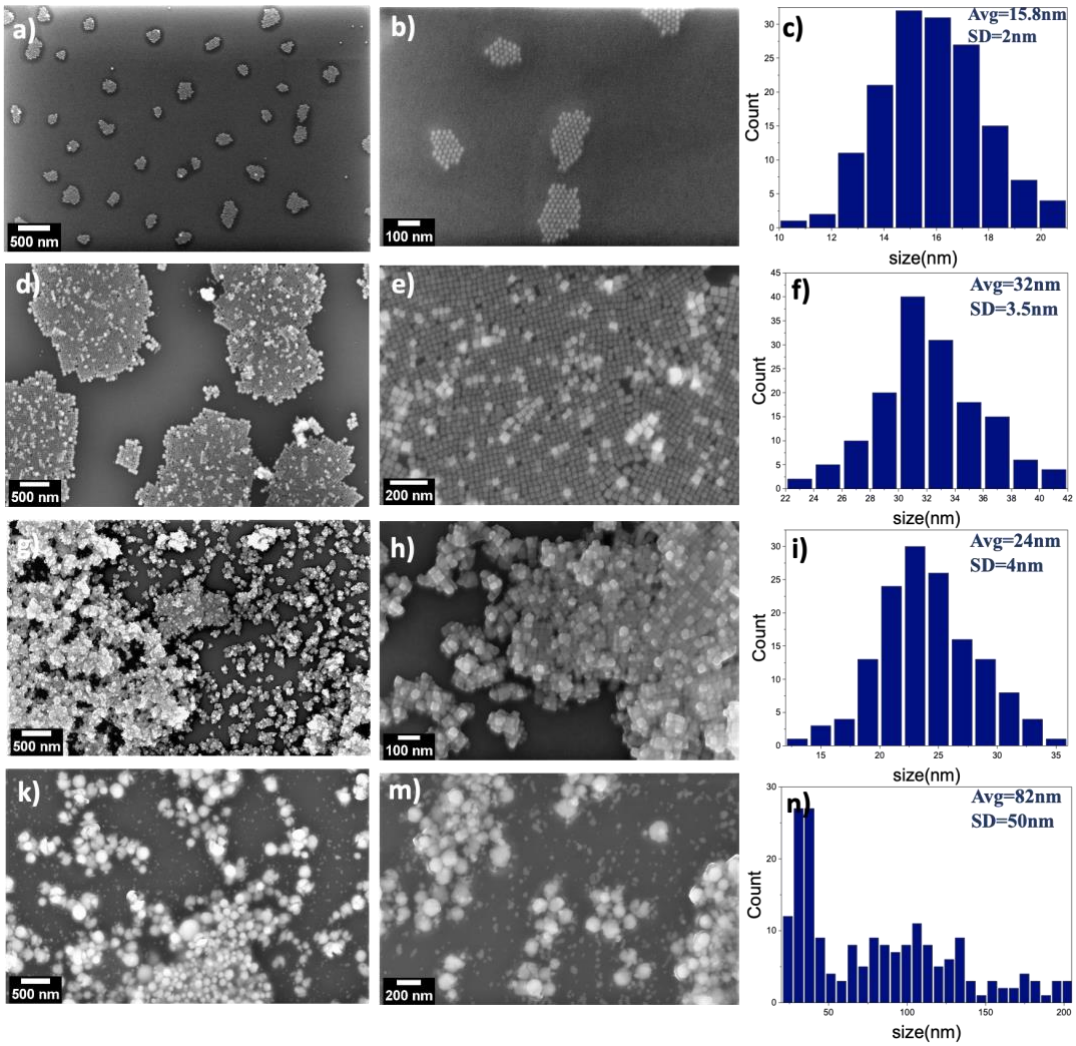

Figure 3.5 - SEM images of PbS QDs/NPs synthesized with the blade coating method and dried in the RTA at various magnifications. SEM and histogram showing size distributions of PbS QDs/NPS heated at (a-c) 250 °C for 10 min, (d-f) 300 °C for 10 min, (g-i) 350 °C for 3 min, and (k-n) 350 °C for 10 min.

Different shapes, such as cubic and spherical shapes of QDs/NPs, are seen in samples heated in the RTA at various temperatures and durations of heating. A series of controlled experiments to investigate the conditions of shape change of as-fabricated PbS QDs/NPs was performed. In Figure 3.6, different samples heated at 350 °C for 3, 4, 5, 8, and 10 min are shown, respectively. It is evident from the figures that in a sample that was heated at 350 °C for 3 min (Fig. 3.6 (a-c)) and 4 min (Fig. 3.6(e-g)), most of the QDs/NPs have cubic shapes. When the duration of heating is increased to 5 min (Fig. 3.6(j-m)), 8 min (Fig. 3.6(o-q)), and 10 min (Fig. 3.6(s-u)), the shape of the QDs/NPs become more spherical as time passes. The size of NPs heated at 350 °C for 3 min

(Fig. 3.6(d)), 4 min (Fig. 3.6(h)), 5 min (Fig. A6.(n)), 8 min (Fig. A6.(r)), and 10 min (Fig. A6.(v)) were about (24±4) nm, (34±15) nm, (41±19) nm, (65±32) nm, and (96±60) nm, respectively. A longer heating duration leads to larger NPs and a wider range of sizes for NPs.

In RTA, the heating process and cooling down cycles are much faster and better controlled compared to the hotplate or vacuum oven. Very intense heating in this process can result in structural changes in the QDs/NPs. This can be similar to nuclear rearrangements in NPs due to melting and fragmentation by heating with intense laser pulses, which was reported by Zhou et al.[48], who achieved spherical and nanorod gold NPs by changing the intensity of the exposed laser. Also, in another report, Al-Nassar et al.[49] discussed the effect of laser pulse energy on ZnO NPs formation. They mentioned that the interaction of the different laser pulses with the zinc could change the shapes, distribution, and sizes of ZnO NPs. In addition, longer heating times can allow for optimization of surface energy of the particles leading to the formation of spherical shapes of PbS QDs/NPs [50,51].

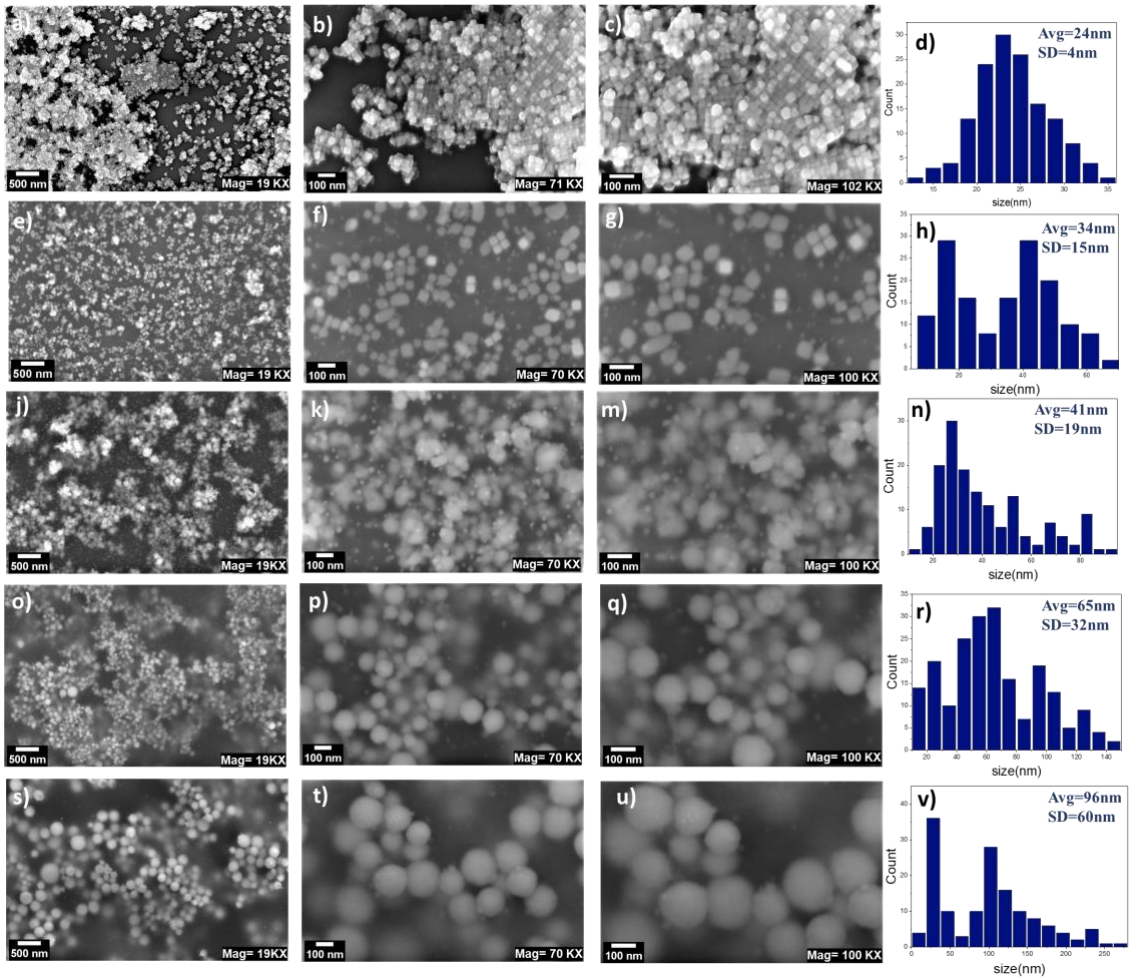

Figure 3.6 - Different magnification SEM images of PbS NPs synthesized with the blade coating method and dried in an RTA at 350 °C for different durations. SEM and histogram of the size distribution of PbS NPs heated in RTA (a-d) at 350 °C for 3 min, (e-h) 4 min, (j-n) 5 min, (o-r) 8 min, and (s-v) 10 min.

Figure 3.7 shows the SEM images of PbS QDs heated on a hotplate in a glovebox at 250 °C for 1 h (Fig. 3.7(a-b)), 250 °C for 2 h (Fig. 3.7(d-e)), 250 °C for 3 h (Fig. 3.7(g-h)), and 300 °C for 1 h (Fig. 3.7(k-m)), respectively. The estimated size of QDs was (6.8±0.8) nm (Fig. 3.7(c)), (8.5±1.4) nm (Fig. 3.7(f)), (9.2±1.2) nm (Fig. 3.7(i)), and (8.4±1.3) nm (Fig. 3.7(n)), respectively. It can be seen that with increasing heating and temperature duration, the QDs' sizes become larger. The temperature range studied in this heating method ranged from higher than 200 °C to lower than 300 °C. Because the films do not fully dry at temperatures lower than 250 °C (for instance, 2 hours heating at 200 °C), only the SEM of the best samples are shown in the Figure.

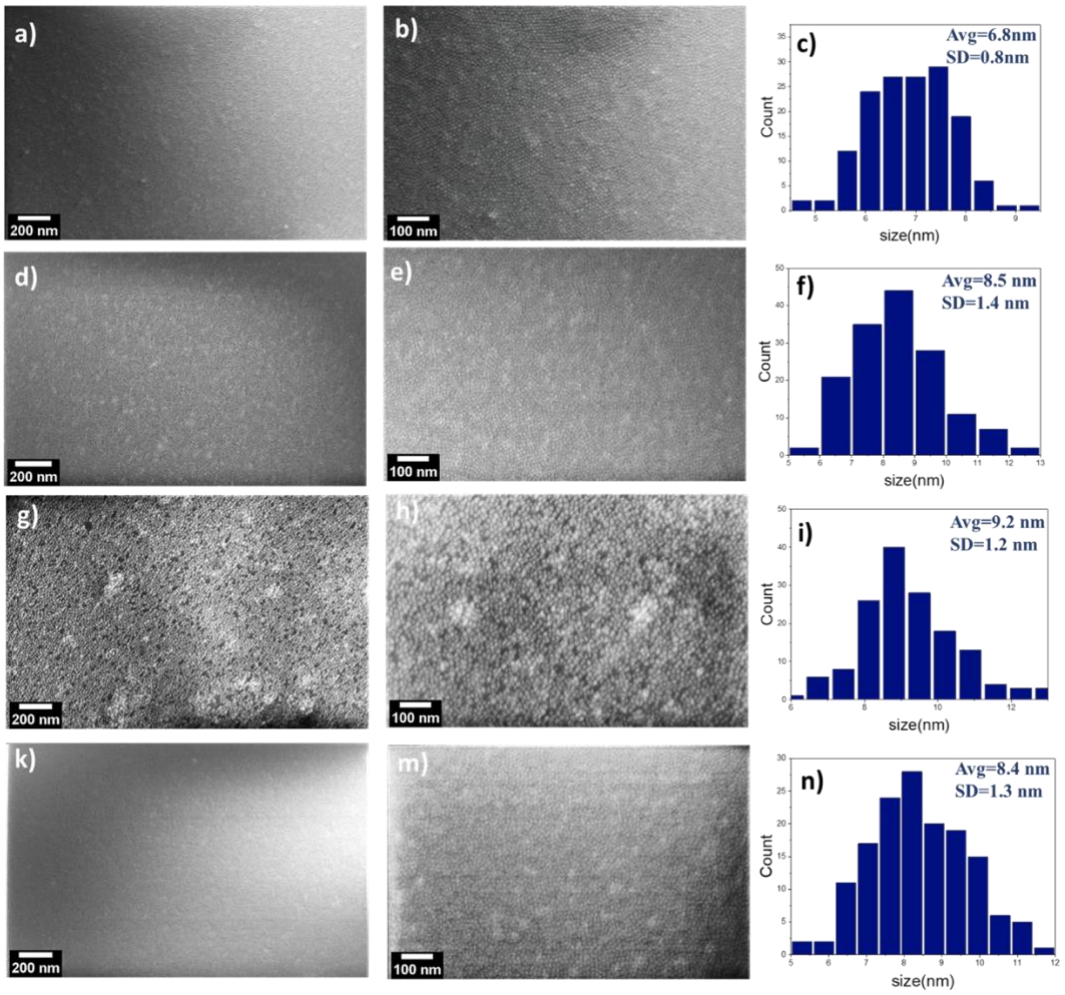

Figure 3.7 - Different magnification SEM images of PbS QDs synthesized with the blade coating method and dried with a hotplate in the glovebox. SEM and histogram of the size distribution of PbS QDs heated at (a-c) 250 °C for 1 h, (d-f) 250 °C for 2h, (g-i) 250 °C for 3 h, and (k-n) 300 °C for 1 h.

Also, Fig. A2 shows SEM images taken for PbS QDs heated on a hotplate in a glovebox for different concentrations of S ink (1 ml of S ink diluted with 3 ml, 4 ml, and 5 ml OLA, respectively) that were used in the blade coating process. QD sizes were (9.2±1.2) nm for diluting the S ink with 3 ml OLA, (9.8±1.5) nm for diluting the S ink with 4 ml OLA, and (9.3±1.3) nm for diluting the S ink with 5 ml OLA, respectively. It can be observed from the estimation of size and the figures that the average sizes of the QDs vary by less than 1 nm as the Sulfur concentration was changed. Zhao et al.[52] synthesized PbS QDs with a solventless system and did a PL test on their samples. They mentioned in their report that as they decreased the concentration of Sulfur source, a blue shift was seen in the PL peaks, which shows the size of QDs was becoming smaller with reducing the amount of Sulfur. Nevertheless, in our experiments, the effect of Sulfur concentration on the

size of QDs was insignificant, which can be attributable to the fact that a different synthesis technique was chosen in our case. Furthermore, since a change in concentration of S ink did not lead to any changes in QD size, changing the concentration of S ink parameter was not tried with other heating techniques.

Fig. 3.8 shows SEM images of PbS QDs/NPs heated with a vacuum oven. Figures 3.8(a-b) and (d-e) are SEM images of samples heated at 250 °C for 2 h and 3 h, respectively. The average size of the particles is (12.8±2.1) nm (Fig. 3.8(c)) and (24±3.8) nm (Fig. 3.8(f)), respectively. As the duration of heating increased from 2 h to 3 h, the size of QDs/NPs became larger. It is worth noting that the PbS sample did not completely dry after 1 hour of heating at 250°C and 3 hours at 200 °C, so only the best samples are shown in Fig. 3.8.

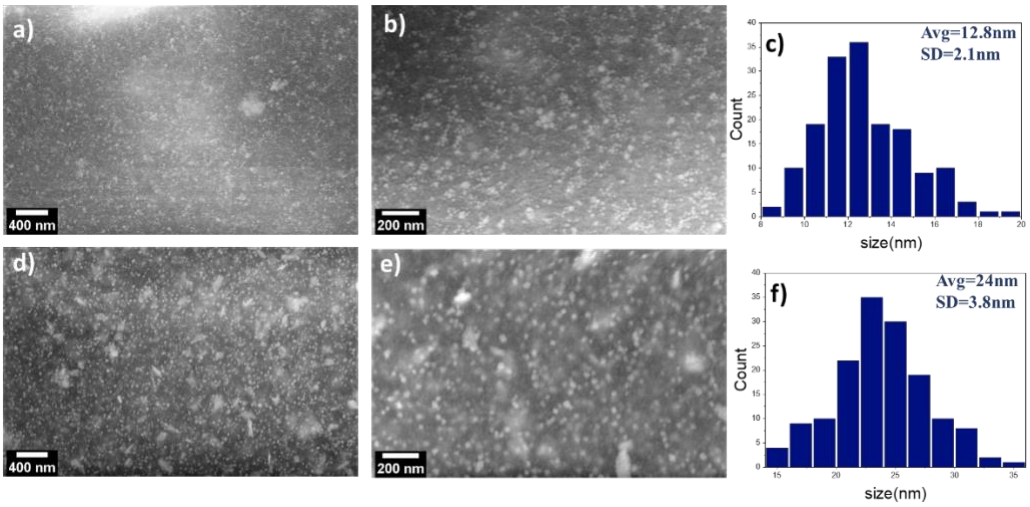

Figure 3.8 - Images with various magnifications of PbS QDs/NPs synthesized with the blade coating method and dried in a vacuum oven. Using a vacuum oven at 250 °C for 2 h, Fig. (a,b) show SEM, and (c) histogram of the size distribution of PbS QDs. Fig. (d,e) show SEM, and (f) a histogram of the size distribution of PbS NPs heated for 3 h at 250 °C.

Figure A3 shows the PbS samples heated in the RTA at 300 °C for 10 min under a nitrogen environment (Fig. A3(a-c)) and oxygen environment (Fig. A3(e-g)). The average size of the observed particles is (32±3.5) nm (Fig. A3(a) inset) and (9±1.5) nm (Fig. A3(e) inset), respectively. Energy-dispersive X-ray spectroscopy (EDS) test results of samples are shown in Fig. A3(d) (for sample heated under nitrogen) and Fig. A3(h) (for sample heated under oxygen). As expected, the EDS data reveals a large oxygen peak for sample heated under oxygen environment and smaller

Pb and S peaks compared to the sample under nitrogen. Also, based on XRD and EDS taken for these samples, most of the particles in the sample under oxygen are $PbSO_4$.

The EDS spectra of PbS QDs/NPs for the above-mentioned heating methods are shown in Fig. 3.9. As shown, all samples confirm the presence of Pb and S. The Si peak is due to the silicon substrate. An artificial carbon (C) peak is visible as a result of the elevated background counts in SEM-EDS. The aperture in the detector is responsible for this artefact [53]. Also, little oxygen peaks can be attributed to the contamination on the silicon substrates (possible presence of silicon oxide). This was confirmed by the EDS data of a bare silicon wafer (Fig. 3.9(d)). Furthermore, according to EDS quantitative measurement, the molar ratio of Pb to S was about 1:1.018, 1:1.017, and 1:1.02 for samples a-c (Fig. 3.9), respectively. These ratios are almost identical to stoichiometric PbS 1:1.

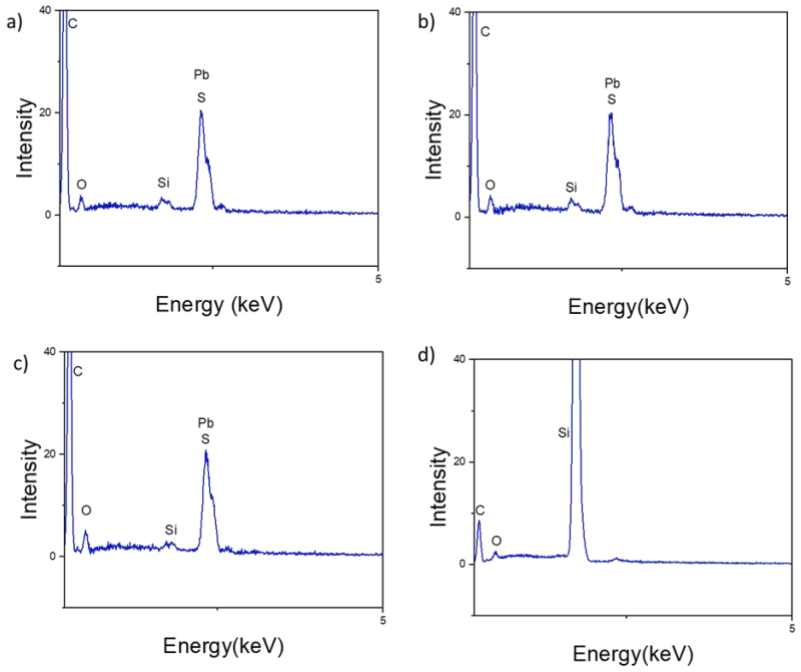

Figure 3.9 - EDS spectrum of PbS sample heated with a) vacuum oven, b) hotplate in the glovebox, c) RTA at 250 °C, and d) EDS spectrum of a bare clean Silicon substrate. (The y axis is cut short to make the smaller peaks visible)

Figures A4, A5, and A6 show the spin-coated PbS samples versus blade-coated samples heated with RTA, hotplate, and vacuum oven, respectively. It can be seen from the figures that for all of the investigated heating methods, the distribution of the QDs/NPs is more homogeneous in blade

coated than the spin coating. This difference may be attributed to the faster drying of spin coated films during the substrate's rapid rotation.

The attractiveness of blade coating lies in the fact that it is more scalable than spin coating because it is more readily adjustable for industrial roll-to-roll (R2R) manufacturing[26,54], compared to spin coating, which cannot be used in such setting[55–57]. The size of QDs/NPs formed with both coating techniques for the same heating method is comparable.

3.4.3 UV-vis absorption measurement

UV-vis measurement of PbS QDs/NPs was investigated in this report. First, the PbS QDs/NPs annealed with different heating methods were dissolved in toluene. Then the UV-vis absorption test was performed on the PbS solution. The absorption spectra of PbS QDs/NPs dissolved in Toluene is shown in Fig. 3.10(a). The estimated absorption band edge was in the range of 380-450 nm. Some works report the absorption of PbS QDs around 1000-1400 nm[58–60], and there are other reports in which they got absorption in the area that we got[61–65]. The reason for seeing this blue shift in wavelength compared to bulk PbS and getting absorption peaks in the UV-vis region was explained in Li et al.[64] and Borhade et al.[61] works. They mentioned that by decreasing the size of PbS particles from bulk to nanometer size, a blue shift is seen from an absorption onset of 3200 nm to UV-vis region absorption due to the quantum size effect. Also, in Zhao et al.[62] work, they explained that these spectra might not correspond to excitonic transitions, but the spectra might be related to transition to higher energy bands.

3.4.4 Photoluminance

Photoluminance (PL) measurement of PbS QDs/NPs was performed in the 400-700 nm range. Figure 3.10(b-d) shows PL emission spectra of PbS samples for the various heating methods. All samples were excited at a wavelength of λ= 350 nm. In Fig. 3.10(b), the PL emission of four different PbS samples heated in a vacuum oven at 200 °C for 3 h, and 250 °C for 1 h, 2 h, and 3 h is shown. The images indicate a slight red shift in the PL peaks with increased heating. Also, comparing the PL peaks for samples heated at 200 °C for 3 h (PL peak at 416 nm) and samples heated at 250 °C for 3 h (PL peak at 423 nm), a red shift is seen. In Fig. 3.10(c), PL emission of PbS QDs/NPs heated at three different temperatures (250 °C,300 °C, and 350 °C) for two different durations (10 min and 3 min) with RTA are shown. The red shift in the PL emission peak is seen

when the temperature is increased from 250 °C (PL peak at 407 nm) to 300 °C (PL peak at 412 nm) and 350 °C (PL peak at 418 nm) for 10 min of heating. With increasing the temperature to 350 °C while heating for a shorter period of time (3 min) (PL peak at 410 nm), a slight red shift is seen compared to 250 °C (10 min heating). In Fig. 3.10(d), PL emission of PbS QDs heated on a hotplate at three different temperatures (200 °C, 250 °C, and 300 °C) for different amounts of times (1 h and 2 h and 3 h) is shown. As the temperature was increased from 250 °C at 1 h (PL peak at 403 nm) to 300 °C at 1 h (PL peak at 410 nm), a slight red shift was observed. Also, a red shift was seen as the temperature was increased from 200 °C (PL peak at 405 nm) to 250 °C (PL peak at 412 nm) for 2 h heating, and as the heating period was extended from 1 h (PL peak at 403 nm) to 2 h (PL peak at 412 nm) and 3 h (PL peak at 418 nm) at 250 °C. For all samples in Fig. 3.10p(b-d), the redshift in PL peaks is attributed to an increase in the size of QDs/NPs (Table 3.1).

The PL tests show that the range of emitted light from the PbS QDs/NPs is in the UV-visible region. Some literature in this field documents an emission in the Near IR region from PbS QDs/NPs[58,63,66,67]. However, there have been several reports on PbS QDs/NPs emitting light in the UV-visible range in a PL test under UV light exciation[61,62,68–73]. Bhatt et al. reported that their 15 nm PbS QDs showed PL emission at 405 nm (λ_{ex} = 345 nm) with an absorption edge at 382 nm. They stated that the reason for getting PL peaks in this range is due to the quantum confinement effect[63]. In another work, Pawar et al. made PbS NPs in the 23-34 nm size range. According to their report, the emission bands found in the UV-vis range (405 nm) were related to electrons transitioning from the conduction band to holes trapped in states such as interstitial Pb^{2+} sites. Another possibility is that the observed peaks are not related to excitonic transition but are related to transitions to higher energy bands[74].

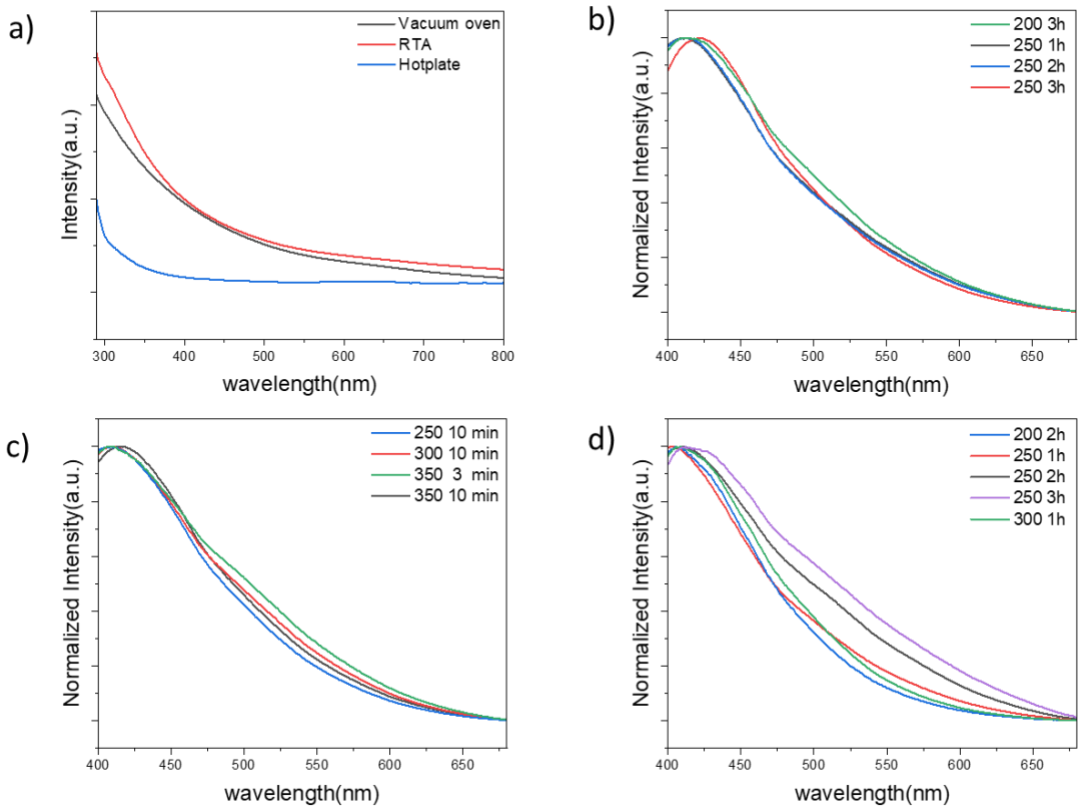

Figure 3.10 - (a) UV-VIS absorption spectrum of PbS QDs/NPs dissolved in toluene heated with oven, hotplate, and RTA at 250 ℃. Photoluminescence spectra of PbS QDs/NPs heated with (b) oven, (c) RTA, and (d) hotplate at different temperatures for different time duration.

3.5 Conclusion

In-situ reactive blade coating procedure was used in this study to demonstrate a one-step synthesis and coating of self-assembled PbS QDs/NPs. Different heating methods were used to treat the blade-coated PbS QDs/NPs, such as a vacuum oven, a hotplate in a glovebox, and RTA. Various heating and synthesizing parameters, such as heating temperature and heating duration, were investigated in each heating method. Based on the characteristics and details of each heating procedure, PbS particles of various shapes and sizes were produced. Using various heating approaches in a reactive blade coating process will allow for specifically manufactured QDs/NPs with adjustable shapes and sizes and various physical and chemical properties. Based on our results, samples heated with RTA had high crystallinity XRD peaks compared to other heating

approaches. Moreover, different shapes of QDs/NPs were obtained when RTA was used, making it a preferable approach for heating and drying PbS particles. Blade coating is compatible with R2R manufacturing and can be instrumental in large scale manufacturing of nanomaterials. This facile approach will help accelerate the development of low-cost production of PbS QDs/NPS and other binary QDs. Furthermore, the blade-coated thin films could be utilized in optoelectronic devices like solar cells, LEDs, and optical sensors, to mention a few.

3.6 References

[1] Murray C B, Norris D J and Bawendi M G 1993 Synthesis and characterization of nearly monodisperse CdE (E = sulfur, selenium, tellurium) semiconductor nanocrystallites *J. Am. Chem. Soc.* **115** 8706–15

[2] Kovalenko M V, Manna L, Cabot A, Hens Z, Talapin D V, Kagan C R, Klimov V I, Rogach A L, Reiss P, Milliron D J, Guyot-Sionnnest P, Konstantatos G, Parak W J, Hyeon T, Korgel B A, Murray C B and Heiss W 2015 Prospects of Nanoscience with Nanocrystals *ACS Nano* **9** 1012–57

[3] Gaponik N, Talapin D V, Rogach A L, Hoppe K, Shevchenko E V, Kornowski A, Eychmüller A and Weller H 2002 Thiol-Capping of CdTe Nanocrystals: An Alternative to Organometallic Synthetic Routes *J. Phys. Chem. B* **106** 7177–85

[4] Jagannadham K, Howe J and Allard L F 2010 Laser physical vapor deposition of nanocrystalline dots using nanopore filters *Appl. Phys. A* **98** 285–92

[5] Zhou J, Yang Y and Zhang C 2015 Toward Biocompatible Semiconductor Quantum Dots: From Biosynthesis and Bioconjugation to Biomedical Application *Chem. Rev.* **115** 11669–717

[6] Owen J and Brus L 2017 Chemical Synthesis and Luminescence Applications of Colloidal Semiconductor Quantum Dots *J. Am. Chem. Soc.* **139** 10939–43

[7] Permatasari F A, Aimon A H, Iskandar F, Ogi T and Okuyama K 2016 Role of C–N Configurations in the Photoluminescence of Graphene Quantum Dots Synthesized by a Hydrothermal Route *Sci Rep* **6** 21042

[8] Yu J, Xu C, Tian Z, Lin Y and Shi Z 2016 Facilely synthesized N-doped carbon quantum dots with high fluorescent yield for sensing Fe 3+ *New Journal of Chemistry* **40** 2083–8

[9] Lin K-F, Cheng H-M, Hsu H-C, Lin L-J and Hsieh W-F 2005 Band gap variation of size-controlled ZnO quantum dots synthesized by sol–gel method *Chemical Physics Letters* **409** 208–11

[10] Allen P M and Bawendi M G 2008 Ternary I−III−VI Quantum Dots Luminescent in the Red to Near-Infrared *J. Am. Chem. Soc.* **130** 9240–1

[11] Tian R, Zhong S, Wu J, Jiang W, Shen Y, Jiang W and Wang T 2016 Solvothermal method to prepare graphene quantum dots by hydrogen peroxide *Optical Materials* **60** 204–8

[12] Jiang Y, Wang B, Meng F, Cheng Y and Zhu C 2015 Microwave-assisted preparation of N-doped carbon dots as a biosensor for electrochemical dopamine detection *Journal of Colloid and Interface Science* **452** 199–202

[13] Haverinen H M, Myllylä R A and Jabbour G E 2009 Inkjet printing of light emitting quantum dots *Appl. Phys. Lett.* **94** 073108

[14] Hu Z, Yin Y, Ali M U, Peng W, Zhang S, Li D, Zou T, Li Y, Jiao S, Chen S, Lee C-Y, Meng H and Zhou H 2020 Inkjet printed uniform quantum dots as color conversion layers for full-color OLED displays *Nanoscale* **12** 2103–10

[15] Jung S, Sou A, Banger K, Ko D-H, Chow P C Y, McNeill C R and Sirringhaus H 2014 All-Inkjet-Printed, All-Air-Processed Solar Cells *Advanced Energy Materials* **4** 1400432

[16] Pace G, Grimoldi A, Sampietro M, Natali D and Caironi M 2015 Printed photodetectors *Semicond. Sci. Technol.* **30** 104006

[17] Facsko S, Kurz H and Dekorsy T 2001 Energy dependence of quantum dot formation by ion sputtering *Phys. Rev. B* **63** 165329

[18] Kumar D, Agarwal G, Tripathi B, Vyas D and Kulshrestha V 2009 Characterization of PbS nanoparticles synthesized by chemical bath deposition *Journal of Alloys and Compounds* **484** 463–6

[19] Anikeeva P O, Madigan C F, Halpert J E, Bawendi M G and Bulović V 2008 Electronic and excitonic processes in light-emitting devices based on organic materials and colloidal quantum dots *Phys. Rev. B* **78** 085434

[20] Chen M, Lee H, Yang J, Xu Z, Huang N, Chan B P and Kim J T 2020 Parallel, Multi-Material Electrohydrodynamic 3D Nanoprinting *Small* **16** 1906402

[21] Kurley J M, Pan J-A, Wang Y, Zhang H, Russell J C, Pach G F, To B, Luther J M and Talapin D V 2021 Roll-To-Roll Friendly Solution-Processing of Ultrathin, Sintered CdTe Nanocrystal Photovoltaics *ACS Appl. Mater. Interfaces* **13** 44165–73

[22] Arango A C, Oertel D C, Xu Y, Bawendi M G and Bulović V 2009 Heterojunction Photovoltaics Using Printed Colloidal Quantum Dots as a Photosensitive Layer *Nano Lett.* **9** 860–3

[23] Cook B, Gong M, Ewing D, Casper M, Stramel A, Elliot A and Wu J 2019 Inkjet Printing Multicolor Pixelated Quantum Dots on Graphene for Broadband Photodetection *ACS Appl. Nano Mater.* **2** 3246–52

[24] Sliz R, Lejay M, Fan J Z, Choi M-J, Kinge S, Hoogland S, Fabritius T, García de Arquer F P and Sargent E H 2019 Stable Colloidal Quantum Dot Inks Enable Inkjet-Printed High-Sensitivity Infrared Photodetectors *ACS Nano* **13** 11988–95

[25] Abulikemu M, Da'as E H, Haverinen H, Cha D, Malik M A and Jabbour G E 2014 In Situ Synthesis of Self-Assembled Gold Nanoparticles on Glass or Silicon Substrates through Reactive Inkjet Printing *Angewandte Chemie* **126** 430–3

[26] Abulikemu M, Tabrizi B E A, Ghobadloo S M, Mofarah H M and Jabbour G E 2022 Silver Nanoparticle-Decorated Personal Protective Equipment for Inhibiting Human Coronavirus Infectivity *ACS Appl. Nano Mater.* **5** 309–17

[27] Shuklov I A, Toknova V F, Lizunova A A and Razumov V F 2020 Controlled aging of PbS colloidal quantum dots under mild conditions *Materials Today Chemistry* **18** 100357

[28] Bertolotti F, Dirin D N, Ibáñez M, Krumeich F, Cervellino A, Frison R, Voznyy O, Sargent E H, Kovalenko M V, Guagliardi A and Masciocchi N 2016 Crystal symmetry breaking and vacancies in colloidal lead chalcogenide quantum dots *Nature Mater* **15** 987–94

[29] Hou B, Cho Y, Kim B-S, Ahn D, Lee S, Bae Park J, Lee Y-W, Hong J, Im H, M. Morris S, Inn Sohn J, Cha S and Min Kim J 2017 Red green blue emissive lead sulfide quantum dots: heterogeneous synthesis and applications *Journal of Materials Chemistry C* **5** 3692–8

[30] Günes S, Fritz K P, Neugebauer H, Sariciftci N S, Kumar S and Scholes G D 2007 Hybrid solar cells using PbS nanoparticles *Solar Energy Materials and Solar Cells* **91** 420–3

[31] Choi J J, Lim Y-F, Santiago-Berrios M B, Oh M, Hyun B-R, Sun L, Bartnik A C, Goedhart A, Malliaras G G, Abruña H D, Wise F W and Hanrath T 2009 PbSe Nanocrystal Excitonic Solar Cells *Nano Lett.* **9** 3749–55

[32] Ren Z, Sun J, Li H, Mao P, Wei Y, Zhong X, Hu J, Yang S and Wang J 2017 Bilayer PbS Quantum Dots for High-Performance Photodetectors *Advanced Materials* **29** 1702055

[33] Torquemada M C, Rodrigo M T, Vergara G, Sánchez F J, Almazán R, Verdú M, Rodríguez P, Villamayor V, Gómez L J, Montojo M T and Muñoz A 2003 Role of halogens in the mechanism of sensitization of uncooled PbSe infrared photodetectors *Journal of Applied Physics* **93** 1778–84

[34] Ma X, Xu F, Benavides J and Cloutier S G 2012 High performance hybrid near-infrared LEDs using benzenedithiol cross-linked PbS colloidal nanocrystals *Organic Electronics* **13** 525–31

[35] Lee S-M, Jun Y, Cho S-N and Cheon J 2002 Single-Crystalline Star-Shaped Nanocrystals and Their Evolution: Programming the Geometry of Nano-Building Blocks *J. Am. Chem. Soc.* **124** 11244–5

[36] Moreels I, Lambert K, Smeets D, De Muynck D, Nollet T, Martins J C, Vanhaecke F, Vantomme A, Delerue C, Allan G and Hens Z 2009 Size-Dependent Optical Properties of Colloidal PbS Quantum Dots *ACS Nano* **3** 3023–30

[37] Hines M A and Scholes G D 2003 Colloidal PbS Nanocrystals with Size-Tunable Near-Infrared Emission: Observation of Post-Synthesis Self-Narrowing of the Particle Size Distribution *Advanced Materials* **15** 1844–9

[38] Rosiles-Perez C, Serrano-Estrada M A, Sidhik S, Alatorre-Ordaz A, Torres-Castro A, Vallejo M A, Jiménez-González A E and López-Luke T 2020 Synthesis of high quality PbS

colloidal quantum dots by ultrasonic bath as photosensitizers in a TiO2 solar cell *Journal of Solid State Chemistry* **292** 121720

[39] Zhang J, Gao J, Miller E M, Luther J M and Beard M C 2014 Diffusion-Controlled Synthesis of PbS and PbSe Quantum Dots with *in Situ* Halide Passivation for Quantum Dot Solar Cells *ACS Nano* **8** 614–22

[40] Mondal A and Mukherjee N 2006 Cubic PbS thin films on TCO glass substrate by galvanic technique *Materials Letters* **60** 2672–4

[41] Wei S, Guo C, Wang L, Xu J and Dong H 2021 Bacterial synthesis of PbS nanocrystallites in one-step with L-cysteine serving as both sulfur source and capping ligand *Sci Rep* **11** 1216

[42] Hong Z, Liu A, Chen L, Chen X and Jing X 2009 Preparation of bioactive glass ceramic nanoparticles by combination of sol–gel and coprecipitation method *Journal of Non-Crystalline Solids* **355** 368–72

[43] Alves Cardoso D, Jansen J A and G. Leeuwenburgh S C 2012 Synthesis and application of nanostructured calcium phosphate ceramics for bone regeneration *Journal of Biomedical Materials Research Part B: Applied Biomaterials* **100B** 2316–26

[44] Pang Y X and Bao X 2003 Influence of temperature, ripening time and calcination on the morphology and crystallinity of hydroxyapatite nanoparticles *Journal of the European Ceramic Society* **23** 1697–704

[45] Ginzburg M, MacLachlan M J, Yang S M, Coombs N, Coyle T W, Raju N P, Greedan J E, Herber R H, Ozin G A and Manners I 2002 Genesis of Nanostructured, Magnetically Tunable Ceramics from the Pyrolysis of Cross-Linked Polyferrocenylsilane Networks and Formation of Shaped Macroscopic Objects and Micron Scale Patterns by Micromolding Inside Silicon Wafers *J. Am. Chem. Soc.* **124** 2625–39

[46] Tavangarian F, Emadi R and Shafyei A 2010 Influence of mechanical activation and thermal treatment time on nanoparticle forsterite formation mechanism *Powder Technology* **198** 412–6

[47] Zhou Q, Jin Z, Li H and Wang J 2016 Enhancing performance and uniformity of CH3NH3PbI3−xClx perovskite solar cells by air-heated-oven assisted annealing under various humidities *Sci Rep* **6** 21257

[48] Link S and El-Sayed M A 2000 Shape and size dependence of radiative, non-radiative and photothermal properties of gold nanocrystals *International Reviews in Physical Chemistry* **19** 409–53

[49] Al-Nassar S I, Hussein F I and M A K 2019 The effect of laser pulse energy on ZnO nanoparticles formation by liquid phase pulsed laser ablation *Journal of Materials Research and Technology* **8** 4026–31

[50] Amendola V and Meneghetti M 2013 What controls the composition and the structure of nanomaterials generated by laser ablation in liquid solution? *Phys. Chem. Chem. Phys.* **15** 3027–46

[51] Kim K J, Han H, Defferriere T, Yoon D, Na S, Kim S J, Dayaghi A M, Son J, Oh T-S, Jang H M and Choi G M 2019 Facet-Dependent *in Situ* Growth of Nanoparticles in Epitaxial Thin Films: The Role of Interfacial Energy *J. Am. Chem. Soc.* **141** 7509–17

[52] Zhao H, Chaker M and Ma D 2009 Bimodal Photoluminescence during the Growth of PbS Quantum Dots *J. Phys. Chem. C* **113** 6497–504

[53] Anon Practical Electron Microscopy and Database - An Online Book

[54] Cheng J, Liu F, Tang Z and Li Y 2021 Scalable Blade Coating: A Technique Accelerating the Commercialization of Perovskite-Based Photovoltaics *Energy Technology* **9** 2100204

[55] Tseng S-R, Meng H-F, Lee K-C and Horng S-F 2008 Multilayer polymer light-emitting diodes by blade coating method *Appl. Phys. Lett.* **93** 153308

[56] Choudhary K, Chen A X, Pitch G M, Runser R, Urbina A, Dunn T J, Kodur M, Kleinschmidt A T, Wang B G, Bunch J A, Fenning D P, Ayzner A L and Lipomi D J 2021 Comparison of the Mechanical Properties of a Conjugated Polymer Deposited Using Spin Coating, Interfacial Spreading, Solution Shearing, and Spray Coating *ACS Appl. Mater. Interfaces* **13** 51436–46

[57] Kim J H, Williams S T, Cho N, Chueh C-C and Jen A K-Y 2015 Enhanced Environmental Stability of Planar Heterojunction Perovskite Solar Cells Based on Blade-Coating *Advanced Energy Materials* **5** 1401229

[58] Bakueva L, Musikhin S, Hines M A, Chang T-W F, Tzolov M, Scholes G D and Sargent E H 2003 Size-tunable infrared (1000–1600 nm) electroluminescence from PbS quantum-dot nanocrystals in a semiconducting polymer *Appl. Phys. Lett.* **82** 2895–7

[59] Debellis D, Gigli G, ten Brinck S, Infante I and Giansante C 2017 Quantum-Confined and Enhanced Optical Absorption of Colloidal PbS Quantum Dots at Wavelengths with Expected Bulk Behavior *Nano Lett.* **17** 1248–54

[60] Ellingson R J, Beard M C, Johnson J C, Yu P, Micic O I, Nozik A J, Shabaev A and Efros A L 2005 Highly Efficient Multiple Exciton Generation in Colloidal PbSe and PbS Quantum Dots *Nano Lett.* **5** 865–71

[61] Borhade A V and Uphade B K 2012 A comparative study on characterization and photocatalytic activities of PbS and Co doped PbS nanoparticles *Chalcogenide Lett* **9** 299–306

[62] Zhao P, Wang J, Cheng G and Huang K 2006 Fabrication of Symmetric Hierarchical Hollow PbS Microcrystals via a Facile Solvothermal Process *J. Phys. Chem. B* **110** 22400–6

[63] Bhatt S V, Deshpande M P, Chaki S H, Patel N H, Pandy N and Soni B H 2011 Chemical Synthesis and Characterization of Lead Sulphide (PbS) Nanoparticles *AIP Conference Proceedings* **1349** 281–2

[64] Li C, Zhao Y, Li F, Shi Z and Feng S 2010 Near-Infrared Absorption of Monodisperse Water-Soluble PbS Colloidal Nanocrystal Clusters *Chem. Mater.* **22** 1901–7

[65] U P, Gowda K M A, M g E, Teja B S, N N and Mohan B R 2017 Biologically synthesized PbS nanoparticles for the detection of arsenic in water *International Biodeterioration & Biodegradation* **119** 78–86

[66] Gao J, Zhang J, van de Lagemaat J, Johnson J C and Beard M C 2014 Charge Generation in PbS Quantum Dot Solar Cells Characterized by Temperature-Dependent Steady-State Photoluminescence *ACS Nano* **8** 12814–25

[67] Liu C, Heo J, Zhang X and Adam J-L 2008 Photoluminescence of PbS quantum dots embedded in glasses *Journal of Non-Crystalline Solids* **354** 618–23

[68] Mamiyev Z Q and Balayeva N O 2015 Preparation and optical studies of PbS nanoparticles *Optical Materials* **46** 522–5

[69] Zhang J 2011 Synthesis via an organic molten salt solvent route and characterization of PbS nanocrystals *Crystal Research and Technology* **46** 1058–64

[70] Kaci S, Keffous A, Trari M, Fellahi O, Menari H, Manseri A and Guerbous L 2010 Relationship between crystal morphology and photoluminescence in polynanocrystalline lead sulfide thin films *Journal of Luminescence* **130** 1849–56

[71] Liu S, Xiong S, Bao K, Cao J and Qian Y 2009 Shape-Controlled Preparation of PbS with Various Dendritic Hierarchical Structures with the Assistance of L -Methionine *J. Phys. Chem. C* **113** 13002–7

[72] Hu Y, Chen J, Jin X and Chen W 2005 Synthesis of hollow lead sulfide microspheres *Materials Letters* **59** 234–7

[73] Hou B, Cho Y, Kim B-S, Ahn D, Lee S, Park J B, Lee Y-W, Hong J, Im H, Morris S M, Sohn J I, Cha S and Kim J M 2017 Red green blue emissive lead sulfide quantum dots: heterogeneous synthesis and applications *J. Mater. Chem. C* **5** 3692–8

[74] Pawar S B, Shaikh J S, Devan R S, Ma Y R, Haranath D, Bhosale P N and Patil P S 2011 Facile and low cost chemosynthesis of nanostructured PbS with tunable optical properties *Applied Surface Science* **258** 1869–75

Supporting Information A: Chapter 3

Synthesis of Self-Assembled PbS Quantum Dots Using Reactive Blade Coating

Kimia Rezaei Shad[1], Mutalifu Abulikemu[1], and Ghassan E. Jabbour[1]*

[1]School of Electrical Engineering and Computer Science, University of Ottawa,

800 King Edward Ave., Ottawa, ON, Canada K1N 6N5

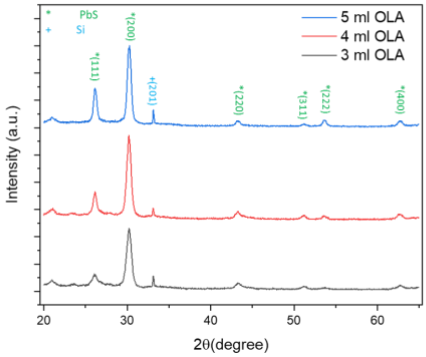

Figure A 1 - XRD patterns of PbS QDs/NPs synthesized using in-situ reactive blade coating method and with different dilutions of S ink, followed by heating on a hotplate in an inert glovebox.

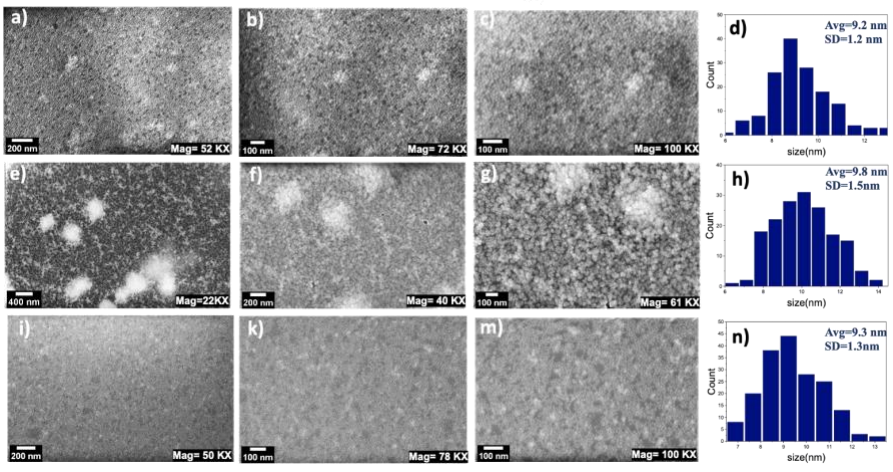

Figure A 2 – a)-c), e)-g), and i)-m) SEM images of different magnifications of PbS QDs synthesized with blade coating method and heated with hotplate in glovebox. d), h), and n) histogram of size

distribution of PbS QDs heated with hotplate at: a)-c) 250 °C for 3 hours with diluted S ink and 3 ml OLA, e)-g) 250 °C for 3 hours with diluted S ink and 4 ml OLA, and i)-m) 250 °C for 3 hours with diluted S ink and 5 ml OLA.

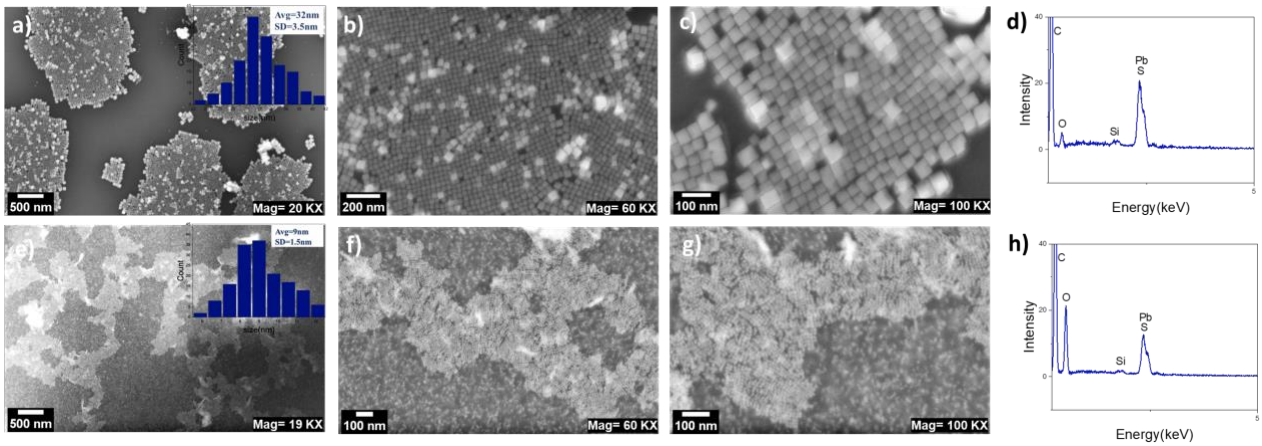

Figure A 3 – a)-c) SEM images and d) EDS spectrum of PbS QDs heated with RTA at 300 °C for 10 min under nitrogen environment. e)-g) SEM and h) EDS spectrum of PbS QDs heated with RTA at 300 °C for 10 min under oxygen environment. Histograms of size distribution of PbS QDs heated with RTA at 300 °C for 10 min under nitrogen and oxygen environments are shown in inset of a) and e), respectively.

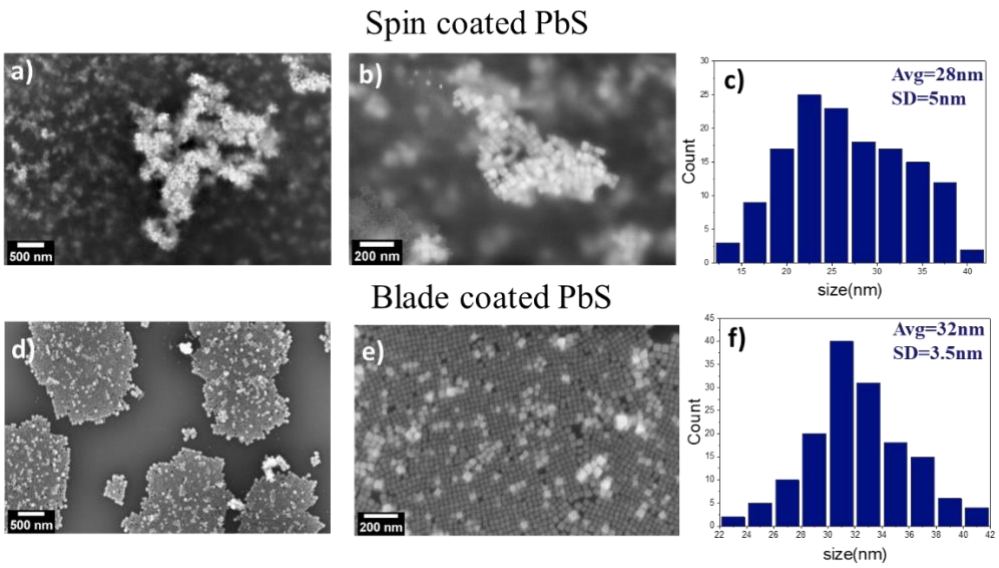

Figure A 4 - Different magnification SEM images of PbS QDs/NPs synthesized with reactive blade coating method and spin coating method, heat treated with RTA at 300 °C for 10 min.

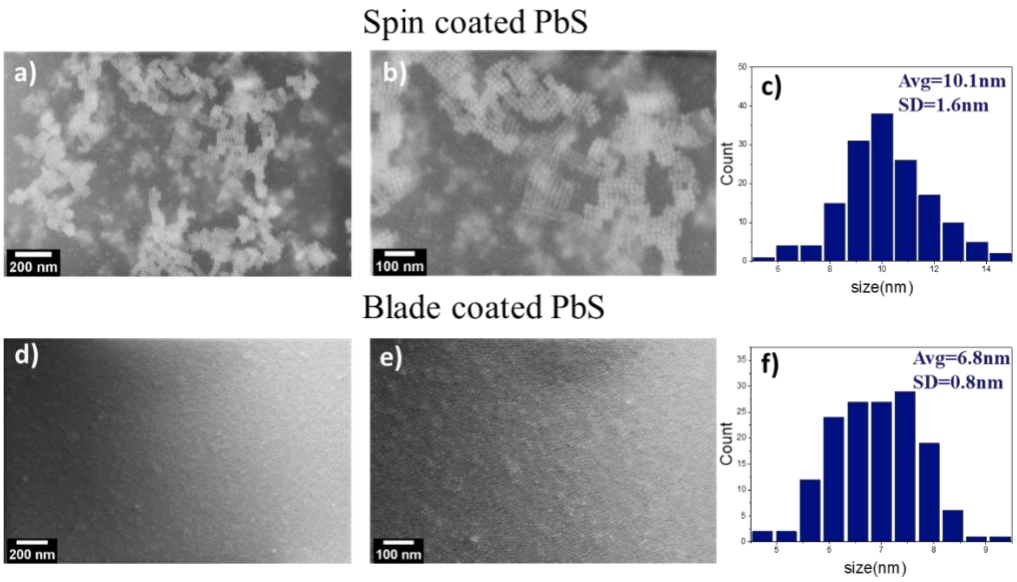

Figure A 5 - Different magnification SEM images of PbS QDs/NPs synthesized with reactive blade coating method and spin coating method and heat treated using a hotplate in an inert environment glovebox at 250 °C for 1 hour duration.

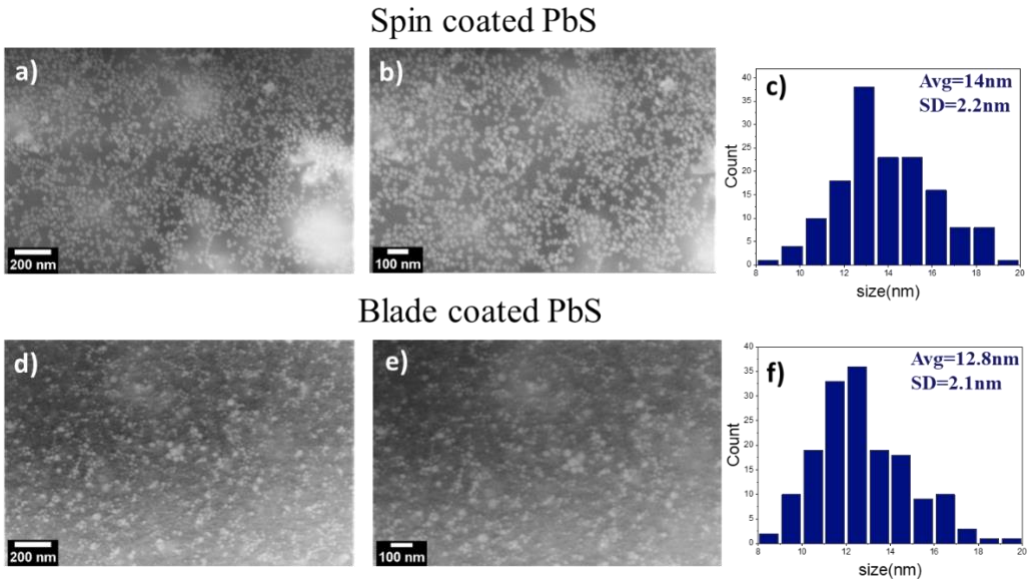

Figure A 6 - Different magnification SEM images of PbS QDs/NPs synthesized with reactive blade coating method and spin coating method, dried with vacuum oven at 250 °C for 2 hours duration.

Chapter 4 . CIS quantum dots

The following article is going to be submitted for publication.

In-situ Reactive $CuInS_2$ Quantum dots synthesis: Impact of selected heating methods

Kimia Rezaei Shad[1], Mutalifu Abulikemu[1], and Ghassan E. Jabbour[1]*

[1]School of Electrical Engineering and Computer Science, University of Ottawa,

800 King Edward Ave., Ottawa, ON, Canada K1N 6N5

*Corresponding Author: gja@uOttawa.ca

4.1 Abstract

Ternary I-III−VI_2 structures such as $CuInS_2$ (CIS), which are low-cost materials free of toxic heavy metals and, consequently, possess little environmental impact, are potential substitutes for hazardous binary structures such as PbS in various applications such as biological, optoelectronic, and bioelectric applications. Most techniques for the synthesis and deposition of CIS quantum dots (QDs) are costly and impractical for large-scale fabrications. Nevertheless, the in-situ reactive synthesis and deposition technique has attracted considerable interest due to its versatility and cost-effectiveness. This report introduces the first systematic in-situ reactive synthesis of CIS QDs/nanoparticles (NPs) produced by the rapid thermal annealing (RTA) heating method. CIS QDs/NPs of various diameters have been investigated by varying synthesis parameters such as heat treatment time and temperature. In addition, efforts have been made to increase the wettability of the substrate in an effort to obtain a more uniform coverage of the CIS thin film on a silicon substrate. In this regard, 1) oxygen plasma was used to activate the substrate surface, and 2) chemical surface modification by incorporating chemical functional groups were performed before coating steps. Post coating characterization using XRD, SEM, TEM, EDS, UV-vis, and photoluminescence experiments were conducted to comprehend some of the structural, morphological and optical properties of the obtained QD/NPs. The results indicate the potential of

reactive blade coating as a facile and scalable fabrication method in the self-assembly of relatively uniform CIS QDs/NPs for use in various optoelectronic applications.

KEYWORDS: CIS QDs, in-situ reactive synthesis, R2R manufacturing technique, self-assembly.

4.2 Introduction

Quantum dots (QDs) containing no toxic heavy metals, such as Pb and Cd, are becoming increasingly popular because of their broader range of applications, including biomedical, optoelectronic, and electrochemical applications. QDs can be based on Si, carbon, I–III–VI structures, and others. Different synthesis techniques, such as microwave/ultrasonic synthesis, hydrothermal approaches, electrochemical synthesis, vacuum and chemical vapor deposition, and laser ablation, have generated nontoxic (less toxic) QDs[1−3].

Ternary Group I-III-VI semiconductor QDs, such as $CuInS_2$ and $CuInSe_2$, are promising alternatives to II-VI binary hazardous QDs, such as PbS and CdS, in applications relevant to optoelectronics, catalysis, and bioengineering. As mentioned before, Cd and Pb toxicity have generated concerns over the environmental impact of the II-VI binary materials. In contrast, structures such as $CuInS_2$ are made of more ecologically friendly components and have demonstrated equivalent or even superior performance in a variety of applications compared to II-VI binary nanocrystals[4,5].

$CuInS_2$ (CIS) QDs and NPs with chemical elements from groups I-III-VI are ternary solids that are inexpensive and nontoxic and have been the subject of numerous studies. Many optoelectronic and biomedical applications, including solar cells, photodetectors, light-emitting diodes, and bioimaging utilizing CIS QDs, have been investigated by researchers [6–8]. CIS has a direct bandgap of 1.5 eV[9]. This bandgap energy has a wavelength of approximately 820 nm, which falls between the visible and near-infrared regions of the electromagnetic spectrum. CIS has three main structures: i) chalcopyrite, ii) wurtzite, and iii) zinc blend. Each structure has specific crystal structure and features[10,11]. For instance, chalcopyrite CIS crystal structure is tetragonal, and has an off-stochiometry tolerance to a wide variety of anions and cations. As a result, the chalcopyrite structure has a high degree of structural flexibility, which permits the insertion of a broad range of

elemental substitutions, producing a family of quaternary and quinary compounds with adjustable optoelectronic characteristics[12]. Moreover, the wurtzite CIS structure has a hexagonal close-packed (HCP) crystal structure. An important property of the wurtzite structure is its anisotropy, which implies that its physical attributes can vary depending on the direction in which they are measured. In addition, the structure of wurtzite exhibits piezoelectric and pyroelectric properties, making it highly suited for various electrical and optoelectronic devices[13,14]. Several approaches, including the hot injection, solvothermal, microwave irradiation, hydrothermal synthesis, and thermolysis, have been employed to manufacture CIS QDs/NPs with various shapes[15–18].

Due to their mass production and adaptability, printed electronic devices have recently attracted much attention[19]. They can provide competitive benefits regarding functionality and manufacturing expenses compared to conventional production techniques such as chemical vapor deposition (CVD) or vacuum deposition[20,21]. Inkjet printing, screen printing, and roll-to-roll (R2R) printing are known printing methods to print QDs[22–24]. Several printing processes were utilized to fabricate thin films of ternary QDs for various electrical and optical applications. One example can be the inkjet printing of Zn_2SnO_4 QDs to be used to detect humidity, in which QDs were prepared with microwave hydrothermal synthesis before the printing step[25]. In another example, $CsPbBr_3$ QDs synthesized with the help of a three-neck flask were printed by electrohydrodynamic inkjet printing to be used in micro-LEDs[26]. However, the printing procedures employed for the QD layers were ex-situ, meaning the QD-containing inks were prepared before printing process. The traditional techniques for synthesizing and printing QDs in distinct stages are expensive and damaging to the environment due to the substantial amount of material waste and the numerous procedures required to synthesize the QDs and deposit them into thin films afterwards[27].

Meanwhile, promising techniques exist for producing thin films of QDs directly via in-situ reactive printing or coating, which allow for the formation and self-assembly of such particles directly on the substrate, thus resulting in simple, inexpensive, quick, and straightforward procedures that lead to cost reduction in the overall materials and device manufacturing process. Moreover, in-situ reactive printing processes produce less chemical waste and are better suited for large-scale environmentally mindful production. Our group’s previous study is an illustration of an in-situ

reactive approach where in-situ reactive inkjet printing approach was demonstrated for the first time to generate Au NPs. Such technique facilitates using Au NPs in delicate optoelectronic applications[28]. Although inkjet printing is a well-suited printing technique, it can be an expensive approach due to the high price of printing cartridges which might also clog over time and the slower speeds compared to traditional R2R processes such as gravure and offset printing and blade coating. In recent work, our group also employed an in-situ reactive blade coating approach to synthesize silver NPs on a glass substrate, textile, and surgical mask for use against SARS-CoV-2 with high disinfection efficacy[27]. To our knowledge, there has been no report of in situ reactive synthesis of binary and ternary non-metallic QDs/NPs.

In this study, the synthesis of CIS QDs/NPs using in-situ reactive deposition technique and the consequent use of rapid thermal annealing (RTA) to produce QDs/NPs will be discussed. Several factors have been studied in synthesizing and heating these QDs/NPs, such as heat treatment temperature and duration. Moreover, efforts were made to get a full-coverage uniform thin film by using various techniques. The in-situ reactive blade coating approach utilized in this study for the synthesis of CIS QDs/NPs is an R2R-compatible methodology that can be applied on a wide scale and reduces the total cost of such materials and devices based on them.

4.3 Experimental

4.3.1 Materials

Copper (I) iodide (CuI), indium (III) acetate ($In(C_2H_3O_2)_3$), oleylamine (OLA) ($C_{18}H_{35}NH_2$), sulfur (100%) were used as received to create the solutions for the blade coating procedure. Isopropyl alcohol (IPA) was utilized to clean silicon substrates, while acetone (C_3H_6O) and toluene (TOL) were employed to dilute the solution containing the particles for the photoluminescence (PL) test. For the blade coating procedure, a carbon-steel blade was utilized. Moreover, (3-mercaptopropyl)trimethoxysilane was used for the silanization process.

4.3.2 CIS QDs synthesis

4.3.2.1 Precursor preparation

Before the blade coating process, two solutions (inks) were prepared. For the first solution (CuIn ink), copper (I) iodide (14.6 mg) and indium (III) acetate (9.5 mg) were dissolved in 5 ml OLA,

followed by 30 minutes of heating at 280 °C while stirring continuously. Similarly, for the second solution (the S ink), 16 mg of sulfur was dissolved in 5 ml of OLA, followed by heat treatment at 180 °C for 30 minutes while stirring.

4.3.2.2 Substrate preparation

Silicon and glass substrates (1 × 1 $inch^2$) were utilized for the blade coating procedure. After washing with soap and rinsing with DI water, these substrates were sonicated for 10 minutes in DI water and IPA, respectively. The substrates were dried after each step with airflow. Prior to the blade coating procedure, the surface was treated with a UV-Ozone cleaning or plasma cleaning for different amounts of time. Both of these surface preparation approaches increase the wetting of the ink over the surface of the substrates. Moreover, for some of the substrates, the silanization process was investigated to get a more uniform and full-coverage thin film, and the details of the process will be discussed thoroughly in the results section.

4.3.2.3 Blade coating process

Figure 4.1 depicts a schematic illustration of CIS QDs/NPs synthesis. Figures 4.1(a) and 4.1(b) illustrate the preparation of CuIn and S ink, respectively. Initially, two droplets of the as-prepared CuIn ink (about 0.05 ml) were coated on silicon using a surgical razor blade (Fig. 4.1(c)). After that, two droplets of the as-prepared S ink (about 0.05 ml) were blade-coated on top of the CuIn ink layer, as seen in Fig. 4.1(d). The angle between the blade and silicon substrate was maintained at 50 degrees throughout the coating process. In the last step (Fig. 4.1(e)), the coated substrates were heated using RTA to generate dark brown CIS QDs/NPs. Various synthesis and heating parameters (time and temperature) were investigated for the prepared samples.

4.3.2.4 Rapid thermal annealing (RTA) heating method

The prepared inks above were blade coated in air on top of the substrates before being put in the RTA immediately. The RTA utilized four primary steps to optimize heating and cooling to room temperature. The initial stage was purging gas into the device chamber. Before heating any of the samples listed in Table 4.1, the chamber of the RTA was purged with nitrogen for 30 minutes to exclude oxygen from the RTA chamber environment. All the other steps were completed while the nitrogen was being used as the purging gas.

The second step was the ramp up step. In this step, the temperature rose to reach the desired temperature. The third step was the holding step. As soon as the substrate reached the desired temperature, it was kept at that temperature for the time given. The studied treatment temperatures and durations are listed in Table 4.1 (stated in the time and temperature column). The fourth step was the ramp-down step. This step involved cooling the chamber from the target temperature to room temperature. After the cooling down step, the sample was removed from the RTA. Before blade coating samples, 1 ml of S ink (described in the ink preparation section) was diluted with 3 ml of OLA to get a pure CIS structure. Table 4.1 shows all the parameters investigated for the prepared samples.

Table 4.1 - CIS QDs & NPs different parameters and size estimation from SEM and TEM.

Heating method	**Sample**	**Temperature**	**Time**	**Average size from SEM (nm)**	**Average size from TEM (nm)**
RTA (Rapid thermal annealing)	S_1	400 °C	2 min	-	2.3
	S_2	400 °C	3 min	3.4	3.2
	S_3	400 °C	4 min	7.8	7
	S_4	400 °C	5 min	10	10.8
	S_5	500 °C	10 sec	9.3	Not taken
	S_6	500 °C	30 sec	11.2	11.3
	S_7	500 °C	1 min	14	13.6
	S_8	500 °C	2 min	19.3	Not taken
	S_9	500 °C	3 min	22	Not taken

4.3.3 Characterization

Different approaches of characterization were employed to analyze the synthesized CIS QDs/NPs. X-ray diffraction (XRD) utilizing a Rigaku Ultima IV Diffractometer with a Cu target (k_α = 1.54 Å) was performed to characterize the crystalline phase. Using a Cu-sealed tube, the range of angle 2θ was between 10-65°, and the scan speed was tuned to 0.5°/min at 40 kV. A scanning electron microscope (SEM) equipment was used to study the morphology, structure, and size distribution

of QDs/NPs (Zeiss Gemini 500 device). In addition, energy-dispersive X-ray spectroscopy (EDS) analysis was conducted on NPs and QDs using a Zeiss Gemini 500 apparatus equipped with an EDS beam. A transmission electron microscope (TEM) (FEI Tecnai G2 Spirit Twin TEM) was also used for investigating the morphology and structure of CIS QDs/NPs. The UV-vis Cary 7000 Measuring Spectrophotometer detected absorption in the 280-800 nm wavelength range. Moreover, the photoluminescence (PL) measurement was studied with a Horiba fluorescence spectrometer in the UV-Vis region (390-600 nm). Also, an Oxygen Plasma Etcher (PE-50 Compact Benchtop Plasma Cleaning System) was used for cleaning the surface of the silicon and glass substrates.

4.4 Results and Discussion

The whole process for blade coating CIS QDs/NPs was discussed in the experimental section and depicted in Fig. 4.1. Two layers of CuIn ink and S ink were blade-coated on top of one another to create the CIS thin film, as shown in Fig. 4.1(c) and Fig. 4.1(d), respectively. The sample was then heat treated using the RTA to form CIS QDs/NPs (Fig. 4.1(e)). Figures 4.1(f) and 4.1(g) display the SEM and TEM images of two samples prepared by the RTA heating process at 400ºC.

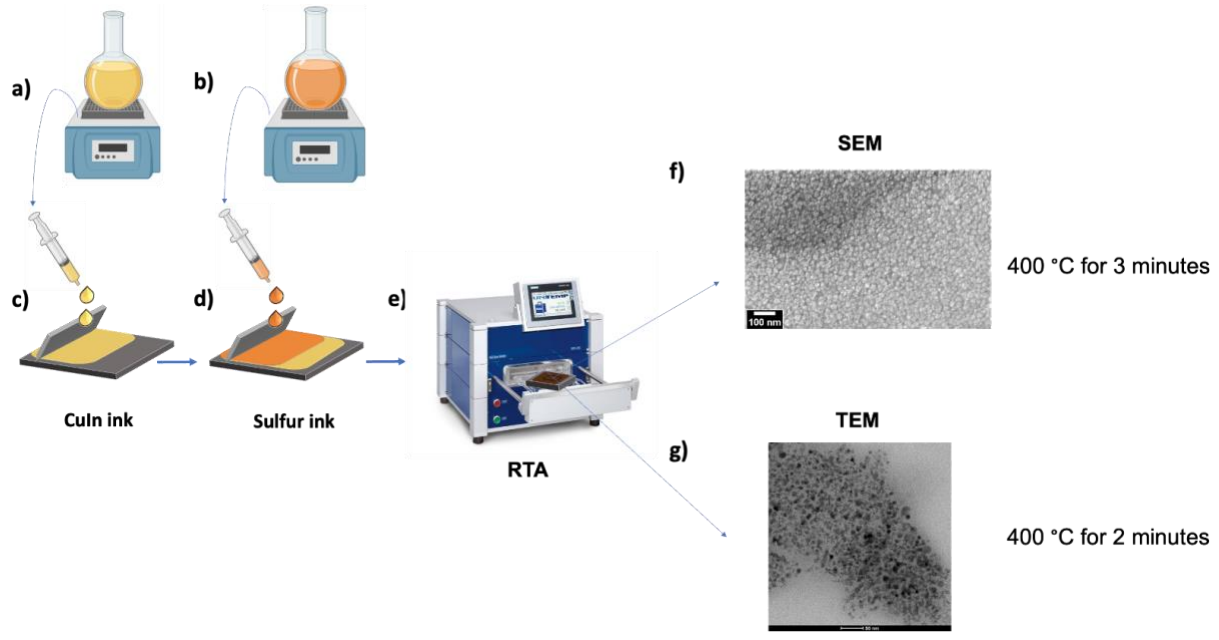

Figure 4.1 - Schematic of in situ reactive blade coating process of self-assembled CIS QDs/NPs. a) preparation of CuIn ink. b) preparation of S ink. c) blade coating the CuIn ink. d) blade coating the Sulfur ink on top of the first ink (CuIn ink). e) heating treatment with RTA. f) SEM and g) TEM Figure of formation of CIS NPs after the heating treatment with RTA.

4.4.1 X-ray diffraction analysis

The crystal structure of the obtained CIS QDs/NPs were analyzed using an XRD technique and is shown in Fig. 4.2. Observed patterns in Fig. 4.2(a) from the sample heated at 400 °C for 5 min showed good agreement with the standard JCPDS CIS chalcopyrite data (No. 47-1372), confirming the structure of synthesized CIS nanocrystals is tetragonal. Also, from the TEM images of the same sample shown in Fig. 4.2(b), it is evident that most of the particles are spherical. Moreover, in Fig. 4.2(d), the XRD pattern of the sample heated at 500 °C for 1 min is shown, which indicates the peaks matching those of mixed chalcopyrite and wurtzite CIS structures. In the TEM image taken from this sample (Fig 4.2(e)), two different morphologies of QDs/NPs (semi-spherical and rice shape) can be seen, which can be attributed to having the above mentioned two structures in the sample.

From other reports, it has been observed that a change in the crystal structure of CIS QDs could lead to a change in the morphology of the particles[10,14,29–31]. For instance, Perera et al. reported that their synthesized spherical QDs were related to the chalcopyrite CIS structure, and the rod-shape QDs were related to wurtzite CIS crystal structure, using SEM and XRD tests. They acquired different crystal structures of CIS QDs by trying different reaction conditions, such as changing the capping agents and heating temperatures[31]. They could get wurtzite structures at higher temperatures and higher growth rates. Therefore, the reason that the current study demonstrates both the chalcopyrite and wurtzite structures at 500 °C can be attributed to faster heating rates (shorter reaction times) and higher temperature, which lead to having kinetically stable wurtzite and chalcopyrite CIS mixed structure. It is worth mentioning that different heating rates and temperatures lead to different lengths of nucleation and growth steps, which will affect the final crystal CIS structure formed[32].

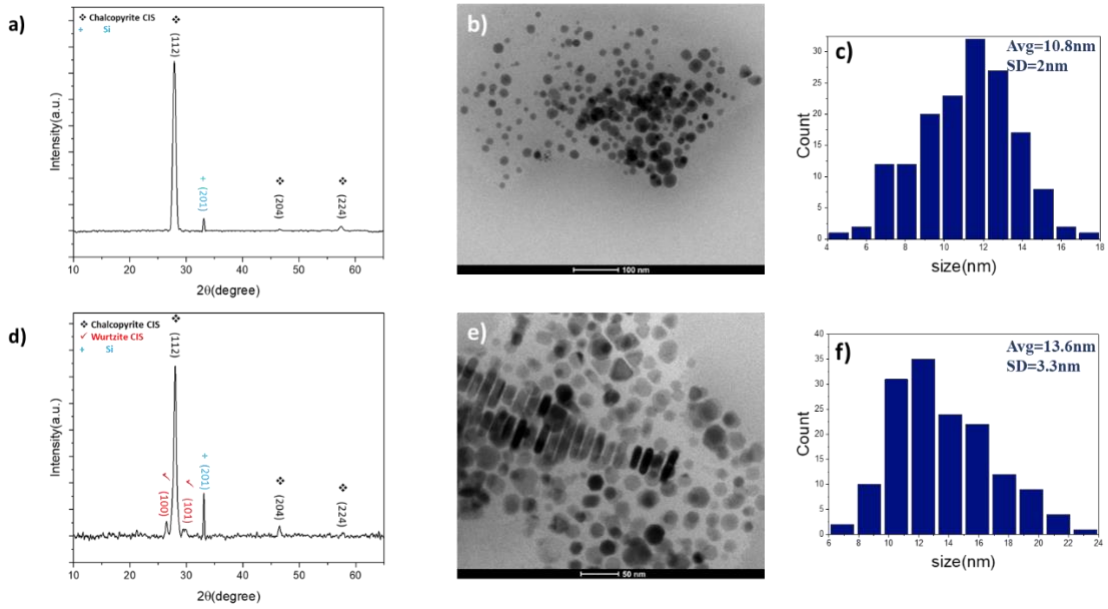

Figure 4.2 - XRD patterns and TEM images of CIS QDs and NPs synthesized with in-situ reactive blade coating method heat treated using RTA. (a) XRD data, (b) TEM image, and (c) size histogram of Chalcopyrite and Wurtzite mixed structure of CIS NPs heat treated at 400 °C for 5 min. (d) XRD data, (e) TEM image, and (f) histogram of particle sizes of mixed structure of CIS NPs heat treated at 500 °C for 1 min.

4.4.2 Scanning Electron Microscope

Figures 4.3 and 4.4 show SEM images of the as-synthesized CIS samples, heat treated using RTA. Figure 4.3(a-b) shows SEM images of CIS QDs after heat treatment at 400 °C for 3 min with an average size of 3.4±0.7 nm (Fig. 4.3(c)). Also, Figures 4.3(d-e) and (g-h) show SEM images of CIS QDs heat treated at 400 °C for 4 min and 5 min showing an average particle size of 7.8±1.4 nm (Fig. 4.3(f)) and 10±1.8 nm (Fig. 4.3(j)), respectively. The images indicate an increase in the size of QDs/NPs as the duration of heating at 400 °C increases.

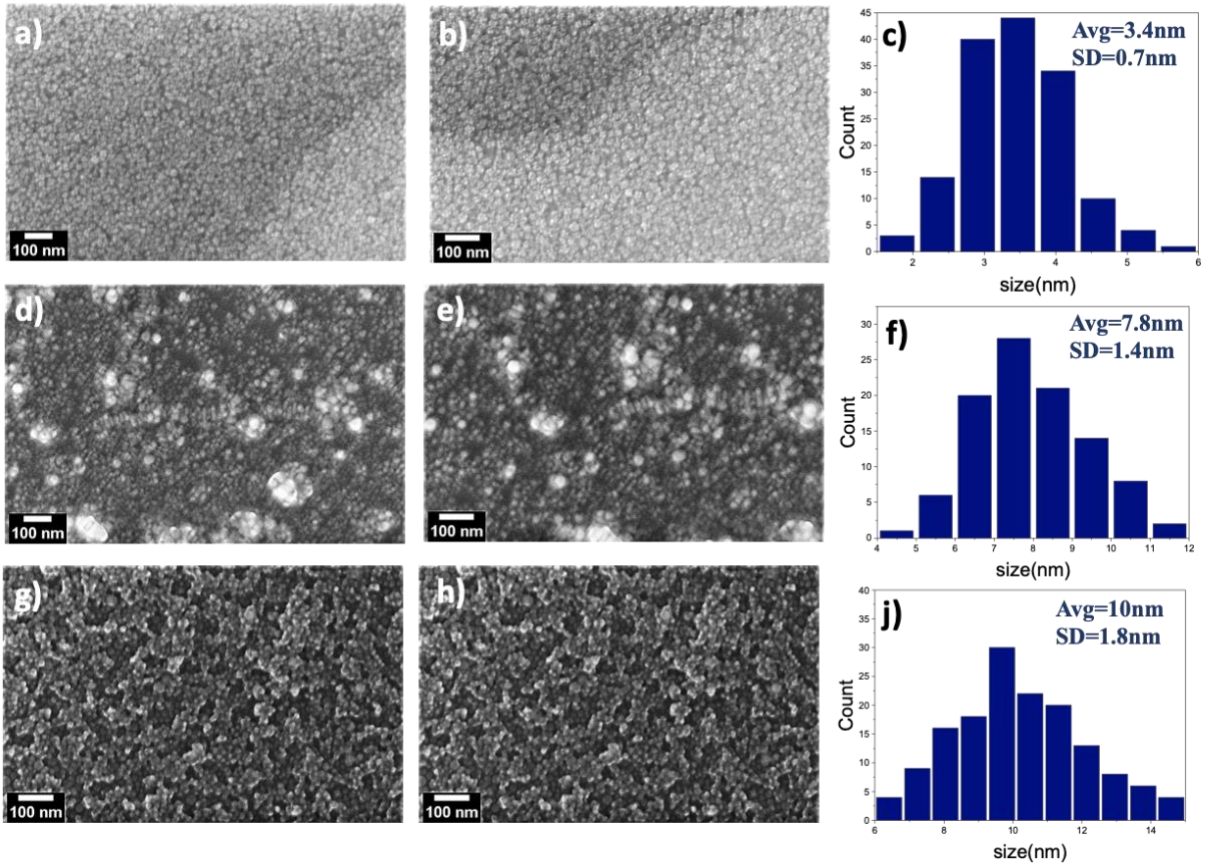

Figure 4.3 - SEM images of CIS QDs and NPs synthesized with blade coating and heat treated with the RTA. (a,b) SEM and (c) histogram of the size distribution of CIS QDs obtained after heating the sample at 400 °C for 3 min. (d,e) SEM and (f) histogram of the size distribution of CIS QDs dried at 400 °C for 4 min. (g,h) SEM and (j) histogram of the size distribution of CIS QDs obtained after heat treatment of the sample at 400 °C for 5 min.

Moreover, SEM images of CIS NPs heat treated with an RTA at 500 °C for 10 sec, 30 sec, 1 min, 2 min, and 3 min are presented in Figs. 4.4(a-b), (d-e), (g-h), (k-m), and (o-p), respectively. The average size of the obtained NPs is (9.3±1.8) nm (Fig. 4.4(c)) for 10 sec, (11.2±2) nm (Fig. 4.4(f)) for 30 sec, (14±3.2) nm (Fig. 4.4(j)) for 1 min, (19.3±3.8) nm (Fig. 4.4(n)) for 2 min, (22±3.9) nm (Fig. 4.4(q)) for 3 min heating duration. As shown in Fig. 4.4, the NPs grow in size as the duration of heating increases at 500 °C. Moreover, the rice-shaped and semi-spherical particles seen in samples heat treated at 500 °C for 30 sec, 1 min, 2 min, and 3 min can be related to having two crystal structures of CIS, chalcopyrite, and wurtzite. The possible reasons behind getting the mixtures of these two crystal structures were discussed in the XRD section.

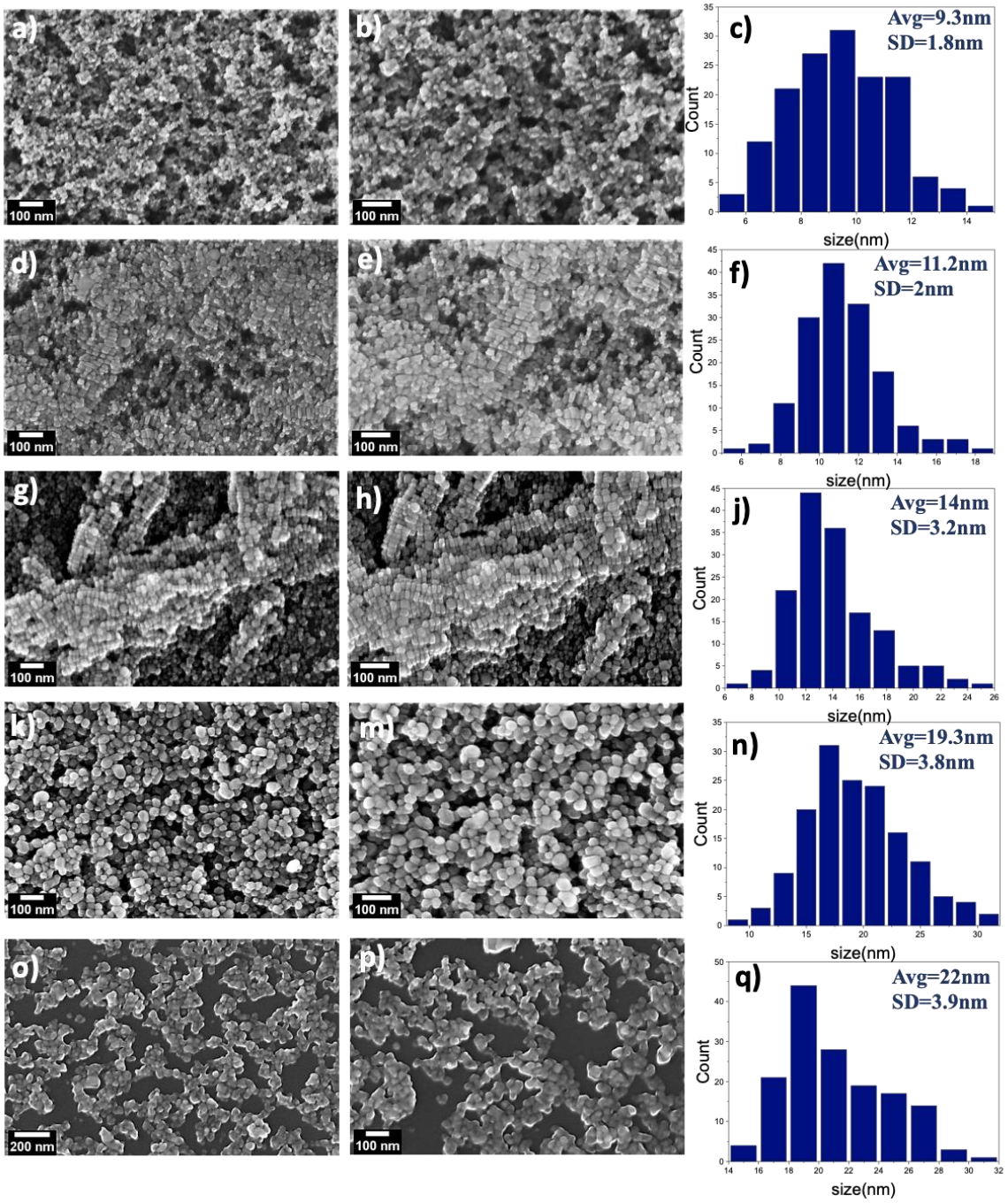

Figure 4.4 – (a, b) and (d, e) SEM images and (c, f) histogram of the size distribution of CIS QDs and NPs synthesized with blade coating and heat treated with the RTA at 500 °C for 10 sec, and 500 °C for 30 sec, respectively; (g, h), (k, m), and (o, p) SEM images and (j,n,q) histogram of size distribution of CIS QDs heated at 500 °C for 1 min, 2min, and 3 min, respectively.

4.4.3 Transmission Electron Microscope

In Fig. 4.5, TEM images for samples heated at 400 °C for 2 min (Fig. 4.5(a)), 400 °C for 3 min (Fig. 4.6(b)), 400 °C for 4 min (Fig. 4.6(c)), and 400 °C for 5 min (Fig. 4.6(d)) are shown. The estimated size of QDs/NPs from the TEM images is (2.3±0.44) nm (Fig. 4.6(e)), (3.2±0.8) nm (Fig. 4.6(f)), (7±2.3) nm (Fig. 4.6(g)), and (10.8±2) nm (Fig. 4.6(h)), respectively.

Moreover, Fig. 4.6 (a) and (b) show the TEM images of samples heated at 500 °C for 30 sec and 1 min, respectively, with an average size estimate of (11.3±2.3) nm (Fig. 4.6(c)) for 30 sec heating and (13.6±3.3) nm (Fig. 4.6(d)) for 1 min heating. In this Figure, different shapes of NPs can be seen at the two heating durations, such as semi-spherical, rice shape, and even hexagonal. The reason for seeing different shapes for the sample heat treated at 500 °C is attributed to the mixture of crystal structures of CIS, such as chalcopyrite and wurtzite, as confirmed by XRD characterization and described in the XRD section. As in the case of PbS QDs/NPs heat treated at 350 °C, the shape change observed here can also result from the rapid and intense heat pulse provided by the RTA. The different shapes observed in the TEM images were corroborated by SEM scans of the various samples studied here.

It can be seen from the Figs. 4.3 and 4.4 that the QDs/NPs are becoming larger with increasing heat treatment temperature and duration. The size of QDs/NPs estimated from TEM images are in tune with the sizes estimated from SEM images.

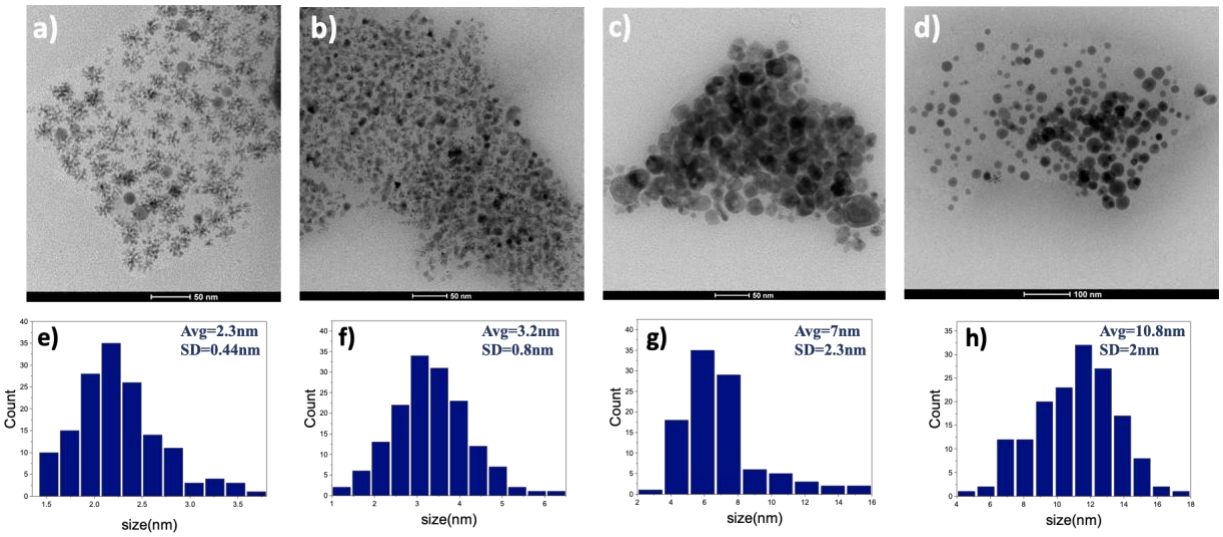

Figure 4.5 - TEM images (a)-(d) of CIS QDs and NPs synthesized using blade coating and the RTA heat treatment and their histogram of the size distribution (e)-(h) for heat treatment conditions of 400 °C for 2 min, 400 °C for 3 min, 400 °C for 4 min, and 400 °C for 5 min, respectively.

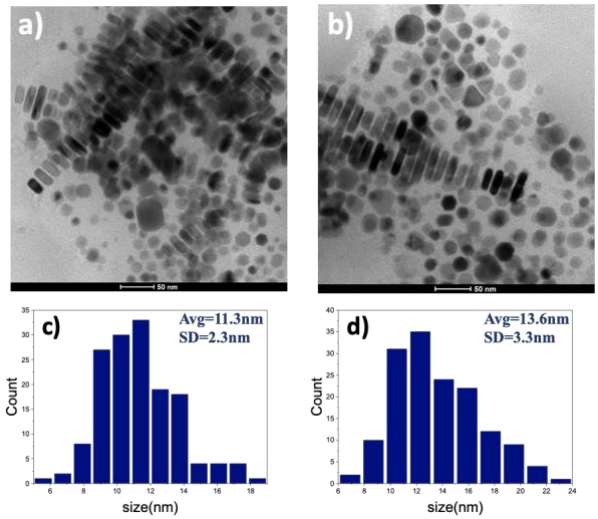

Figure 4.6 - TEM images (a), (b) of CIS QDs and NPs obtained using blade coating method and the RTA heat treatment approach, and the resulting histogram of the size distribution for samples heat treated at 500 °C for 30 sec (c) and 500 °C for 1 min (d), respectively.

4.4.4 UV-vis absorption measurement

UV-Vis measurement of CIS QDs/NPs was investigated in this report. First, the CIS QDs/NPs formed on the silicon substrate were dissolved in toluene. Then the UV-Vis absorption test was performed on the CIS solution. In this case, the estimated absorption band edge is in the range of 360-475 nm. Also, the absorption spectra of CIS QDs/NPs formed on a glass substrate, which the

UV-Vis test was taken from the glass substrate and not the solution in this case, are shown in Fig. 4.7(b). The estimated absorption band edge was in the range of 450-530 nm. The reason for differences in the absorbed ranges of QDs formed on glass substrates and silicon substrates is differences in the surface chemistry (roughness), energy band alignment, and crystallographic structure of glass and silicon substrates[33–35]. Moreover, the reason for trying to take the UV-Vis test from particles formed on glass substrate was the potential of the particles formed on this substrate to be used in future optoelectronic applications. Formation of particles on silicon substrates was also tried because of ease of getting SEM and TEM pictures from particles formed on silicon substrates. Our UV-Vis absorption test results are similar to other literatures[14,36–38]. For instance, In one of the reports, colloidal CIS QDs dispersed in hexanes or toluene synthesized from a single source precursor showed absorption in the mentioned range above[37]. Also, in Pein et al. report, they synthesized CIS QDs with chalcopyrite structure, with 2-10 nm size at different parameters, with almost the same precursors and ligand that we used and disperse the QDs in chloroform for taking the UV-Vis test. Their UV Vis spectra was similar to our UV-Vis graph[36].

4.4.5 Photoluminance

Photoluminance (PL) measurements of CIS QDs/NPs on silicon substrates were performed in the 390-600 nm range. Figure 4.7(c-d) shows PL emission spectra of CIS samples on silicon and glass substrates heat treated with the RTA right after the material deposition process. Upon the formation of the particles on the surface of silicon substrates, they were dissolved in toluene and consequently excited at a wavelength of $\lambda = 360$ nm. This was done due to the opacity of silicon to the excitation wavelength used. For samples formed on glass substrates, the PL test was taken directly using excitation at $\lambda = 370$ nm wavelength. In Fig. 4.7(c), PL emissions of CIS QDs/NPs heated with the RTA at two different temperatures (400 °C and 500 °C) for different durations (1 min, 2 min, 3 min, 4 min, and 5 min). A red shift in the PL emission peak is seen when the temperature is increased from 400 °C (PL peak at 407 nm) to 500 °C (PL peak at 438 nm) for 2 min of heat treatment. Also, with increasing the duration of heating at 400 °C from 2 min (PL peak at 407 nm) to 3 min (PL peak at 410 nm), 4 min (PL peak at 420 nm), and 5 min (PL peak at 427 nm), a red shift can also be seen as the time increases. Furthermore, at 500 °C, with increasing the duration of heating from 1 min (PL peak at 430 nm) to 2 min (PL peak at 438 nm), a red shift in the peaks is also seen.

In Fig. 4.7(d), the PL response of samples formed on a glass substrate is shown. A redshift in all spectra can be seen with increasing temperature and duration of heating. It is noted that the peaks here are wider compared to corresponding samples formed on silicon substrates. The possible reason for this observation can be attributed to the differences between the surface chemistry (roughness), energy band alignment and crystallographic structure of glass substrate and silicon substrate themselves[33,34]. The fact, as mentioned above, that the PL spectra performed on the particles formed on silicon were actually taken for particles dissolved in toluene, and not in the solid compact film can also contribute to the observed differences between the PL for the particles in the liquid vs. in the solid film on the glass samples. It is known that dispersing particles in a given liquid will lead to reduced particle-particle interactions, thus weakening the broading and red shift of the spectra.

In addition to the above, in all of the samples in Fig. 4.7(c-d), the increase in the size (Table 4.1) of QDs/NPs can also contribute to the observed shift and broadening in the emitted spectra. In this regard, our PL results are in accord with published literature[15,39]. Although an exhaustive study in this venue is beyond the scope of this thesis, it is worth mentioning that other variables, including precursors, ligands, reaction temperature, precursor reactivity, Cu/In ratio, method of synthesis, etc., can affect the position of the PL peak of CIS QDs/NPs[15].

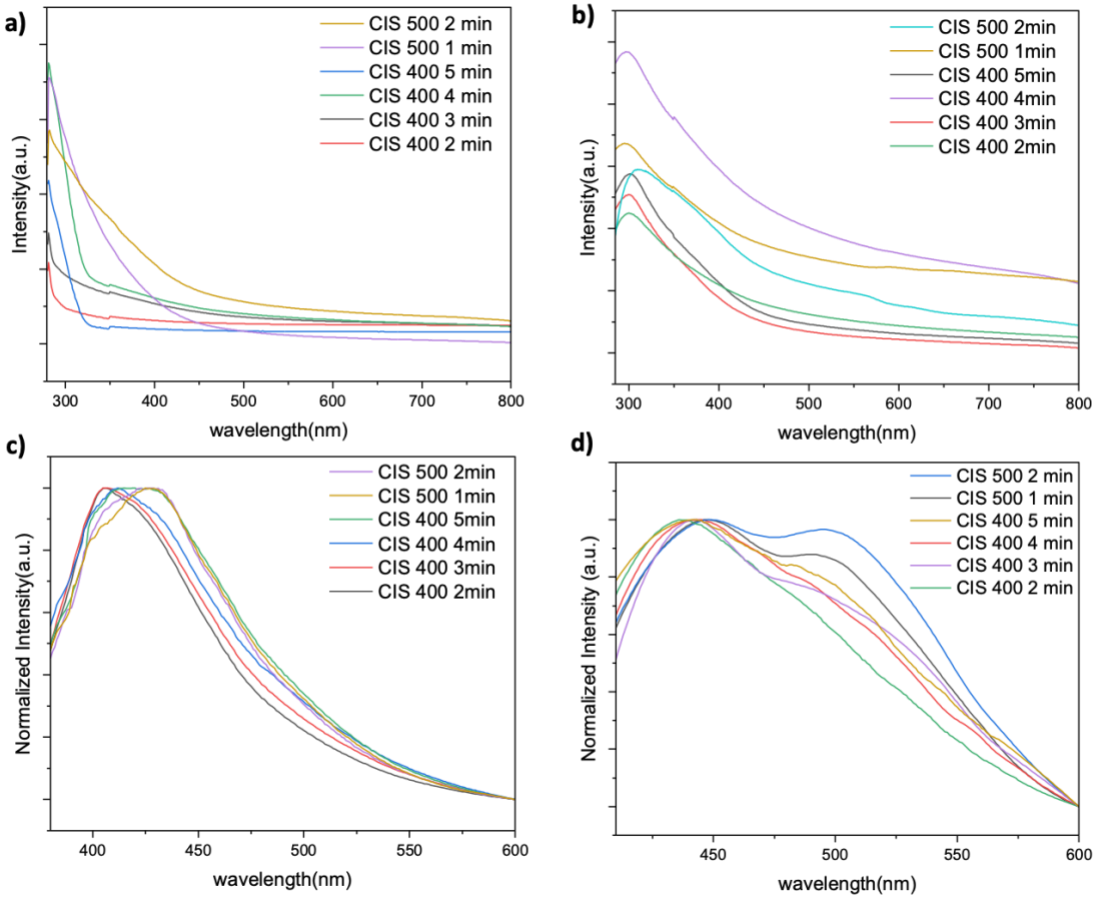

Figure 4.7 - (a) UV-Vis absorption spectrum of CIS NPs and QDs formed on a glass substrate and (b) dissolved in toluene (for the silicon substrate case). All samples were heat treated using RTA at different temperatures and different durations. (c) Photoluminescence spectra of CIS NPs and QDs formed on silicon substrate (particles dissolved in toluene) and (d) glass substrate heated with RTA excited with 360 nm wavelength (silicon) and 370 nm wavelength (glass) at different temperatures for different times.

4.4.6 Surface modification

In this section, substrate surface modification was performed, prior to deposition process, using UV-ozone cleaning, oxygen plasma etching (cleaning), and chemical surface modification (e.g., silanization treatment).

Using a UV-ozone or plasma cleaning (ashing) before the coating procedure can optimize the free energy and leads to enhanced wettability of the ink on the substrate surface. Using these cleaning techniques, a substantial amount of the contaminants on top of the surfaces of the substrates will

be eliminated. The plasma cleaning process involves bombarding a surface with ions and electrons of high energy. Physical and chemical properties of the upper layer of the surface, as well as the surface's wettability and functionalization, are altered by this bombardment[34,40]. An Oxygen plasma asher/etcher (PE-50 Compact Benchtop Plasma Cleaning System) was used to clean the silicon substrates' surface before blade-coating. The optimal power and the duration for plasma cleaning was 100 W for 5 min. This allowed for a full-coverage of the thin film coating over the substrate surface area. In Figure 4.8, digital images of the CIS film formed on silicon substrates without plasma cleaning (Fig. 4.8(a,c)) and with plasma cleaning step (Fig. 4.8(b,d)) are shown. It can be seen that the coverage of the thin film has been improved as a result of the Oxygen-plasma cleaning step.

The UV-ozone cleaning process involves the breakdown of organic molecules into gases by ultraviolet radiation and intense oxidation through the creation and decomposition of O_3, which are then removed from the surface[41]. UV-ozone cleaning was also carried out on the substrates before the blade coating step. Upon optimization of this cleaning process, a 10-minute UV-ozone cleaning process was the optimal timing.

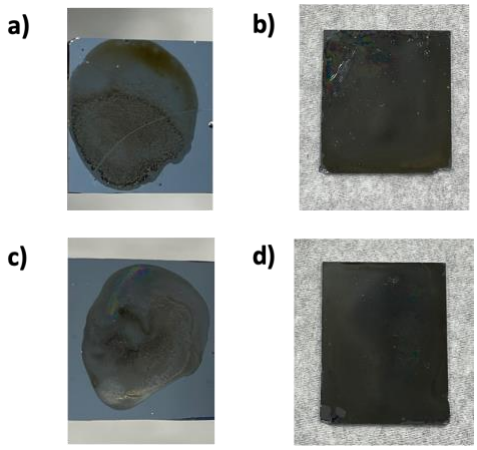

Figure 4.8 - Digital images of coated silicon substrates after heat treatment with RTA at (a) 400 °C 2 min and (b) 400 °C 3 min, and for silicon substrates cleaned with plasma before heating the samples at (b) 400 °C 2 min and (d) 400 °C 3 min.

Silanization is another treatment to change the wettability of the silicon substrate. In this technique, a silane molecule, containing reactive groups is attached to the surface of the substrate with a covalent bond, which alters the surface chemistry and improves the surface energy of the substrate and, in turn, its wettability[42,43]. Figure 4.9 shows the silicon samples with the resulting thin

films upon post-deposition heating using the RTA. The surface of the substrates was functionalized with silane before the blade-coating. For the silanization procedure, 1 ml of (3-mercaptopropyl)trimethoxysilane was added to 15 ml TOL and stirred to obtain uniform solution. The clean silicon substrates were then placed in this solution for 3 hours while heated on the hotplate at 60 °C. Upon the termination of this step, the substrates were removed from the solution, soaked in clean TOL for 30 sec, and dried with air.

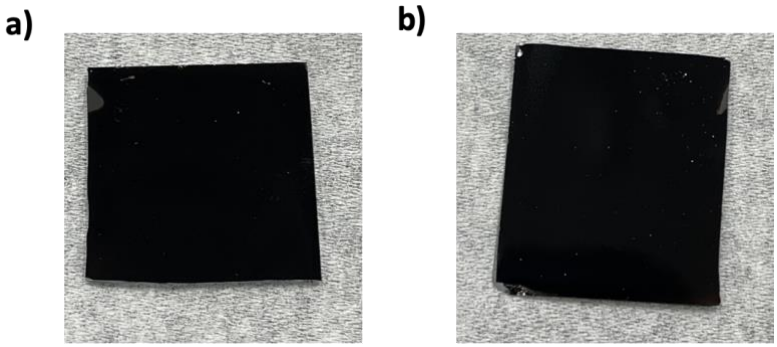

Figure 4.9 - Digital images of silicon substrates treated with silane and blade-coated to yield a uniform film of CIS QDs over the substrate surface upon heat treatment with RTA at (a) 400 °C 2 min and (b) 400 °C 3 min.

4.5 Conclusion

The in-situ reactive blade coating procedure in conjunction with RTA heat treatment of the coated films was used in this study to demonstrate a rapid synthesis and coating of self-assembled CIS QDs/NPs. Different heating parameters, such as temperature and heat treatment duration, were studied and found to impact the formation and crystal structure of the obtained CIS QDs/NPs. The study also demonstrates that substrate surface modification steps such as oxygen plasma cleaning and silanization are critical to improve the surface's wettability and allow for a full coverage of the coated thin film on the silicon substrate, and in turn the formation of packed layers of CIS QDs/NPs. Blade coating is compatible with R2R manufacturing and can be scaled up to large-scale industrial fabricating levels, which gives our approach a great potential in the low cost and environmentally more friendly fabrication of CIS QDs/NPs and other ternary nontoxic QDs than the current techniques of liquid pot chemistry and vacuum deposition and CVD processes.

4.6 References

[1] García de Arquer F P, Talapin D V, Klimov V I, Arakawa Y, Bayer M and Sargent E H 2021 Semiconductor quantum dots: Technological progress and future challenges *Science* **373** eaaz8541

[2] Efros A L and Brus L E 2021 Nanocrystal Quantum Dots: From Discovery to Modern Development *ACS Nano* **15** 6192−210

[3] Das A and Snee P T 2016 Synthetic Developments of Nontoxic Quantum Dots *ChemPhysChem* **17** 598−617

[4] Liu S and Su X 2014 The synthesis and application of I−III−VI type quantum dots *RSC Adv.* **4** 43415−28

[5] Girma W M, Fahmi M Z, Permadi A, Abate M A and Chang J-Y 2017 Synthetic strategies and biomedical applications of I−III−VI ternary quantum dots *J. Mater. Chem. B* **5** 6193−216

[6] Lv M, Zhu J, Huang Y, Li Y, Shao Z, Xu Y and Dai S 2015 Colloidal $CuInS_2$ Quantum Dots as Inorganic Hole-Transporting Material in Perovskite Solar Cells *ACS Appl. Mater. Interfaces* **7** 17482−8

[7] Liu S, Zhang H, Qiao Y and Su X 2012 One-pot synthesis of ternary CuInS 2 quantum dots with near-infrared fluorescence in aqueous solution *RSC Advances* **2** 819−25

[8] Jara D H, Yoon S J, Stamplecoskie K G and Kamat P V 2014 Size-Dependent Photovoltaic Performance of CuInS2 Quantum Dot-Sensitized Solar Cells *Chem. Mater.* **26** 7221−8

[9] Luo J, Wei H, Huang Q, Hu X, Zhao H, Yu R, Li D, Luo Y and Meng Q 2013 Highly efficient core−shell CuInS2−Mn doped CdS quantum dot sensitized solar cells *Chem. Commun.* **49** 3881

[10] Xie B-B, Hu B-B, Jiang L-F, Li G and Du Z-L 2015 The phase transformation of CuInS2 from chalcopyrite to wurtzite *Nanoscale Res Lett* **10** 86

[11] Pan D, An L, Sun Z, Hou W, Yang Y, Yang Z and Lu Y 2008 Synthesis of Cu−In−S Ternary Nanocrystals with Tunable Structure and Composition *J. Am. Chem. Soc.* **130** 5620−1

[12] Li T-L and Teng H 2010 Solution synthesis of high-quality CuInS 2 quantum dots as sensitizers for TiO 2 photoelectrodes *Journal of Materials Chemistry* **20** 3656−64

[13] Xia C, Wu W, Yu T, Xie X, van Oversteeg C, Gerritsen H C and de Mello Donega C 2018 Size-Dependent Band-Gap and Molar Absorption Coefficients of Colloidal $CuInS_2$ Quantum Dots *ACS Nano* **12** 8350−61

[14] Liu L, Li H, Liu Z and Xie Y-H 2018 Structure and band gap tunable CuInS2 nanocrystal synthesized by hot-injection method with altering the dose of oleylamine *Materials & Design* **149** 145–52

[15] Long Z, Zhang W, Tian J, Chen G, Liu Y and Liu R 2021 Recent research on the luminous mechanism, synthetic strategies, and applications of $CuInS_2$ quantum dots *Inorg. Chem. Front.* **8** 880–97

[16] Liu Z, Ma Q, Wang X, Lin Z, Zhang H, Liu L and Su X 2014 A novel fluorescent nanosensor for detection of heparin and heparinase based on CuInS2 quantum dots *Biosensors and Bioelectronics* **54** 617–22

[17] Shi A, Wang X, Meng X, Liu X, Li H and Zhao J 2012 Temperature-dependent photoluminescence of CuInS2 quantum dots *Journal of Luminescence* **132** 1819–23

[18] Yue W, Han S, Peng R, Shen W, Geng H, Wu F, Tao S and Wang M 2010 CuInS2 quantum dots synthesized by a solvothermal route and their application as effective electron acceptors for hybrid solar cells *J. Mater. Chem.* **20** 7570

[19] Pandey M, Rashiku M and Bhattacharya S 2021 Recent progress in the development of printed electronic devices *Chemical Solution Synthesis for Materials Design and Thin Film Device Applications* (Elsevier) pp 349–68

[20] Roy P, Ota J R and Srivastava S K 2006 Crystalline ZnS thin films by chemical bath deposition method and its characterization *Thin Solid Films* **515** 1912–7

[21] Petrus R Yu, Ilchuk H A, Kashuba A I, Semkiv I V and Zmiiovska E O 2019 Optical-Energy Properties of CdS Thin Films Obtained by the Method of High-Frequency Magnetron Sputtering *Opt. Spectrosc.* **126** 220–5

[22] Jia S, Tang H, Ma J, Ding S, Qu X, Xu B, Wu Z, Li G, Liu P, Wang K and Sun X W 2021 High Performance Inkjet-Printed Quantum-Dot Light-Emitting Diodes with High Operational Stability *Advanced Optical Materials* **9** 2101069

[23] Ma Y-F, Wang Y-M, Wen J, Li A, Li X-L, Leng M, Zhao Y-B and Lu Z-H 2023 Review of roll-to-roll fabrication techniques for colloidal quantum dot solar cells *Journal of Electronic Science and Technology* **21** 100189

[24] Aumaitre C, Joly D, Aldakov D and Demadrille R 2018 Alternative Binary and Ternary Metal Oxides for Dye- and Quantum Dot-Sensitized Solar Cells *The Future of Semiconductor Oxides in Next-Generation Solar Cells* (Elsevier) pp 85–115

[25] Lehnen T, Zopes D and Mathur S 2012 Phase-selective microwave synthesis and inkjet printing applications of Zn2SnO4 (ZTO) quantum dots *J. Mater. Chem.* **22** 17732

[26] Yang X, Yan Z-J, Zhong C-M, Jia H, Chen G-L, Fan X-T, Wang S-L, Wu T-Z, Lin Y and Chen Z Electrohydrodynamically Printed High-resolution Arrays Based on Stabilized CsPbBr3 Quantum Dot Inks *Advanced Optical Materials* **n/a** 2202673

[27] Abulikemu M, Tabrizi B E A, Ghobadloo S M, Mofarah H M and Jabbour G E 2022 Silver Nanoparticle-Decorated Personal Protective Equipment for Inhibiting Human Coronavirus Infectivity *ACS Appl. Nano Mater.* **5** 309–17

[28] Abulikemu M, Da′as E H, Haverinen H, Cha D, Malik M A and Jabbour G E 2014 In Situ Synthesis of Self-Assembled Gold Nanoparticles on Glass or Silicon Substrates through Reactive Inkjet Printing *Angewandte Chemie* **126** 430–3

[29] Qi Y, Liu Q, Tang K, Liang Z, Ren Z and Liu X 2009 Synthesis and Characterization of Nanostructured Wurtzite $CuInS_2$: A New Cation Disordered Polymorph of $CuInS_2$ *J. Phys. Chem. C* **113** 3939–44

[30] Kuzuya T, Hamanaka Y, Itoh K, Kino T, Sumiyama K, Fukunaka Y and Hirai S 2012 Phase control and its mechanism of CuInS2 nanoparticles *Journal of Colloid and Interface Science* **388** 137–43

[31] Perera S D, Zhang H, Ding X, Nelson A and Robinson R D 2015 Nanocluster seed-mediated synthesis of $CuInS_2$ quantum dots, nanodisks, nanorods, and doped Zn-$CuInGaS_2$ quantum dots *J. Mater. Chem. C* **3** 1044–55

[32] Nose K, Soma Y, Omata T and Otsuka-Yao-Matsuo S 2009 Synthesis of Ternary $CuInS_2$ Nanocrystals; Phase Determination by Complex Ligand Species *Chem. Mater.* **21** 2607–13

[33] Malinský P, Slepička P, Hnatowicz V and Švorčík V 2012 Early stages of growth of gold layers sputter deposited on glass and silicon substrates *Nanoscale Res Lett* **7** 241

[34] Chen G and Hui P 1999 Thermal conductivities of evaporated gold films on silicon and glass *Appl. Phys. Lett.* **74** 2942–4

[35] Potocky S, Kromka A, Potmesil J, Remes Z, Vorlicek V, Vanecek M and Michalka M 2007 Investigation of nanocrystalline diamond films grown on silicon and glass at substrate temperature below 400 °C *Diamond and Related Materials* **16** 744–7

[36] Pein A, Baghbanzadeh M, Rath T, Haas W, Maier E, Amenitsch H, Hofer F, Kappe C O and Trimmel G 2011 Investigation of the Formation of $CuInS_2$ Nanoparticles by the Oleylamine Route: Comparison of Microwave-Assisted and Conventional Syntheses *Inorg. Chem.* **50** 193–200

[37] Castro S L, Bailey S G, Raffaelle R P, Banger K K and Hepp A F 2004 Synthesis and Characterization of Colloidal $CuInS_2$ Nanoparticles from a Molecular Single-Source Precursor *J. Phys. Chem. B* **108** 12429–35

[38] Chen Y, He X, Zhao X, Song M and Gu X 2007 Preparation and characterization of copper indium disulfide films by facile chemical method *Materials Science and Engineering: B* **139** 88–94

[39] Chuang P-H, Lin C C and Liu R-S 2014 Emission-Tunable CuInS $_2$ /ZnS Quantum Dots: Structure, Optical Properties, and Application in White Light-Emitting Diodes with High Color Rendering Index *ACS Appl. Mater. Interfaces* **6** 15379–87

[40] O′Kane D F and Mittal K L Plasma cleaning of metal surfaces

[41] Vig J R 1985 UV/ozone cleaning of surfaces *J. Vac. Sci. Technol. A* **3**

[42] Brehm M, Scheiger J M, Welle A and Levkin P A 2020 Reversible Surface Wettability by Silanization *Adv. Mater. Interfaces* **7** 1902134

[43] Metwalli E, Haines D, Becker O, Conzone S and Pantano C G 2006 Surface characterizations of mono-, di-, and tri-aminosilane treated glass substrates *Journal of Colloid and Interface Science* **298** 825–31

Supporting Information B: Chapter 4

In-situ Reactive $CuInS_2$ Quantum dots synthesis: Impact of selected heating methods

Kimia Rezaei Shad[1], Mutalifu Abulikemu[1], and Ghassan E. Jabbour[1]*

[1]School of Electrical Engineering and Computer Science, University of Ottawa,

800 King Edward Ave., Ottawa, ON, Canada K1N 6N5

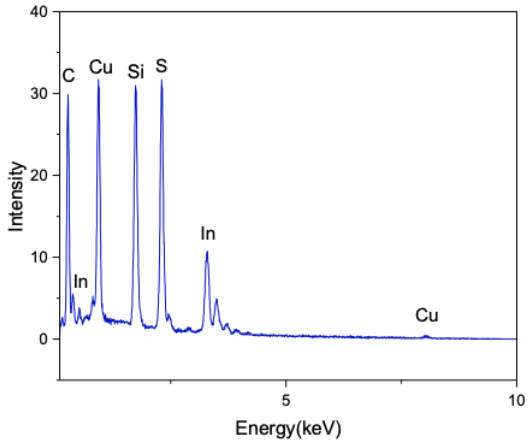

Figure B 1 - EDS spectrum of CIS QDs formed on silicon substrate heat treated with RTA.

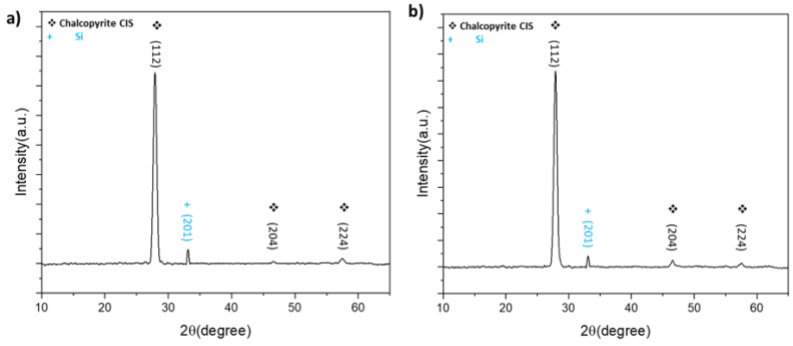

Figure B 2 - XRD patterns of CIS nanoparticles synthesized with in-situ reactive blade coating method and heat treated using RTA at a) 400 °C for 2 min, and b) 400 °C for 3 min.

Chapter 5 . Conclusion and Future Works

5.1 Conclusion

This research intended to demonstrate the potential of the large-scale coating technique for the direct fabrication and deposition of binary and ternary quantum dots, nanoparticle materials, and thin films. Blade coating of the starting materials and consequent heat treatment allowed for the in-situ self-assembly of quantum dots and nanoparticles into thin films. The fabrication of two binary and ternary quantum dots based on PbS and $CuInS_2$ was demonstrated successfully.

To fabricate PbS QD thin films, two precursors were prepared, mainly Pb ink as a lead precursor and S ink as a sulfur precursor. The two inks were subsequently blade coated on top of each other on glass or silicon substrates. SEM imaging, EDS characterization, and XRD crystalline phase analysis revealed that crystalline PbS QDs/NPs were formed on the substrate following the post-coating heat treatment step. Different heat treatments, such as hotplate in the glovebox, vacuum oven, and rapid thermal annealing (RTA), and their impact on the formation of PbS QDs/NPs with different shapes and size distribution were documented. By changing the concentration of the reactants in the prepared inks, the heat treatment temperature and its duration, the average particle size can be controlled. Furthermore, in order to assess the potential of such materials in optoelectronics, UV-vis absorption and photoluminescence (PL) tests were carried.

Particles with an average diameter of 6-7 nm with homogenous distribution were formed by heating the blade-coated sample using a hotplate in a glovebox. Increasing the temperature and duration of heating led to an increased average size of 8-10 nm. Moreover, for samples heated in a vacuum oven, the average particle size was 12-14 nm, which increased to 24-27 nm with increased heat treatment duration. When the RTA was used for the heat treatment of the coated samples, a temperature of 250 °C allowed the self-assembly of spherical particles of PbS QDS having an average size of 15-18 nm. Increasing the temperature to 300 °C and 350 °C, most spherical shapes undergone a transformation to cubic structure. Chapter 3 discussed an investigation of the conditions that lead to shape change through a series of controlled experiments. One possible reason for shape change can be due to the intense heating pulse provided by RTA during the establishment of the required treatment temperature. The RTA heating approach provided the highest crystalline order for the samples, as indicated in the XRD characterization. In

addition, through simple alteration of the heating parameters, different shapes of QDs/NPs were obtained when using the RTA, as documented in the SEM scans.

Spin coating was also utilized as a deposition method of the precursor inks in order to compare such approach to blade coating. In this case, thin films of PbS QDs/NPs were obtained. The SEM study of the resulting films points to the superiority of the blade coating approach in obtaining uniform distribution of QDs/NPs. This is an encouraging result, as blade coating is more scalable than spin coating for large-scale fabrication.

Despite the benefits of PbS QDs and the potential of these QDs for various applications (such as photodetectors, sensors, and other optoelectronic applications), their use on a large scale is limited because of the toxicity of lead. One solution to this problem is to use ternary I-III−VI_2 QDs such as $CuInS_2$ (CIS). These structures are economical, heavy-metal-free materials, and with low toxicity. In this venue, an investigation of the fabrication of self-assembled thin films of CIS QDs/NPs using in-situ reactive blade coating was presented. The results indicate compact films of self-assembled CIS QDs/NPs with a size distribution between 2-3 nm that can be obtained at 400 °C, and 9-11 nm at 500 °C, using RTA for heat treatment. The size distribution of QDs/NPs seems to increase to 10-12 nm at 400 °C and 22-26 nm at 500 °C, and is dependent on the duration of RTA heating period.

Prior to the fabrication of CIS thin films, two precursor inks were prepared and blade coated on top of each other, followed by heat treatment of the samples. The first ink was the CuIn ink (copper (I) iodide + indium (III) acetate + oleylamine), and the second ink was sulfur ink (sulfur powder + oleylamine). Following the post-coating heat treatment, crystalline CIS QDs/NPs were formed on the substrate, as revealed by SEM and TEM imaging. Such structures were also characterized by EDS and XRD. Moreover, UV-Vis absorption and photoluminescence (PL) spectroscopy were performed on the resulting thin films.

The coverage of the deposited films was successfully achieved over a silicon substrate of 1 in × 1 in area. UV-ozone cleaning, oxygen plasma cleaning, and surface silanization were different techniques that were studied to promote better coverage of the CIS thin layers on silicon substrates.

It is worth noting that the results of the characterization tests of PbS and CIS QDs and NPs thin films were comparable to those obtained from other techniques with prepared inks, according to

other reports. The essential aspect of the reactive approach is it provides an extended shelf lifetime for starting inks and greater control over the QDs/NPs size compared to an ink containing QDs/NPs with a fixed size and limited shelf lifetime. Moreover, blade-coating technique is exceptionally significant in roll-to-roll industrial manufacturing and can provide quicker and more cost-effective processing of important materials such as QDs and NPs, and directly self-assemble them as layers for large area devices.

5.2 Future works

This study focused on an in-situ reactive blade coating method for manufacturing binary and ternary QDs/NPs such as PbS and CIS. Such reactive deposition approach was capable of manufacturing small size QDs/NPs reaching particle size below 5 nm. The roll-to-roll nature of blade coating positions our results for a facile transition to large-scale industrial manufacturing. Although these results are world's first time demonstration, more efforts need to be made to extend the full-coverage and self-assembly of QDs/NPs on much larger scale than the 1 in x 1in demonstrated above. This can involve more modification of chemical content of the inks, substrate surface preparation approaches, and flexible substrate characteristics. Extending this work to flexible substrates such as glass and plastics will be highly beneficial to portable device industry (e.g., solar cells, medical sensors, smart textile, and mobile displays, to mention a few). One aspect to focus on in this venue could be the investigation of suitable surfactants to allow optimum wetting. Another effort here is to identify relevant ligand exchange processes that are also beneficial for getting uniform full coverage of the coated films. Such efforts will prove beneficial in manufacturing optoelectronic devices such as LEDs, solar cells, photodetectors, and sensors based on the above thin films.

It is worth mentioning that although the focus of this study is reactive blade coating, the findings are readily applicable to other roll-to-roll coating/printing techniques, such as screen printing, slot-die printing, gravure and flexography printing, etc. The current work is the spark for empowering low carbon footprint, low-cost and environmentally friendly approaches for advanced electrical and optoelectronic materials and device manufacturing.